

Generalized Bose-Einstein Condensation in Driven-dissipative Quantum Gases

Dissertation
zur Erlangung des wissenschaftlichen Grades
Doctor rerum naturalium

vorgelegt von

Daniel Christian Vorberg
geboren am 21. Dezember 1987 in Dresden

Institut für Theoretische Physik
Fakultät Physik
Technische Universität Dresden

Max-Planck-Institut
für Physik komplexer Systeme
Dresden



MAX-PLANCK-GESELLSCHAFT

Eingereicht am 20. Oktober 2017

Verteidigt am 7. Februar 2018

Erster Gutachter: Prof. Dr. Roland Ketzmerick

Zweiter Gutachter: Prof. Dr. Sebastian Diehl

Dritter Gutachter: Dr. André Eckardt

Für Kerstin, die mir Jakob schenkte.

Abstract

Bose-Einstein condensation is a collective quantum phenomenon where a macroscopic number of bosons occupies the lowest quantum state. For fixed temperature, bosons condense above a critical particle density. This phenomenon is a consequence of the Bose-Einstein distribution which dictates that excited states can host only a finite number of particles so that all remaining particles must form a condensate in the ground state. This reasoning applies to thermal equilibrium.

We investigate the fate of Bose condensation in nonisolated systems of noninteracting Bose gases driven far away from equilibrium. An example of such a driven-dissipative scenario is a Floquet system coupled to a heat bath. In these time-periodically driven systems, the particles are distributed among the Floquet states, which are the solutions of the Schrödinger equation that are time periodic up to a phase factor. The absence of the definition of a ground state in Floquet systems raises the question, whether Bose condensation survives far from equilibrium. We show that Bose condensation generalizes to an unambiguous selection of multiple states each acquiring a large occupation proportional to the total particle number. In contrast, the occupation numbers of nonselected states are bounded from above. We observe this phenomenon not only in various Floquet systems, i.a. time-periodically-driven quartic oscillators and tight-binding chains, but also in systems coupled to two baths where the population of one bath is inverted. In many cases, the occupation numbers of the selected states are macroscopic such that a fragmented condensation is formed according to the Penrose-Onsager criterion. We propose to control the heat conductivity through a chain by switching between a single and several selected states. Furthermore, the number of selected states is always odd except for fine-tuning. We provide a criterion, whether a single state (e.g., Bose condensation) or several states are selected.

In open systems, which exchange also particles with their environment, the nonequilibrium steady state is determined by the interplay between the particle-number-conserving intermode kinetics and particle-number-changing pumping and loss processes. For a large class of model systems, we find the following generic sequence when increasing the pumping: For small pumping, no state is selected. The first threshold, where the stimulated emission from the gain medium exceeds the loss in a state, is equivalent to the classical lasing threshold. Due to the competition between gain, loss and intermode kinetics, further transitions may occur. At each transition, a single state becomes either selected or deselected. Counterintuitively, at sufficiently strong pumping, the set of selected states is independent of the details of the gain and loss. Instead, it is solely determined by the intermode kinetics like in closed systems. This implies equilibrium condensation when the intermode kinetics is caused by a thermal environment. These findings agree well with observations of exciton-polariton gases in microcavities. In a collaboration with experimentalists, we observe and explain the pump-power-driven mode switching in a bimodal quantum-dot micropillar cavity.

Zusammenfassung

Die Bose-Einstein-Kondensation ist ein Quantenphänomen, bei dem eine makroskopische Zahl von Bosonen den tiefsten Quantenzustand besetzt. Die Teilchen kondensieren, wenn bei konstanter Temperatur die Teilchendichte einen kritischen Wert übersteigt. Da die Besetzungen von angeregten Zuständen nach der Bose-Einstein-Statistik begrenzt sind, bilden alle verbleibenden Teilchen ein Kondensat im Grundzustand. Diese Argumentation ist im thermischen Gleichgewicht gültig.

In dieser Arbeit untersuchen wir, ob die Bose-Einstein-Kondensation in nicht wechselwirkenden Gasen fern des Gleichgewichtes überlebt. Diese Frage stellt sich beispielsweise in Floquet-Systemen, welche Energie mit einer thermischen Umgebung austauschen. In diesen zeitperiodisch getriebenen Systemen verteilen sich die Teilchen auf Floquet-Zustände, die bis auf einen Phasenfaktor zeitperiodischen Lösungen der Schrödinger-Gleichung. Die fehlende Definition eines Grundzustandes wirft die Frage nach der Existenz eines Bose-Kondensates auf. Wir finden eine Generalisierung der Bose-Kondensation in Form einer Selektion mehrerer Zustände. Die Besetzung in jedem selektierten Zustand ist proportional zur Gesamtteilchenzahl, während die Besetzung aller übrigen Zustände begrenzt bleibt. Wir beobachten diesen Effekt nicht nur in Floquet-Systemen, z.B. getriebenen quartischen Fallen, sondern auch in Systemen die an zwei Wärmebäder gekoppelt sind, wobei die Besetzung des einen invertiert ist. In vielen Fällen ist die Teilchenzahl in den selektierten Zuständen makroskopisch, sodass nach dem Penrose-Onsager Kriterium ein fragmentiertes Kondensat vorliegt. Die Wärmeleitfähigkeit des Systems kann durch den Wechsel zwischen einem und mehreren selektierten Zuständen kontrolliert werden. Die Anzahl der selektierten Zustände ist stets ungerade, außer im Falle von Feintuning. Wir beschreiben ein Kriterium, welches bestimmt, ob es nur einen selektierten Zustand (z.B. Bose-Kondensation) oder viele selektierte Zustände gibt.

In offenen Systemen, die auch Teilchen mit der Umgebung austauschen, ist der stationäre Nichtgleichgewichtszustand durch ein Wechselspiel zwischen der (Teilchenzahl-erhaltenden) Intermodenkinetik und den (Teilchenzahl-ändernden) Pump- und Verlustprozessen bestimmt. Für eine Vielzahl an Modellsystemen zeigen wir folgendes typisches Verhalten mit steigender Pumpleistung: Zunächst ist kein Zustand selektiert. Die erste Schwelle tritt auf, wenn der Gewinn den Verlust in einer Mode ausgleicht und entspricht der klassischen Laserschwelle. Bei stärkerem Pumpen treten weitere Übergänge auf, an denen je ein einzelner Zustand entweder selektiert oder deselektiert wird. Schließlich ist die Selektion überraschenderweise unabhängig von der Charakteristik des Pumpens und der Verlustprozesse. Die Selektion ist vielmehr ausschließlich durch die Intermodenkinetik bestimmt und entspricht damit den oben beschriebenen geschlossenen Systemen. Ist die Kinetik durch ein thermisches Bad hervorgerufen, tritt wie im Gleichgewicht eine Grundzustands-Kondensation auf. Unsere Theorie ist in Übereinstimmung mit experimentellen Beobachtungen von Exziton-Polariton-Gasen in Mikrokavitäten. In einer Kooperation mit experimentellen Gruppen konnten wir den Modenwechsel in einem bimodalen Quantenpunkt-Mikrolaser erklären.

Contents

Abstract	v
English	v
German	vii
Table of contents	xi
1. Introduction	1
1.1. Bose-Einstein condensates and lasers	1
1.2. Outline	6
I. Closed Systems	11
2. Theoretical framework	13
2.1. Driven-dissipative quantum gases	13
2.2. Floquet systems	14
2.3. Floquet-Born-Markov theory	15
2.4. Nonequilibrium steady state	21
2.5. Master equation of ideal quantum gases	22
2.6. Monte-Carlo simulations	23
3. Model systems	27
3.1. Tight-binding chain in contact with two heat baths	27
3.2. Time-periodically driven tight-binding in contact with a heat bath	29
3.3. Driven quartic oscillator	29
3.4. Random-rate matrix	32
4. Equilibrium Bose condensation	33
5. Bose selection	35
6. Mean-field theory	39
7. Asymptotic theory	41
7.1. Selection criterion	41

7.2. Properties of Bose selection	43
7.3. Systematic high-density expansion	45
8. Transitions	49
9. Beyond the mean-field approximation	55
10. Heat current	59
11. Small and zero rates	63
11.1. Small rates	63
11.2. Zero rates	65
12. Lotka-Volterra systems and evolutionary game theory	71
II. Open Systems	73
13. Framework	75
13.1. Introduction	75
13.2. Kinetic equations	76
14. Exciton-polaritons in a micro-cavity	79
15. Multi-mode condensation	83
16. Transitions	87
16.1. Phase diagram of a photonic system	87
16.2. Theoretical description by the asymptotic theory	89
16.3. Bose selection in open and closed systems	92
17. Mode-switching in a microcavity	95
17.1. Theoretical description	96
17.2. Phase diagram	99
18. Conclusion	101
18.1. Summary	101
18.2. Outlook	103
Appendix	105
A. Many-body rate equation	105
B. Equations of motion for mean occupations	105
C. Existence and uniqueness of the set of selected states	106
D. Relaxation dynamics of a double-pillar polariton system	108

E. Augmented mean-field equation	110
F. Extracting parameters of a bimodal laser	111
List of figures	113
Bibliography	115
List of publications	127
Acknowledgments	129
Assurance	131

1. Introduction

1.1. Bose-Einstein condensates and lasers

Bose-Einstein condensation [1], a collective behavior of a macroscopic number of bosonic particles, is one of the most fascinating quantum phenomena. This macroscopic accumulation of bosons in the ground state induces quantum coherence in matter waves even on macroscopic scales, e.g., interferences between entire atom clouds [2]. Moreover, superconductivity is a very consequence of this phenomenon in interacting systems. In the years 1924 and 1925, Albert Einstein [3, 4] predicted this phenomenon based on Satyendranath Bose's work on quantum statistics, which placed the concepts of thermodynamic on the foundation of the new arising quantum physics. First, Bose regarded quantum particles as indistinguishable. This theory applies for bosons (named after Bose), one of the two classes of quantum particles besides fermions. Later, Einstein predicted that when the number of bosons exceeds a critical value, all further particles must condensate in the single-particle ground states of the system, akin to the condensation of water vapor when the pressure exceeds the equilibrium vapor pressure.

Experimentally, Bose-Einstein condensates have been first created by Anderson *et al.* [5] with ^{23}Na atoms and Davis *et al.* [6] with ^{87}Rb atoms in 1995 by cooling these atoms down to very low temperatures of a few microkelvin. Since then, condensation has been realized in various systems, among them are exciton-polaritons [7, 8], magnons [9, 10], bosonic molecules of fermionic atoms [11], and photons [12, 13]. Even before these realizations, Bose-Einstein condensation was proposed to explain the observed superfluidity in ^4He [14] and superconductivity [15]. Bose-Einstein condensates are widely used to explore quantum physics nowadays.

The prediction of Bose-Einstein condensation seventy years before its experimental realization is a consequence of the success of the fundamental concepts of equilibrium physics. These concepts have been derived for classical systems by Kelvin, Boltzmann, Gibbs, and Maxwell in the nineteenth century and for quantum gases by Bose, Einstein, Fermi, Dirac, Jaynes, and others in the last century. In thermodynamic equilibrium, the system is in the Gibbs state given by the principle of maximum entropy [16]. The states of quantum systems are described by density operators $\hat{\rho}$. The Gibbs state for a quantum system reads $\hat{\rho} \propto e^{-\beta(\hat{H}-\mu)}$. Apart from the details of the system given by its Hamiltonian \hat{H} , the environment determines a few thermodynamic properties, such as (inverse) temperature β or chemical potential μ , only. For an increasing number of noninteracting bosons, the chemical potential increases until it approaches the ground-state energy and the occupations of all

excited states saturate while all additional particles must accumulate in the ground state [Fig. 1.1(a)]. In the thermodynamic limit, which is the limit of infinite volume at fixed particle density, the system undergoes a phase transition and a Bose condensate forms. According to the Mermin-Wagner theorem [17], no long-range order exists in one and two-dimensional systems at finite temperatures so that true Bose condensation is prevented. In finite systems of any dimensionality, one finds a crossover to a state with a significant fraction of particles occupying the ground state corresponding to finite-size Bose condensation [18]. Whenever Bose condensation is discussed in this thesis, we refer to this finite-size effect.

Most systems found in nature operate only far from equilibrium. They require a permanent flow of, e.g., energy [19–21] or particles [22]. Among these systems are heat engines, electrical devices, and of course living organisms.

Nonequilibrium steady states are stationary states, which exhibit nonzero fluxes of probability as well as energy or particles. These fluxes are caused by the coupling to an environment. In contrast to equilibrium, the nonequilibrium steady state depends on the very details of not only the system but also the environment and the system-environment coupling¹. Thus, finding concepts for nonequilibrium effects as general as the concepts for equilibrium is still a remaining challenge, even though many fruitful results have been found, e.g., the fluctuation-dissipation theorem [23, 24], the Kibble-Zurek scaling [25], the dynamical critical behavior [26], and many others [27]. However, this dependence on all details allows for quantum bath engineering, where the environment and its coupling to the system are designed to prepare specific states of interest. Examples are the creation of arbitrary coherent superpositions [28–31], dark state cooling [32, 33], or the preparation of topological states by dissipation [34, 35]. These opportunities have triggered the recent interest in exploring nonequilibrium physics.

Besides bath engineering, Floquet engineering is another very fruitful approach of quantum engineering based on time-periodic driving instead of an environment. Floquet systems [36, 37] are time-periodically driven systems. Various artificial systems [38] have been created by time-periodic driving. Examples include artificial tunable gauge fields [39, 40], the realization of topological insulators [41], the quantum simulation of frustrated magnetism [42, 43], and the control of the superfluid-to-Mott-insulator transition [44, 45]. Like eigenstates of time-independent Hamiltonians, Floquet states solve the time-dependent Schrödinger equation for time-periodic Hamiltonians $\hat{H}(t) = \hat{H}(t + 2\pi/\omega)$ with an angular frequency ω . These Floquet states $|\varphi_i(t)\rangle = e^{-i\varepsilon_i t/\hbar}|u_i(t)\rangle$ are time-periodic states $|u_i(t)\rangle = |u_i(t + 2\pi/\omega)\rangle$ with an additional phase rotation, which is determined by quasienergies ε_i . In contrast to eigenenergies, quasienergies are defined only up to multiples of the quantum $\hbar\omega$. This causes the notable difference that an ordering of the Floquet states according to their quasienergies is ambiguous. Especially, there is no definition of a ground state in Floquet systems.

The investigation of open Floquet systems [46] opened a new field which has been termed “periodic

¹In equilibrium, the steady state is given by Gibbs ensemble. This state is independent of the details about the environment except for its temperature and chemical potential.

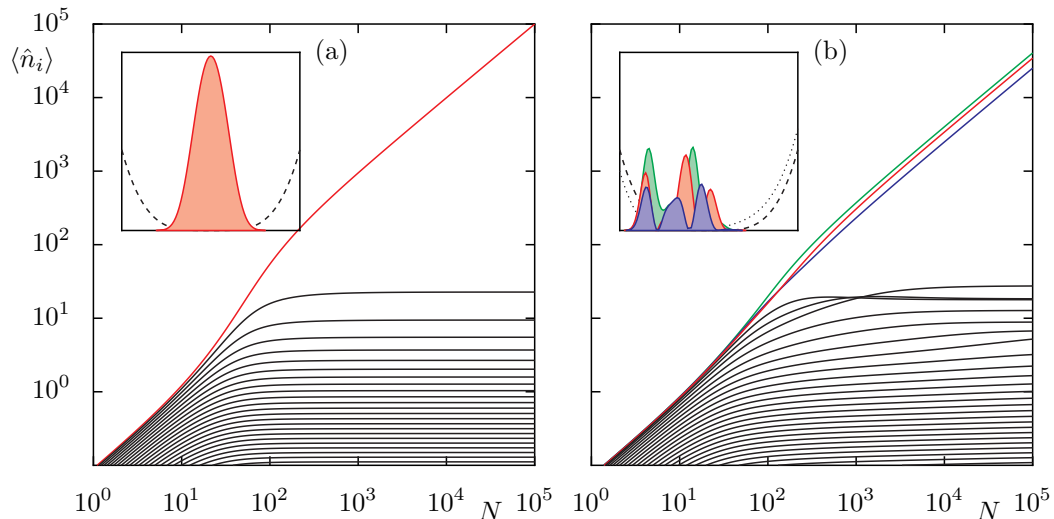


Figure 1.1.: (a) Bose condensation versus (b) Bose selection. (a) Bose-Einstein condensation in a quartic trap in thermal equilibrium. The dependence of the mean occupation numbers $\langle \hat{n}_i \rangle$ of the eigenstates on the total particle number N is shown. Bose-Einstein condensation forms above a characteristic total particle number. All further particles condensate in the ground state while the occupation in any other state saturates. The inset shows the condensate density (shaded area) and the quartic trap (dashed line). (b) Bose selection in a driven quartic oscillator in contact with a thermal environment. The dependence of the mean occupation numbers $\langle \hat{n}_i \rangle$ of the Floquet states on the total particle number N is shown. In the limit of large particle numbers N , multiple states acquire macroscopic occupation numbers $\langle \hat{n}_i \rangle$ each. The occupation of any other state saturates like the occupations of excited states in equilibrium. The inset shows the condensate densities (shaded areas) and the potential of the quartic trap, namely the time-averaged potential (dashed line) and the maximal tilted trap (dotted line). The latter case of the maximal tilt towards the left corresponds to the time where the snapshot of the condensate shapes was taken. The system is discussed in detail in Sec. 3.3 and all parameters of panel (b) are the same as in the Fig. 3.5; the only difference to panel (a) is the absence of driving.

thermodynamics” by Kohn [47]. In open Floquet systems, the bath and Floquet engineering are united since a quantum system is coupled to a (thermal) environment and driven away from equilibrium by a time-periodic force. When the system-environment coupling is weak, the system approaches a nonequilibrium steady state in the long-time limit. This state is quasistationary only since it still exhibits the time periodicity of the Floquet states. The absence of the ordering of the Floquet states by the quasienergy shows vividly that nonequilibrium steady states are not described by the Gibbs ensemble. Indeed, the steady state is determined not only by the energetics (like in Gibbs ensemble) but also by the kinetics. I.e., the Hamiltonian of the system (its spectrum and eigenstates) and the thermodynamic potentials are not sufficient to determine the steady state since the knowledge of the relaxation kinetics is necessary. A common framework to describe this dynamics is the Born-Markov approach [48] and its generalization to time-periodic systems, the Floquet-Born-Markov approach [49–51]. Various effects were investigated in single-particle systems, e.g., dynamical localizations of Rydberg atoms in noisy environments [49], signatures of chaotic and regular dynamics in steady states [51, 52], and heat flows in nonequilibrium steady states [53]. Avoided crossings intrinsically appear in the quasienergy spectrum under parameter variation. Since they affect the steady states

strongly [54, 55], they can be exploited to control the steady state via dissipation [56]. In contrast to these single-particle effects, we will discuss many-particle effects based on quantum statistics in open Floquet gases in this thesis.

We investigate the fate of Bose condensation far from thermal equilibrium. A Floquet gas coupled to a thermal bath provides an example where such nonequilibrium situations exist. The absence of a ground state raises the question: “Does Bose condensation survive under nonequilibrium condition?” And, if so, “which state hosts the condensate”? Figure 1.1(b) exemplarily shows the answers for a Bose gas trapped in a time-periodically-driven, quartic oscillator and coupled to a heat bath. We find that the Bose condensation generalizes to an unambiguous *selection* of a group of states far from equilibrium [57, 58]. Each of these *Bose-selected* states acquires a large number $\langle \hat{n}_i \rangle$ of particles, which increase with the total particle number N . In contrast, the occupation number $\langle \hat{n}_i \rangle$ of any other state saturates and remains orders of magnitude smaller, like the occupation of each excited state in thermal equilibrium. Surprisingly, we find that the number of selected states is always odd except for fine-tuned situations. The insight into the mechanism of this phenomenon is one of the key results of this thesis.

Steady states with a persistent particle flow through the system make up another type of nonequilibrium steady states. This scenario generalizes systems which are driven out of equilibrium only via an energy flow through the system, which were discussed until now. In this thesis, we use the definitions of statistical mechanics: *open* systems exchange energy and particles with their environment, *closed* systems only energy but no particles, and *isolated* systems are not coupled to any environment².

Photonic systems are intrinsically open systems since their particle loss must be balanced by pumping. The loss of particles is caused by the short lifetime of photonic particles in a cavity due to the leakage. The interplay between the intermode kinetics (which is particle-number conserving like the kinetics in closed systems) and the pumping and loss determine the nonequilibrium steady state. This interplay enables many fascinating effects, e.g., multi-mode condensation [59]. We will focus on these photonic systems in the second part of this thesis. Prime examples are exciton-polariton fluids [60, 61], lasers [62], and photons in dye-filled cavities [12, 13, 63, 64], which currently raise huge interest.

Lasers [65–67] and Bose-Einstein condensates share the fact that in both the coherence is caused by bosons occupying a single mode. A laser is a device that emits coherent light due to “light amplification by stimulated emission of radiation”. However, while a laser accumulates (massless) photons and operates far from equilibrium, a Bose condensate is formed by massive particles (e.g., atoms) and is an equilibrium phenomenon. This demarcation between lasing and Bose condensation based on whether atoms or photons accumulate in a single state, and, whether this occurs in or out-of equilibrium is not very sharp. Exciton-polaritons, hybridisations of photons and excitons, show this vividly since

²Note, that these definitions from statistical mechanics differ from the terminology in quantum systems, where open systems are nonisolated systems while closed and isolated systems are used synonymously.

they are light yet massive particles with a short lifetime [68]. This has led to the discussion [68–73] of how to distinguish between polariton lasing and Bose-Einstein condensation of polaritons. Both phenomena are taken together in the term “polariton condensation”. Only in Bose-Einstein condensates of polaritons, the polariton gas is almost thermalized, i.e., obeys the Bose-Einstein statistics. Furthermore, the nonequilibrium condition manifests itself in the sensitivity of the condensate density on the pump spot [74].

Another possible criterion to distinguish between Bose condensation and lasing is based on the dynamic mechanism causing the different effects [72, 75, 76]. Lasing is caused by emissions from a gain medium. The gain medium provides new particles and coherence is built up when the gain due to *stimulated emission* exceeds the (spontaneous) loss. The steady state is determined by *kinetics*. Namely, the steady state depends on all rates (i.e., the Einstein coefficients) which describe the dynamics, since it is a nonequilibrium steady state. Furthermore, Bose-Einstein condensation is caused by *stimulated cooling*. The scattering into the emerging condensate is enhanced by bosonic final-state stimulations. In thermal equilibrium, the steady state is determined by the *energetics*, i.e., the spectrum of the system (besides the temperature and the chemical potential). Bose condensation forms when the chemical potential approaches the energy of the single-particle ground state such that its occupation becomes macroscopic.

For completeness, let us also mention *isolated* systems, which exchange neither energy nor particles with any environment [27]. In these systems, a pure state remains pure for all times under unitary time evolution. However, according to the eigenstate thermalization hypothesis [77, 78], which is justified by numerical observations [79], interacting systems can thermalize via dephasing since the expectation values of simple observables are thermal for almost all eigenstates. The system provides the bath for its own subsystems such that these subsystems can thermalize. Exceptions where information of the initial state remains for arbitrary long times are integrable systems and many-body-localized systems [80–82]. For integrable systems, the steady states can be found in the form of generalized Gibbs ensembles, which are determined by the conserved quantities (in addition to temperature or chemical potential) [83, 84]. Also for many-body localization, the system fails to act as its own bath [85]. Similar results have been obtained for isolated Floquet systems. However, here not even the total energy is conserved. Generic nonintegrable systems lose eventually all initial information [86] and heat up to infinite-temperature states [87]. On intermediate timescales, a Floquet condensate, which is a many-body state with coherence properties of a macroscopically occupied single-particle state, can exist for large driving frequencies [44, 88, 89]. However, preventing these systems from heating up on experimental timescales in order to investigate Floquet-engineered systems is a challenge [90–94]. For integrable systems, the system approaches a periodic Gibbs ensemble, a generalized Gibbs ensemble not restricted to a given energy [95]. Many-body localization is also proposed to survive in Floquet systems [96], e.g., in form of discrete time crystals [97, 98]. We will not discuss isolated system in this thesis. Possible connections between the Bose selection in open and closed systems and effects in isolated systems remain for future investigation.

1.2. Outline

In this thesis, we discuss nonequilibrium steady states of driven-dissipative ideal Bose gases. This discussion is divided into two parts focusing on closed and open quantum gases. In Part I, we investigate closed quantum gases, which exchange energy with their environment and whose total particle number is conserved. In Part II, we discuss open quantum gases, where the loss of particles is compensated by their coupling to an externally-pumped particle reservoir.

Chapter 2 presents the theoretical framework. Two generic scenarios to drive systems far from equilibrium are presented: firstly, a quantum Floquet gas coupled to a heat bath, and, secondly, a quantum gas coupled to two heat baths of different temperatures. The time-evolutions of these systems are described by master equations, which are obtained within the Born-Markov approach and the Floquet-Born-Markov approach for the autonomous and the time-periodically-driven system, respectively. The incoherent dynamics is given by a Pauli master equation, whose rates are given by Fermi's-golden-rule-type expressions. Starting from the single-particle case, the generalization of the master equation to an ideal gas follows in a straight-forward fashion. In the long-time limit, the systems approach a stationary state. Note, for Floquet systems this state is quasistationary since it exhibits still the time-periodicity of the modulation. However, finding this nonequilibrium steady state of the many-body system is not just a simple generalization of the single-particle problem. This is different from the equilibrium state, where the many-body state is obtained by entropy maximization and given by Gibbs ensemble and, thus, determined by single-particle properties only. Thus, away from equilibrium, even ideal gases constitute a (classical) many-body problem. Numerically exact results are obtained by quantum-jump Monte-Carlo simulations.

In Chapter 3, we introduce several model systems. The first system is a noninteracting Bose gas trapped in a quartic potential, subjected to a time-periodic force, and coupled to a single heat bath. Furthermore, two model systems are based on tight-binding chains, where particles tunnel coherently between neighboring sites. In the first chain model, the system is subjected to a time-periodic force and coupled to a heat bath. In the second chain model, the system is coupled to two heat baths, whereby the second heat bath is population-inverted. Implementations of such model systems with the help of cold atoms in optical lattices [99] and traps are sketched. These systems are examples for the two above-mentioned scenarios. To obtain results not relying on specific system properties, we also introduce random-rate models where all rates determining their dynamics are chosen randomly.

Chapter 4 briefly recapitulates Bose gases in thermal equilibrium. In particular, the consequences of detailed balance in the steady state and the emergence of Bose-Einstein condensation in the limit of high particle densities are discussed.

An intriguing phenomenon in the nonequilibrium steady state is presented in Chap. 5: the selection of a group of states where each state acquires a large and often even macroscopic occupation [Fig. 1.1(b)]. All other states, the nonselected states, have finite occupations in the high-density limit. We observe that the number of selected states is odd except for fine-tuned situations and that

the set of selected states is independent of the temperature(s) of the heat bath(s). Various model systems illustrate these findings. We find that Bose selection causes fragmented condensation when the occupations of several states are macroscopic. This effect, which generalizes Bose condensation to nonequilibrium steady states and which we term Bose selection in the following, is a central result and starting point for further investigation.

Chapter 6 presents a mean-field approximation for the master equation leading to kinetic equations for the mean occupation numbers. The assumption of neglecting the two-particle correlations, which are induced by nonequilibrium effects and by the conserved particle number, is justified by comparisons to results of Monte-Carlo simulations.

An analytical theory of Bose selection is derived in Chap. 7. This theory is based on a Bogoliubov-like approximation of the mean-field equations where the rates between nonselected states are neglected. This theory unveils the underlying mechanism of Bose selection. We formulate a transparent criterion, which determines the set of selected states. Furthermore, all numerical observations of Chap. 5 are explained by analytical arguments.

In Chapter 8, we discuss that the variation of a system parameter can trigger sudden jumps in the mean occupation numbers. These jumps are caused by transitions where the set of selected states changes. We find that at these transitions generically two states are involved ensuring an odd number of selected states also after the transition. At each transition, the number of selected states is even. These transitions are fine-tuned situations, where the number of selected states is not odd. In finite-size systems, these transitions have finite widths. Moreover, the theory of transitions allows for an algorithm for efficiently finding all selected states even in large systems.

Two-particle fluctuations beyond the mean-field results are discussed in Chap. 9. Nontrivial correlations are not only caused by the restriction to a fixed particle number like for the canonical ensemble but also by nonequilibrium effects. We present an augmented mean-field method taking into account these correlations.

In Chapter 10, we discuss the heat current from the population-inverted bath to the colder bath and from the driven system to the bath. We find that the heat current sensitively depends on the set of Bose-selected states, in particular, whether one or several states are selected. We propose a quantum switch to control the heat current by switching between one and three selected states.

The limit of small and even vanishing rates is discussed in Chap. 11. In systems where some rates are much smaller than others, we find a preasymptotic regime at intermediate particle numbers. In this regime, the selection is determined by a rate matrix where small rates have been neglected. A careful analysis shows that the selection criterion is altered in this case (as a consequence of the fact that the rate matrix is not fully connected anymore) and that the number of selected states can also be even.

Chapter 12 briefly highlights the connection between the dynamics of driven ideal Bose gases and population dynamics in biological systems described by Lotka-Volterra equations [100]. We discuss

this analogy, which manifests itself in the correspondence between selected states and surviving species, respectively.

In Part II, we discuss open driven-dissipative systems, i.e., systems whose total particle number is not conserved due to particle exchange with their environment. This scenario generically arises in photonic systems, like lasers, exciton-polariton systems, or photons in dye-filled cavities.

Chapter 13 starts with a brief motivation and introduces a generic model system. In contrast to a closed system, this model is extended by processes of particle loss and the coupling to an externally-pumped particle reservoir. In the following, different systems are modeled in this way.

Chapter 14 focuses on exciton-polariton gases. We sketch a specific system motivated by experimental observations of polariton condensates in “photonic molecules” [101]. Here excited-state condensation emerges when ramping up the pumping. Increasing the pumping further, a single condensate in the ground state eventually forms at the expense of all other.

In Chapter 15, we present a criterion for multi-mode condensation in open driven-dissipative Bose gases. This criterion is derived in an asymptotic theory in the limit where the particle lifetime is short compared to the (single-particle-)thermalization timescale (due to the heat bath). It unveils the mechanism of multi-mode condensation and determines the modes that acquire large occupations. Applying this criterion to exciton-polariton systems, we find good agreement with the input-output characteristics observed in the photonic molecule. Moreover we find for intermediate pumping strength a phase where two condensates coexist.

Varying the pumping can trigger transitions at which a single condensate appears or disappears. By investigating these transitions in Chap. 16, we find a generic behavior of the system when ramping up the pump power: For sufficiently small pumping, no state is selected. The first state is selected by the criterion for simple lasing, namely that the gain exceeds the loss for this state. Subsequently, several phases with different sets of selected states (determined by the interplay between gain, loss, and intermode kinetics) follow. The reservoir occupation reaches a plateau whenever the number of selected states is odd. Eventually, in the limit of strong pumping, the set of selected states is determined only by the intermode kinetics like in closed systems. This implies ground-state condensation when the intermode kinetics is caused by a thermal bath.

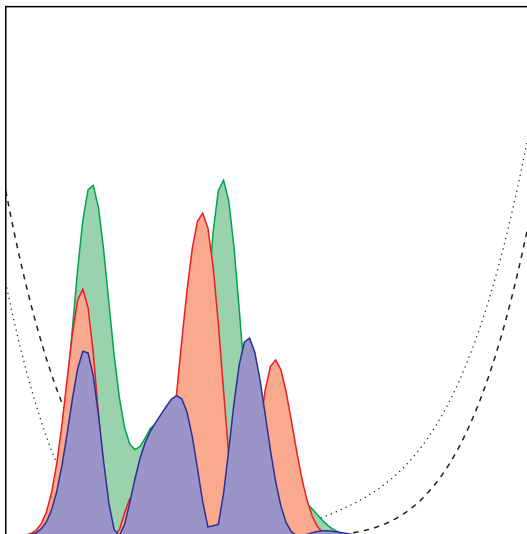
A minimal instance of a transition from lasing to Bose-Einstein condensation is presented in Chap. 17. We consider a bimodal quantum-dot micropillar cavity where the polarization direction switches with respect to the pumping power. We show that the mode which coherently emits light is selected by the gain-loss ratio above the lasing threshold when ramping up the pumping power, while for strong pumping the mode is selected by the intermode kinetics alone akin to equilibrium Bose-Einstein condensation. If these two conditions favor different modes, the selected mode switches at intermediate pumping. Hereby the experimental data from our collaboration with the groups of Reitzenstein and Höfling [102], the numerical results, and the results from the selection criterion agree very well.

Chapter 18 concludes by summarizing this thesis and discussing open questions and future directions of research.

We have published the phenomenon of Bose selection in closed systems in Ref. [57] and have discussed many consequences, e.g., transitions, in Ref. [58]. In another paper [103], we propose to induce Bose condensation by a hot bath which is locally coupled to the system. We observe that in a chain which is in contact to a thermal environment, a condensate forms when this hot “needle” is coupled to the system. This intriguing nonequilibrium effect is not part of this thesis. We have published the results of the mode switching in the bimodel microcavity in Ref. [102]. The results on the general Bose selection in open systems are first published here.

Part I.

Closed Systems



2. Theoretical framework

Driven-dissipative quantum gases are fascinating physical systems showing many intriguing phenomena. Here, we consider ideal Bose gases driven out of equilibrium. Within this framework, we focus on nonequilibrium steady states which exhibit an energy flow through the system. Even though the particles are noninteracting, the gas is not just a straight-forward generalization of the single-particle problem (like in equilibrium) but a true many-body problem. Obtaining the nonequilibrium steady state requires the solution of the full master equation. The derivation of this equation within the (Floquet-)Born-Markov approach is described [Sec. 2.3] and generalized to ideal quantum gases [Sec. 2.5]. The nonequilibrium steady states [Sec. 2.4] can be numerically obtained using quantum-jump Monte-Carlo simulations [Sec. 2.6].

2.1. Driven-dissipative quantum gases

Systems can be driven far away from equilibrium in different scenarios. Two generic scenarios, which will be investigated in the following, are shown in Fig. 2.1. Despite the distinct driving schemes, we will see that both scenarios share many similarities.

In the first scenario, the quantum gas is subjected to a time-periodic force and coupled to a thermal environment [Fig. 2.1(a)]. The system reaches a quasistationary (i.e., time-periodic) state. In this steady state, energy flows from the driving through the system into the heat bath [53]. In cold atom experiments, time-periodic driving is a standard technique. Heat baths can also be implemented in such systems by a different species of atoms [see Chap. 3]. We will present several models of this type to illustrate our findings.

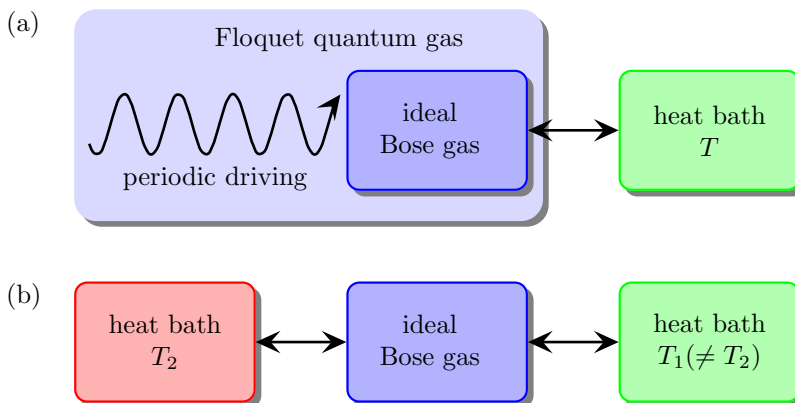


Figure 2.1: Sketch of two scenarios of driven-dissipative ideal Bose gases. (a) A time-periodically driven gas (Floquet gas) in contact with a single heat bath. (b) An ideal Bose gas in contact with two heat baths at different temperatures.

In the second scenario, the quantum gas is coupled to two heat baths [Fig. 2.1(b)]. The system relaxes to a nonequilibrium steady state, where heat flows from the hotter bath into the colder one. We will also discuss situations where one heat bath is population-inverted. This could be described by a negative temperature of the bath. Such a situation has been realized for a gas in an optical lattice recently [104].

2.2. Floquet systems

Subjecting quantum systems to time-periodic forces is a very successful technique of control. Examples span from the Rabi oscillation in atoms subjected to laser fields, to Floquet engineered many-body systems, e.g., the control of the superfluid-to-Mott-insulator transition in cold atoms in an optical lattice via shaking [44, 45].

The theoretical foundations of these time-periodically driven quantum systems are based on the Floquet theorem [36, 37]. It states that for time-periodic Hamiltonians $\hat{H}(t) = \hat{H}(t + 2\pi/\omega)$, the time-dependent Schrödinger equation is solved by a set of Floquet states

$$|\varphi_n(t)\rangle = e^{-i\varepsilon_n t/\hbar} |u_n(t)\rangle. \quad (2.1)$$

These Floquet states are given by time-periodic Floquet modes $|u_n(t)\rangle = |u_n(t+2\pi/\omega)\rangle$ and additional phase rotations characterized by the quasienergies ε_n . The name quasienergy reflects that all energies are defined only up to integer multiples of the energy of the driving quantum $\hbar\omega$. Namely the transformation $\varepsilon_n \rightarrow \varepsilon_n + n\hbar\omega$ and $|u_n(t)\rangle \rightarrow e^{in\omega t} |u_n(t)\rangle$ leaves all Floquet states (2.1) unchanged. This causes an ambiguous definition of the quasienergy. For numerical purposes, we require that all quasienergies ε_n lie in the interval $[0, \hbar\omega)$. The Floquet states form an orthogonal basis at all times. Thus the time-evolution operator can be written as

$$\hat{U}_H(t) = \sum_n e^{-i\varepsilon_n t/\hbar} |u_n(t)\rangle \langle u_n(0)|. \quad (2.2)$$

The Floquet formalism provides a powerful theory to describe time-periodically-driven systems.

The ambiguous definition of the quasienergy prevents a physically meaningful order of the Floquet states with respect to quasienergy. This is different to undriven systems, where all eigenstates are well-ordered by their eigenenergies. We will see that due to this absence of an order, many concepts of equilibrium systems, such as the ground state or the concept of temperature¹, become meaningless in Floquet systems. To have at least some kind of order, we will use the cycle-averaged energy

$$\bar{E}_n = \frac{1}{T} \int_0^T dt \langle u_n(t) | \hat{H}(t) | u_n(t) \rangle, \quad (2.3)$$

¹In some cases the concept of an effective temperature survives [52] approximately.

where $T = 2\pi/\omega$ denotes the period. This is a natural choice since these averaged energies approach the eigenenergies in the limit of weak driving.

2.3. Floquet-Born-Markov theory

Many systems are not perfectly isolated from their environment but weakly coupled to it. Describing their dynamics requires to take into account the impact of the environment. Unfortunately, the knowledge about the state of the environment and its dynamics is usually very little due to its huge number of degrees of freedom. However, under the assumption of weak coupling, the environment can be traced out in a perturbation theory. In this section, we describe such a derivation of a master equation from a microscopic theory by the Born-Markov [48, 105, 106] (Floquet-Markov [47, 49–51, 55, 107]) approach for autonomous systems (Floquet systems), respectively.

The composite Hamiltonian of a system which is coupled with a heat bath reads

$$\hat{H}_{\text{tot}}(t) = \hat{H}(t) + \hat{H}_{\text{sb}} + \hat{H}_{\text{b}}, \quad (2.4)$$

with the system Hamiltonian $\hat{H}(t)$, the bath Hamiltonian \hat{H}_{b} , and the system-bath interaction

$$\hat{H}_{\text{sb}} = \hat{A} \otimes \hat{B}, \quad (2.5)$$

where \hat{A} and \hat{B} act on the Hilbert space of the system and the bath only, respectively. The system Hamiltonian is time-independent, $\hat{H}(t) = \hat{H}$, in the case of an autonomous system and time-periodic, $\hat{H}(t) = \hat{H}(t + 2\pi/\omega)$, for a Floquet system driven at the angular frequency ω .

We apply a perturbation theory for weak system-bath interactions. We switch to the interaction picture with respect to the Hamiltonian $\hat{H}(t) + \hat{H}_{\text{b}}$ and label all operators in the interaction picture by the tilde. This is the Floquet picture in the time-periodically driven case. The time evolution of the total density operator of the system and the environment $\tilde{\rho}_{\text{tot}}$ is given by the Liouville-von Neumann equation,

$$\frac{d}{dt} \tilde{\rho}_{\text{tot}}(t) = -\frac{i}{\hbar} [\tilde{H}_{\text{sb}}(t), \tilde{\rho}_{\text{tot}}(t)]. \quad (2.6)$$

We obtain an integro-differential equation by integrating the Liouville-von Neumann Eq. (2.6) from time t_0 , when the system was prepared in the initial state $\tilde{\rho}_{\text{tot}}(t_0)$, up to time t and plugging the result back into Eq. (2.6). The result reads

$$\frac{d}{dt} \tilde{\rho}_{\text{tot}}(t) = -\frac{i}{\hbar} [\tilde{H}_{\text{sb}}(t), \tilde{\rho}_{\text{tot}}(t_0)] - \frac{1}{\hbar^2} \int_{t_0}^t d\tau \left[\tilde{H}_{\text{sb}}(t), \left[\tilde{H}_{\text{sb}}(\tau), \tilde{\rho}_{\text{tot}}(\tau) \right] \right]. \quad (2.7)$$

The equation of motion for the reduced density operator of the system $\tilde{\rho}(t) = \text{tr}_{\text{b}} \tilde{\rho}_{\text{tot}}(t)$ is obtained

by tracing out all bath degrees of freedom,

$$\frac{d}{dt}\tilde{\rho}(t) = -\frac{1}{\hbar^2} \int_{t_0}^t d\tau \operatorname{tr}_b \left[\tilde{H}_{\text{sb}}(t), \left[\tilde{H}_{\text{sb}}(\tau), \tilde{\rho}_{\text{tot}}(\tau) \right] \right]. \quad (2.8)$$

The linear term $-\frac{i}{\hbar} \operatorname{tr}_b[\tilde{H}_{\text{sb}}(t), \tilde{\rho}_{\text{tot}}(t_0)]$ is omitted (without loss of generality) by assuming that the interaction term has a vanishing mean in the initial state.

First, we perform the *Born approximation* assuming that the environment remains unaffected by its coupling to the system. Namely, we assume a large environment so that it thermalizes fast. Thus, the system and the bath are uncorrelated (i.e., no entanglement builds up), $\hat{\rho}_{\text{tot}}(\tau) \approx \hat{\rho}(\tau) \otimes \hat{\rho}_b$, and the bath remains in its thermal equilibrium $\hat{\rho}_b \sim e^{-\beta \hat{H}_b}$ with inverse bath temperature β .

We decompose the operator $\tilde{A}(t)$ of the system-bath interaction [Eq. (2.5)] as

$$\tilde{A}(t) = \sum_{\Omega \in \Delta} e^{i\Omega t} \hat{A}_\Omega, \quad (2.9)$$

where the sum runs over all eigenenergy or quasienergy differences

$$\Delta = \begin{cases} \{E_j - E_i \mid \forall i, j\} & \text{for autonomous Hamiltonian with eigenenergies } E_i \\ \{\varepsilon_j - \varepsilon_i + K\hbar\omega \mid \forall i, j, \forall K \in \mathbb{Z}\} & \text{for Floquet systems with quasienergies } \varepsilon_i. \end{cases} \quad (2.10)$$

The details of this decomposition, i.e., the operators \hat{A}_Ω , are described below for both cases separately. Note that the property $\hat{A}_\Omega = \hat{A}_{-\Omega}^\dagger$ holds since $\tilde{A}(t)$ is Hermitian. With the substitution $s = t - \tau$, Eq. (2.8) simplifies to

$$\frac{d}{dt}\tilde{\rho}(t) = \frac{1}{\hbar^2} \sum_{\Omega, \Omega'} \int_0^{t-t_0} ds G(s) e^{-i\Omega s} e^{i(\Omega - \Omega')t} [\hat{A}_\Omega \tilde{\rho}(t-s) \hat{A}_{\Omega'}^\dagger - \hat{A}_{\Omega'}^\dagger \hat{A}_\Omega \tilde{\rho}(t-s)] + \text{h.c.}, \quad (2.11)$$

where we defined the bath-correlation function

$$G(s) = \operatorname{tr} \hat{\rho}_b \tilde{B}^\dagger(t) \tilde{B}(t-s) = \left\langle \tilde{B}^\dagger(s) \tilde{B}(0) \right\rangle. \quad (2.12)$$

We assume a *Markovian* time-evolution, i.e., a dynamics independent of its history. This is valid on a coarse-grained timescale when bath excitations decay on timescales much smaller than the coarse-grained one. It means that this approximation is allowed when only a small interval of the integral in Eq. (2.11) contributes, i.e., when the bath-correlation function $G(s)$ decays rapidly compared to the timescale on which $\tilde{\rho}(t)$ changes due to the system-bath coupling. This approximation allows us to replace past states with current ones, $\tilde{\rho}(t-s) \rightarrow \tilde{\rho}(t)$, and to extend the upper integration boundary

to infinity, $t_0 \rightarrow -\infty$, in Eq. (2.11). We obtain

$$\frac{d}{dt}\tilde{\rho}(t) = \frac{1}{\hbar^2} \sum_{\Omega, \Omega'} \int_0^\infty ds G(s) e^{-i\Omega s} e^{i(\Omega - \Omega')t} [\hat{A}_\Omega \tilde{\rho}(t) \hat{A}_{\Omega'}^\dagger - \hat{A}_{\Omega'}^\dagger \hat{A}_\Omega \tilde{\rho}(t)] + \text{h.c.} \quad (2.13)$$

The bath-correlation function $G(s)$ contains all the properties of the bath. The one-sided Fourier transformation of the bath-correlation function is given by

$$\int_0^\infty ds e^{-i\Omega s} G(s) = \pi \hbar g(\hbar\Omega) + i\hbar \mathcal{P} \int_{-\infty}^\infty dE \frac{g(E)}{E - \hbar\Omega}, \quad (2.14)$$

with the Fourier-transformed bath-correlation function

$$g(E) = \frac{1}{2\pi\hbar} \int_{-\infty}^\infty ds e^{-iEs/\hbar} G(s), \quad (2.15)$$

and the Cauchy principal value \mathcal{P} . The principal value corresponds to the Lamb shift [108]. We neglect this Lamb shift by assuming that it is small compared to typical eigenenergy or quasienergy splittings. Note that the Lamb shift might change the position of (avoided) crossings with respect to a parameter variation [109]. Since the bath is in thermal equilibrium, the bath-correlation function obeys the Kubo-Martin-Schwinger condition $\langle \tilde{B}^\dagger(t) \tilde{B}(0) \rangle = \langle \tilde{B}(0) \tilde{B}^\dagger(t + i\hbar\beta) \rangle$, which implies

$$g(-E) = e^{\beta E} g(E). \quad (2.16)$$

We assume the bath to be given by an ensemble of harmonic oscillators,

$$\hat{H}_b(t) = \sum_n \left[\frac{\hat{p}_n^2}{2m_n} + \frac{m_n \omega_n^2}{2} \hat{x}_n^2 \right], \quad (2.17)$$

with masses m_n and frequencies ω_n . This bath is coupled to the system via the operator

$$\hat{B} = \sum_n c_n \hat{x}_n. \quad (2.18)$$

In this case, the bath-correlation function reads

$$g(E) = \frac{J(E)}{e^{\beta E} - 1}, \quad (2.19)$$

where the spectral density is given by

$$J(E) = \frac{\pi}{2} \sum_n \frac{c_n^2}{m_n \omega_n} [\delta(E - \hbar\omega_n) - \delta(E + \hbar\omega_n)]. \quad (2.20)$$

We assume an Ohmic bath so that the spectral density is linear, $J(E) \propto E$.

From the Markov approximation, we obtain the Redfield equation,

$$\frac{d}{dt}\tilde{\rho}(t) = \frac{\pi}{\hbar} \sum_{\Omega, \Omega'} g(\hbar\Omega) e^{i(\Omega - \Omega')t} [\hat{A}_\Omega \tilde{\rho}(t) \hat{A}_{\Omega'}^\dagger - \hat{A}_{\Omega'}^\dagger \hat{A}_\Omega \tilde{\rho}(t)] + \text{h.c.} \quad (2.21)$$

In the weak-coupling regime, where the timescales due to the system-bath coupling are much longer than the timescales of the system, a rotating-wave approximation (i.e., a secular approximation) is justified [110]. This approximation requires that the line broadening, which is caused by the coupling to the environment, is much smaller than all (quasi)energy differences of the discrete spectrum. In this case, the contributions of all summands with $\Omega \neq \Omega'$ are negligible (in a time average) due to their fast oscillation. We obtain a master equation of Lindblad form [111],

$$\frac{d}{dt}\tilde{\rho}(t) = \frac{\pi}{\hbar} \sum_{\Omega} g(\hbar\Omega) [2\hat{A}_\Omega \tilde{\rho}(t) \hat{A}_\Omega^\dagger - \hat{A}_\Omega^\dagger \hat{A}_\Omega \tilde{\rho}(t) - \tilde{\rho}(t) \hat{A}_\Omega^\dagger \hat{A}_\Omega]. \quad (2.22)$$

By expressing Eq. (2.22) in the (quasi)energy eigenbasis $\{|n\rangle\}$ (also the Floquet states are time independent in the interaction picture), we obtain the master equation

$$\frac{d}{dt}\tilde{\rho}(t) = \sum_{n,m} R_{nm} \left(\hat{L}_{nm} \tilde{\rho}(t) \hat{L}_{nm}^\dagger - \frac{1}{2} \{ \tilde{\rho}(t), \hat{L}_{nm}^\dagger \hat{L}_{nm} \} \right), \quad (2.23)$$

where $\hat{L}_{nm} = |n\rangle\langle m|$ denote the jump operators and R_{nm} denote the rates, which are given by the Fermi's-golden-rule-type expressions

$$R_{nm} = \frac{2\pi}{\hbar} \sum_{\Omega} |\langle n | \hat{A}_\Omega | m \rangle|^2 g(\hbar\Omega). \quad (2.24)$$

Below, we provide an explicit derivation of the rates, firstly, for autonomous systems and, subsequently, for Floquet systems.

The equation of motion for each diagonal element $p_n(t) = \langle n | \tilde{\rho}(t) | n \rangle$ is given by the Pauli master equation

$$\frac{d}{dt}p_n(t) = \sum_m [R_{nm}p_m(t) - R_{mn}p_n(t)]. \quad (2.25)$$

These diagonal elements are decoupled from all off-diagonal elements of the density operator $\langle n | \tilde{\rho}(t) | m \rangle$. The off-diagonal elements decay exponentially since the first term in Eq. (2.23) contributes to diagonal elements only. Thus the asymptotic state is diagonal and given by the stationary state of the Pauli master equation (2.25).

Let us finally discuss the limits of validity for the approximations made above. The dynamics takes place on various timescales. The system dynamics causes phase oscillations on timescales up to $\tau_s = \max_{i \neq j} \hbar / |\varepsilon_i - \varepsilon_j|$ given by the smallest (quasi)energy difference. The second timescale, the

bath-correlation time τ_c , is the timescale on which bath correlations decay. The larger the bath is, the faster it thermalizes, and the shorter this bath-correlation time τ_c is. The third timescale is the relaxation time Γ^{-1} , which is given by the typical rate Γ at which the state changes due to the system-bath coupling. This rate can be approximated by $\Gamma \approx \tau_C \langle \hat{A}^2 \rangle \langle \hat{B}^2 \rangle / \hbar$. The fourth timescale is the period of the driving $T = 2\pi/\omega$. Both the Born and the Markov approximation are justified when the bath-correlation time is much shorter than the relaxation time, $\tau_C \Gamma \ll 1$ [55]. The (full-)rotating-wave approximation requires that the state changes slowly due to its system-bath coupling compared to typical system times, $T\Gamma < \tau_s \Gamma \ll 1$ [55, 112, 113]. The last condition causes a problem in Floquet systems with infinite-dimensional Hilbert spaces. Due to the infinite number of Floquet states, the quasienergies fill the finite interval $[0, \hbar\omega)$ densely. However, near degeneracies of quasienergies, which are much smaller than the line width due to the coupling to the bath, are not resolved by the dynamics. The steady state is diagonal in the diabatic basis, which is thus appropriate to overcome the problem of near degeneracies [55].

Autonomous systems

In the following, we describe the rates among the eigenstates of a system whose Hamiltonian $\hat{H}(t) = \hat{H}$ is time independent. The coupling operator in the interaction picture reads

$$\tilde{\hat{A}}(t) = \hat{U}_H^\dagger(t) \hat{A} \hat{U}_H(t) = \sum_{nm} |n\rangle \langle m| \langle n|\hat{A}|m\rangle e^{i(E_n - E_m)t/\hbar} \quad (2.26)$$

$$= \sum_{\Omega} \hat{A}_{\Omega} e^{i\Omega t}. \quad (2.27)$$

The sum in the second line runs over all eigenenergy differences Ω given in Eq. (2.10) and the operators \hat{A}_{Ω} are eigenoperators of the Hamiltonian \hat{H} ,

$$\hat{A}_{\Omega} = \sum_{\substack{nm \\ E_n - E_m = \hbar\Omega}} |n\rangle \langle m| \langle n|\hat{A}|m\rangle. \quad (2.28)$$

The rates are obtained by plugging Eq. (2.28) in Eq. (2.24),

$$R_{nm} = \frac{2\pi}{\hbar} |\langle n|\hat{A}|m\rangle|^2 g(E_n - E_m). \quad (2.29)$$

Due to the Kubo-Martin-Schwinger condition (2.16), these rates fulfill the condition

$$\frac{R_{nm}}{R_{mn}} = e^{-\beta(E_n - E_m)}, \quad (2.30)$$

which leads to detailed balance so that the system thermalizes to the Gibbs state, as discussed in Sec. 2.4. However this is only the case for a single heat bath. When several heat baths with different

temperatures are present, the total rates are given by the sum of the individual rates of all baths,

$$R_{nm} = \sum_b R_{nm}^{(b)}. \quad (2.31)$$

These total rates R_{nm} violate condition (2.30) and thus do not describe thermal equilibrium anymore. Note that the rate differences are independent of the temperatures of the baths,

$$R_{nm} - R_{mn} = \frac{2\pi}{\hbar} \sum_b |\langle n | \hat{A}^{(b)} | m \rangle|^2 J(E_n - E_m). \quad (2.32)$$

Floquet systems

We determine the rates in Floquet systems. These rates correspond to the transitions among the time-periodic states $|u_n(t)\rangle$. With the time-evolution operator expressed by the time-periodic states [Eq. (2.2)], the coupling operator in the interaction picture can be written in the form

$$\tilde{\hat{A}}(t) = \hat{U}_H^\dagger(t) \hat{A} \hat{U}_H(t) = \sum_{n,m} |u_n(0)\rangle \langle u_n(t) | \hat{A} | u_m(t) \rangle \langle u_m(0) | e^{i(\varepsilon_n - \varepsilon_m)t/\hbar}. \quad (2.33)$$

With the Fourier series $|u_n(t)\rangle = \sum_{k=-\infty}^{\infty} e^{-ik\omega t} |n, k\rangle$, this equation simplifies to

$$\tilde{\hat{A}}(t) = \sum_{n,m,K} \sum_k |u_n(0)\rangle \langle n, k | \hat{A} | m, k + K \rangle \langle u_m(0) | e^{i(\varepsilon_n - \varepsilon_m - K\hbar\omega)t/\hbar} \quad (2.34)$$

$$= \sum_{n,m,K} e^{i(\varepsilon_n - \varepsilon_m - K\hbar\omega)t/\hbar} A_{nm}(K) |u_n(0)\rangle \langle u_m(0)|, \quad (2.35)$$

where the Fourier coefficients $A_{nm}(K)$ of the matrix elements of the operator \hat{A} are given by

$$A_{nm}(K) = \sum_k \langle n, k | \hat{A} | m, k + K \rangle = \frac{1}{T} \int_0^T dt e^{-iK\omega t} \langle u_n(t) | \hat{A} | u_m(t) \rangle. \quad (2.36)$$

According to Eq. (2.35), the decomposition of Eq. (2.9) is given by the operators

$$\hat{A}_\Omega = \sum_{\substack{n,m,K \\ \varepsilon_n - \varepsilon_m - K\hbar\omega = \hbar\Omega}} A_{nm}(K) |u_n(0)\rangle \langle u_m(0)|. \quad (2.37)$$

Plugging this decomposition into Eq. (2.24), the rates for the Floquet system read

$$R_{nm} = \sum_K R_{nm}^K \quad \text{with} \quad R_{nm}^K = \frac{2\pi}{\hbar} |A_{nm}(K)|^2 g(\varepsilon_n - \varepsilon_m - K\hbar\Omega). \quad (2.38)$$

Here R_{nm}^K denotes the rate for transferring a particle from the time-periodic state $|u_m(t)\rangle$ to state $|u_n(t)\rangle$ while K driving quanta of total energy $K\hbar\omega$ are absorbed (or emitted). These rates generally violate the condition (2.30) so that the steady state is not detail-balanced, as discussed below. Note

that the rate differences are temperature-independent,

$$R_{nm} - R_{mn} = \frac{2\pi}{\hbar} \sum_K |A_{nm}(K)|^2 J(\varepsilon_n - \varepsilon_m - K\hbar\omega). \quad (2.39)$$

2.4. Nonequilibrium steady state

A system which is coupled to an environment relaxes in the asymptotic limit to a steady state. According to the master equation (2.25), the probabilities p_i of the steady state, $\dot{p}_i = 0$, are determined by

$$0 = \sum_j [R_{ij}p_j - R_{ji}p_i]. \quad (2.40)$$

Note that in a Floquet system, this asymptotic state is stationary only in the interaction picture, $\tilde{\rho}(t) = \tilde{\rho}$, while it exhibits the periodic time dependence due to the time-periodicity of the Floquet states in the Schrödinger picture, $\hat{\rho}(t) = \hat{\rho}(t + 2\pi/\omega)$. This steady state is unique when every state i is connected to every other state j by a sequence of quantum jumps with nonzero rates. From now on, we assume positive rates, $R_{ij} > 0 \forall i \neq j$ (the case of vanishing rates will be discussed in Chap. 11).

In equilibrium, the steady state is independent of the details of the bath and the system-bath coupling. Since the rates fulfill condition (2.30), the steady state is given by the Gibbs distribution $p_i \propto \exp(-\beta E_i)$. This equilibrium state is not only in global balance [Eq. (2.40)] but also in detailed balance, where each net flow I_{ij} between the two states i and j [the terms of the r.h.s. of Eq. (2.40)] vanishes individually,

$$0 = R_{ij}p_j(t) - R_{ji}p_i(t) =: I_{ij}. \quad (2.41)$$

Thus, the steady state becomes independent of the system-bath coupling and depends only on the bath temperature $1/\beta$ and the eigenenergies E_i of the system.

This situation is altered under nonequilibrium conditions. Detailed balance is generically broken since the rates violate condition (2.30), e.g., due to the photon-assisted transitions in the Floquet system [Eq. (2.38)]. Immediate consequences of the broken detailed balance are nonzero probability flows I_{ij} between the states. Furthermore, the nonequilibrium steady state depends on the very details of the system, the bath, and the system-bath coupling via the rates R_{ij} . This new freedom can be exploited to engineer desired properties of the steady state.

In contrast to the equilibrium, dissipative Floquet systems do not possess a pure steady state even at zero bath temperature. A zero-temperature bath can only absorb energy. For an autonomous system in contact with such a heat bath, the system energy can decrease only. In consequence, its equilibrium state is the pure ground state. For driven systems, however, the driving can provide energy such that the rates in both directions between two Floquet states are nonzero. Thus the

steady state is generally not a pure state [cf. Fig. 5.3 below].

Under certain conditions, even the steady states of Floquet systems are approximately detail-balanced. Examples are systems where only neighboring states (ordered according to their cycle-averaged energy) couple to each other approximately [51, 52]. Here, the steady state is given by the Boltzmann distribution with an effective temperature and the cycle-averaged energies. Another such situation arises when only a single term significantly contributes to the rates (2.38) so that these rates obey the relation

$$R_{ji}e^{-\beta(\varepsilon_i+\hbar\omega m_i)} = R_{ij}e^{-\beta(\varepsilon_j+\hbar\omega m_j)}, \quad (2.42)$$

where m_i are arbitrary integer numbers [114]. The steady state is given by the Floquet-Gibbs distribution $p_i \propto e^{-\beta(\varepsilon_i+\hbar\omega m_i)}$, fulfills detailed balance, and is independent of the details of the bath. Thus it is similar to the steady state for rates fulfilling condition (2.16).

2.5. Master equation of ideal quantum gases

We generalize the single-particle problem to gases of N indistinguishable, noninteracting particles (see Refs. [57, 58]). Even though we mainly focus on bosons in this thesis, this derivation is done for fermions as well for illustrative purpose and completeness. Throughout the first part in this thesis, the total particle number shall be conserved like in the canonical ensemble so that its value N is fixed by the initial conditions.

Even in the ideal gas, the bath induces only single-particle transition. The many-body Hilbert space is spanned by Fock states enumerated by the occupation numbers of the M single-particle states, $\mathbf{n} = (n_0, n_1, \dots, n_{M-1})$. We generalize the rate equation by replacing single-particle jump operators $\hat{L}_{ij} = |i\rangle\langle j|$ in Eq. (2.23) by their many-particle operators

$$\hat{L}_{ij} = \hat{a}_i^\dagger \hat{a}_j. \quad (2.43)$$

Here \hat{a}_j denotes the annihilation operator of a particle in the single-particle mode j . Starting from a Fock-state \mathbf{n} , this operator transfers a single particle from state j to state i . The final state is $\mathbf{n}_{ji} = (n_0, \dots, n_j - 1, \dots, n_i + 1, \dots)$. The validity of the rotating-wave approximation is, thus, still determined by the single-particle problem. The jump operators [Eq. (2.43)] conserve the particle total number.

As before, the dynamics of the many-body occupation probabilities $p_{\mathbf{n}} = \langle \mathbf{n} | \hat{\rho} | \mathbf{n} \rangle$ decouples from the off-diagonal elements, which decay over time. The corresponding equation of motion, (derived in Appendix A) reads

$$\dot{p}_{\mathbf{n}}(t) = \sum_{ij} (1 + \sigma n_i) n_j [R_{ij} p_{\mathbf{n}_{ij}}(t) - R_{ij} p_{\mathbf{n}}(t)]. \quad (2.44)$$

This is the generalization of the Pauli master equation (2.25). The many-body transition rate $R_{\mathbf{n}_{ij}, \mathbf{n}} = n_j(1 + \sigma n_i)R_{ij}$ depends on the quantum statistics via the choice of σ , with $\sigma = 1$ for bosons (reflecting the stimulated process by the bosonic enhancement of transitions into occupied states) and $\sigma = -1$ for fermions (reflecting the Pauli exclusion principle). The classical case of distinguishable (Boltzmann) particles corresponds to $\sigma = 0$; here the transition rates are independent of the occupation of the final state.

We will focus entirely on the steady state $\dot{p}_{\mathbf{n}}(t) = 0$ of the ideal quantum gas determined by

$$0 = \sum_{ij} (1 + \sigma n_i) n_j [R_{ij} p_{\mathbf{n}_{ij}}(t) - R_{ij} p_{\mathbf{n}}(t)]. \quad (2.45)$$

2.6. Monte-Carlo simulations

The many-particle rate equation (2.44) becomes numerically intractable even for moderate particle numbers N and system sizes M . Before we discuss several approximations, we sketch a quasiexact quantum-jump Monte-Carlo method [115, 116]. This simulation allows for calculating expectation values of simple operators up to a desired uncertainty and is described in Refs. [57, 58].

The dissipation is caused by sudden particle jumps from one single-particle eigenstate (or Floquet state) to another one. These processes are given by the jump operators [Eq. (2.43)]. We encounter the convenient situation that all occupation numbers are conserved by the evolution generated by the system Hamiltonian since the particles are noninteracting. Therefore, the time evolution is exhausted by taking into account quantum jumps. The dynamics corresponds to a random walk in the classical space spanned by the Fock states $|\mathbf{n}\rangle$ (and not their superpositions). The Monte-Carlo wave function $|\mathbf{n}(t)\rangle$ jumps between Fock states $|\mathbf{n}_k\rangle$, where it resides for time intervals of length t_k ,

$$|\mathbf{n}(t)\rangle = |\mathbf{n}_k\rangle, \text{ where } k \text{ is such that } T_{k-1} \leq t < T_k \quad (2.46)$$

with $T_k = \sum_{l=1}^k t_l$.

We use the Gillespie algorithm [117] in order to compute the time evolution. Initially, the system is prepared according to a given density operator. Then, the algorithm alternates between the following two steps: First, the time interval t_k , which determines how long the system remains in the current state, is randomly drawn from an exponential distribution $P(t_k) \propto \exp(-t_k/\bar{t}(\mathbf{n}_k))$ with mean dwell time

$$\bar{t}(\mathbf{n}_k) = \frac{1}{\sum_{i,j} R_{ij}(1 + \sigma n_i) n_j}. \quad (2.47)$$

Second, a single-particle transition $i \rightarrow j$ is randomly drawn with probabilities proportional to the many-particle rates, $P(i, j) \propto R_{ji}(1 + \sigma n_j) n_i$ and the new state \mathbf{n}_{k+1} is obtained from the current state \mathbf{n}_k by transferring a particle from state i to state j . These two steps are repeated until the

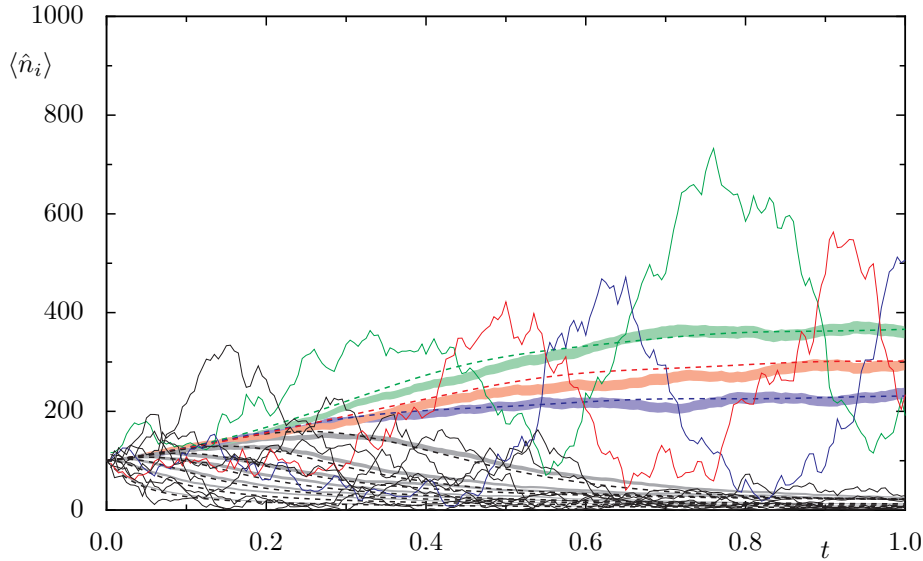


Figure 2.2.: Time evolution of the mean occupation numbers $\langle \hat{n}_i \rangle$ in a driven quartic oscillator computed by Monte-Carlo simulations. The system and its parameters are the same as in Figs. 1.1 and 3.5 including the same color code of the states. A single Monte-Carlo wave function (solid lines) exhibits strong fluctuations. Furthermore, a cyclic behavior is visible, namely maxima are reached in a red-blue-green cycle. The ensemble average of 300 Monte-Carlo wave functions (shaded areas correspond to single standard deviation) shows the relaxation to the steady state. For comparison, the mean-field results are also shown (dashed lines), which are discussed below.

time $T_k = \sum_{l=1}^k t_l$ reaches the desired evolution time T .

From an ensemble of L Monte-Carlo wave functions $|\mathbf{n}^{(\alpha)}(t)\rangle$ labeled by $\alpha \in \{1, 2, \dots, L\}$, the expectation value of an observable \hat{o} is computed via

$$\langle \hat{o} \rangle_{\text{ensemble}}(t) = \frac{1}{L} \sum_{\alpha=1}^L \langle \mathbf{n}^{(\alpha)}(t) | \hat{o} | \mathbf{n}^{(\alpha)}(t) \rangle. \quad (2.48)$$

Figure 2.2 shows the time evolution of the mean occupations $\langle \hat{n}_i \rangle(t)$ for $N = 1000$ particles in a time-periodically driven quartic trap for a single Monte-Carlo wave function (solid lines) and for an ensemble of $L = 300$ Monte-Carlo wave functions (shaded areas). The occupations of a single Monte-Carlo wave function fluctuate strongly. We can observe that their ensemble average relaxes to the steady state. The mean-field theory (dashed lines), which will be described in Chap. 6, predicts the mean occupations of the ensemble average well.

When computing steady-state expectation values $\langle \hat{o} \rangle$, the effect of temporal fluctuations is reduced by combining ensemble averaging with time averaging,

$$\langle \hat{o} \rangle = \frac{1}{LT} \sum_{\alpha=1}^L \sum_k t_k \langle \mathbf{n}_k^{(\alpha)} | \hat{o} | \mathbf{n}_k^{(\alpha)} \rangle. \quad (2.49)$$

It is useful to exclude the transient relaxation process for $t < t_r$ from the time average by constraining the inner sum to $k > k_r^{(\alpha)}$ with $k_r^{(\alpha)}$ such that $T_{k_r^{(\alpha)}} > t_r$. Here, we disregard the first half of the time evolution, $t_r = T/2$. Furthermore, we require that the relaxation time t_r is sufficiently long such that

$$\frac{|\langle \hat{n}_i \rangle_{\text{mf}}(t_r) - \langle \hat{n}_i \rangle_{\text{mf}}|}{\langle \hat{n}_i \rangle_{\text{mf}}} < \varepsilon \quad \forall i, \quad (2.50)$$

where ε denotes the error due to nonperfect relaxation for which we use $\varepsilon = 0.03$ and $\langle \hat{n}_i \rangle_{\text{mf}}(t)$ ($\langle \hat{n}_i \rangle_{\text{mf}}$) denote the mean occupations obtained by the mean-field method [Chap. 6] at time t (in the steady state), respectively. We determine the uncertainties according to the Gelman-Rubin criterion [118], generally setting the relative uncertainty of each state below three percent (barely noticeable in any figure showing steady-state properties). For a bosonic system, this allows us to access particle numbers up to $N \sim 10^5$ for $M \sim 100$ single-particle states.

3. Model systems

We introduce several model systems to illustrate our findings: two versions of tight-binding chains in contact with their environment [57, 58], a quartic driven oscillator [57], and a more abstract model where all rates are chosen randomly [57, 58].

The tight-binding chains and the quartic oscillator are motivated by systems, where a gas of cold atoms is trapped in an optical potential. In many situations, such gases are well isolated so that particle losses are negligible. However, due to their good isolation, the heat bath must be realized artificially. An example is a Bose-Einstein condensate of trapped atoms of a different specie where the system is immersed [32, 33, 119]. This forms a reservoir of Bogoliubov phonons. Generating an optical lattice by a standing-wave pattern is a standard technique for these systems [99]. In the first model, the chain is in contact with two heat baths at different temperatures [compare to Fig. 2.1(b)]. The second model is a chain subjected to a time-periodic force coupled to a single heat bath [compare to Fig. 2.1(a)].

3.1. Tight-binding chain in contact with two heat baths

We discuss a tight-binding chain in contact with two heat baths at different temperatures. Such a configuration where these baths are coupled to the first and the next-to-last site is shown in Fig. 3.1.

The particles in the chain tunnel from one site to neighboring sites. The system Hamiltonian reads

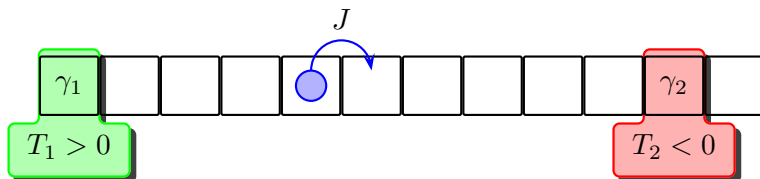


Figure 3.1.: A gas in a lattice is coupled to two heat baths. A tight-binding chain with tunneling strength J is locally coupled to two heat baths. The first bath with temperature T_1 is coupled at the leftmost site with coupling strength γ_1 and the second bath with temperature T_2 is coupled at the next-to-last site with coupling strength γ_2 . We focus on a situation where the second bath is population-inverted and described by a “negative” temperature $T_2 < 0$.

$$\hat{H} = -J \sum_{\ell=1}^{M-1} \left(\hat{c}_{\ell}^{\dagger} \hat{c}_{\ell+1} + \text{h.c.} \right), \quad (3.1)$$

where $J > 0$ denotes the tunneling strength, M the number of sites, and \hat{c}_{ℓ} (\hat{c}_{ℓ}^{\dagger}) the annihilation (creation) operator for a particle at the site ℓ , respectively. All eigenstates $|n\rangle$ with $n \in \{0, 1, 2, \dots, M-1\}$ are delocalized and the wave functions have the spatial form $\langle \ell | n \rangle = \sqrt{2/(M+1)} \sin(k_n \ell)$ with the wave numbers $k_n = (n+1)\pi/(M+1)$. The dispersion relation is $E_n = E(k_n) = -2J \cos(k_n)$. In order to obtain dimensionless quantities, we measure all energies in units of the tunneling strength J .

The system is coupled to two heat baths, one at the first site $s_1 = 1$ and another one at the next-to-last site $s_2 = M-1$. The temperature and coupling strength are T_1 (T_2) and γ_1 (γ_2) for the first (second) bath, respectively. The contact with each heat bath is modeled via the local system-bath interaction

$$\hat{H}_{\text{sb}} = \gamma_b \hat{c}_{s_b}^{\dagger} \hat{c}_{s_b} \otimes \hat{B}, \quad (3.2)$$

where \hat{B} is the operator acting in the Hilbert space of the bath [Eq. (2.18)]. The total rates consist of the contribution from both the left and the right bath, $R_{nm} = R_{nm}^{(1)} + R_{nm}^{(2)}$. These rates read

$$R_{nm}^b = \frac{2\pi\gamma_b^2}{\hbar} \frac{2}{M+1} \sin^2(k_n s_b) \sin^2(k_m s_b) g(E_n - E_m), \quad (3.3)$$

and are shown in Fig. 3.2.

Even though the system is already driven away from equilibrium when $T_1 \neq T_2$, we also investigate the scenario where the second heat bath is population-inverted. Some nonequilibrium effects are only

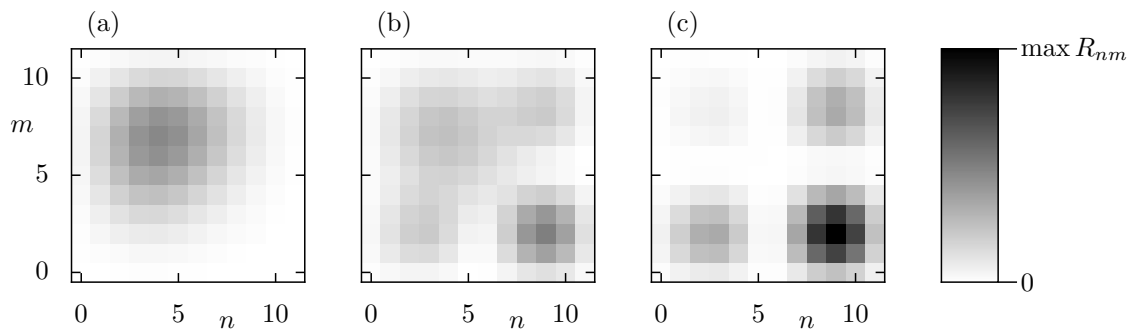


Figure 3.2.: Rates in the tight-binding chain coupled to two heat baths. The matrix of rates R_{nm} for the single-particle transition from state m to state n in a chain with $M = 12$ sites is shown as grayscale plot. While panel (a) shows the rates $R_{nm}^{(1)}$ induced by the left bath at temperature $T_1 = J$ coupled to the leftmost site, and panel (c) shows the rates $R_{nm}^{(2)}$ induced by the right bath at temperature $T_2 = -J$ coupled to the next-to-last site. The panel (b) shows the total rates $R_{nm} = (R_{nm}^{(1)} + R_{nm}^{(2)})/2$ where both baths are coupled to the system with equal strength, $\gamma_1 = \gamma_2$.

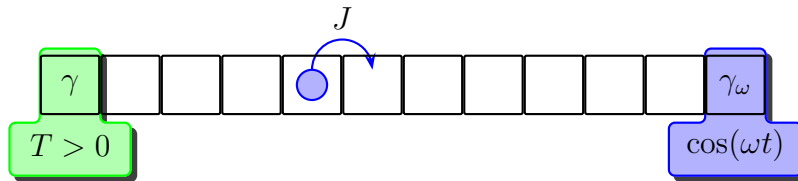


Figure 3.3.: Time-periodically driven tight-binding chain in contact with a heat bath. This tight-binding chain with neighbor tunneling strength J is driven time-periodically with angular frequency ω and driving strength γ_ω at the rightmost site. Furthermore the chain is coupled to a heat bath with temperature T at the leftmost site with coupling strength γ .

present in this case. We describe the population inversion by a negative temperature $T_2 < 0$. Such a negative temperature can be defined in systems with bounded spectra [120]. It has recently been realized for atoms in an optical lattice [104]. Another approach is to transfer a condensate to the top of the dispersion relation of a bounded spectrum via a quasimomentum kick. We use the term “negative” temperature despite a recent controversy [121–123].

3.2. Time-periodically driven tight-binding in contact with a heat bath

The second model is a time-periodically driven tight-binding chain in contact with single a heat bath as sketched in Fig. 3.3. The time-periodic Hamiltonian of the system reads

$$\hat{H}(t) = -J \sum_{\ell=1}^{M-1} \left(\hat{c}_\ell^\dagger \hat{c}_{\ell+1} + \text{h.c.} \right) + \gamma_\omega J \cos(\omega t) \hat{c}_M^\dagger \hat{c}_M. \quad (3.4)$$

In addition to Eq. (3.1), ω denotes the angular frequency of the driving and γ_ω the dimensionless driving strength. The driving is realized by a periodic modulation of the on-site energy at the rightmost site.

A single heat bath is coupled to the first site as before [Eq. (3.2)]. The rates are given by Eq. (2.38) and are obtained from numerically computing the Floquet states. Figure 3.4 shows these rates for an example system, which we will use in the following. While the driving strength γ_ω determines the Floquet modes and thus the rates R_{nm} and the asymptotic state, the coupling strength γ of the heat bath determines only the relaxation rate towards the asymptotic state ¹.

3.3. Driven quartic oscillator

Another illustrative model is a gas trapped in a quartic potential [124] or a quartic double well, subjected to a time-periodic force, and coupled to a thermal environment. The single-particle case of

¹As long as the coupling is still weak.

such quartic oscillators was discussed in Ref. [109] and that of a double well in Refs. [56, 112, 125]. Here we introduce this Floquet system and discuss its single-particle rate matrix. The single-particle results are mentioned only briefly.

The Hamiltonian of a time-periodically-driven quartic oscillator reads

$$\hat{H}(t) = \frac{\hat{p}^2}{2m} + \alpha \hat{x}^4 + \gamma_\omega \hat{x} \cos(\omega t). \quad (3.5)$$

Based on the mass m , the coefficient α , and the reduced Planck constant \hbar , we introduce the units for length x_0 , momentum p_0 , energy V_0 , and time t_0 by

$$x_0 = \sqrt[6]{\frac{\hbar^2}{m\alpha}}, \quad p_0 = \frac{\hbar}{x_0}, \quad V_0 = \frac{\hbar^2}{mx_0^2}, \quad t_0 = \frac{mx_0^2}{\hbar}. \quad (3.6)$$

By switching to the dimensionless quantities $\hat{x}/x_0 \rightarrow \hat{x}$, $\hat{p}/p_0 \rightarrow \hat{p}$, $\hat{H}/V_0 \rightarrow \hat{H}$, $t/t_0 \rightarrow t$, $\omega t_0 \rightarrow \omega$, and $\gamma_\omega x_0/V_0 \rightarrow \gamma_\omega$, the Hamiltonian reads

$$\hat{H}(t) = \frac{\hat{p}^2}{2} + \hat{x}^4 + \gamma_\omega \hat{x} \cos(\omega t) \quad (3.7)$$

and the (dimensionless) Schrödinger equation is

$$\frac{d}{dt}\varphi(x, t) = -i\hat{H}\varphi(x, t). \quad (3.8)$$

Thus the (undriven) quartic oscillator, for which $\gamma_\omega = 0$, has no free parameters. The splittings among nearest eigenenergies of its spectrum increase with the energy monotonically. The smallest splittings are

$$E_1 - E_0 = 1.73, \quad E_2 - E_1 = 2.30, \quad \text{and} \quad E_3 - E_2 = 2.63. \quad (3.9)$$

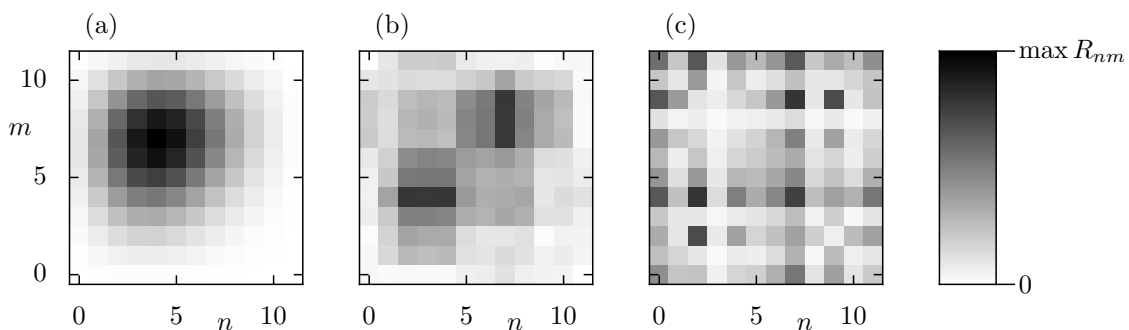


Figure 3.4.: Rates in the time-periodically driven tight-binding chain coupled to a single bath. The matrix of rates R_{nm} for the single-particle transition from Floquet state m to state n (ordered according to their cycle-averaged energy) in a chain with $M = 12$ sites is shown as grayscale plot. The driving strength increases from left to right by (a) $\gamma_\omega = 0$, (b) $\gamma_\omega = 1.5$, and (c) $\gamma_\omega = 3$. Note that panel (a) is the same situation as in Fig. 3.3(a).

The driven quartic oscillator, $\gamma_\omega > 0$, is characterized by the two (dimensionless) parameters of driving strength γ_ω and angular frequency ω . The Floquet states, which are solutions of the time-dependent Schrödinger equation, are obtained using the (t, t') -technique [126, 127].

The semiclassical eigenfunction hypothesis [128–130] states that almost all states can be classified as either regular or chaotic in the semiclassical limit. This distinction also manifests itself in the Husimi representations, quasiprobability phase-space distributions, of the states [131]. The insets in Fig. 3.5(b) show typical chaotic and regular Floquet states. The chaotic states live in the same phase space region (which is in Fig. 3.5(b) in the center). All states with larger cycle-averaged energy are regular and localize on the regular tori of that system which is the classical counterpart. The semiclassical limit (where Planck's constant is small compared to typical actions in the system, $\hbar \rightarrow 0$) corresponds to strong driving limit since the switching to dimensionless reads $\frac{\sqrt{\alpha}}{\hbar\sqrt{m}}\gamma_\omega \rightarrow \gamma_\omega$. For weak driving, this classification becomes less sharp as shown in the insets of Fig. 3.5(a), which corresponds to the example situation discussed in the introduction [Fig. 1.1]. This hierarchy of the Floquet states given by semiclassical theory also affects the steady-state properties of the quantum gas, as discussed in the following.

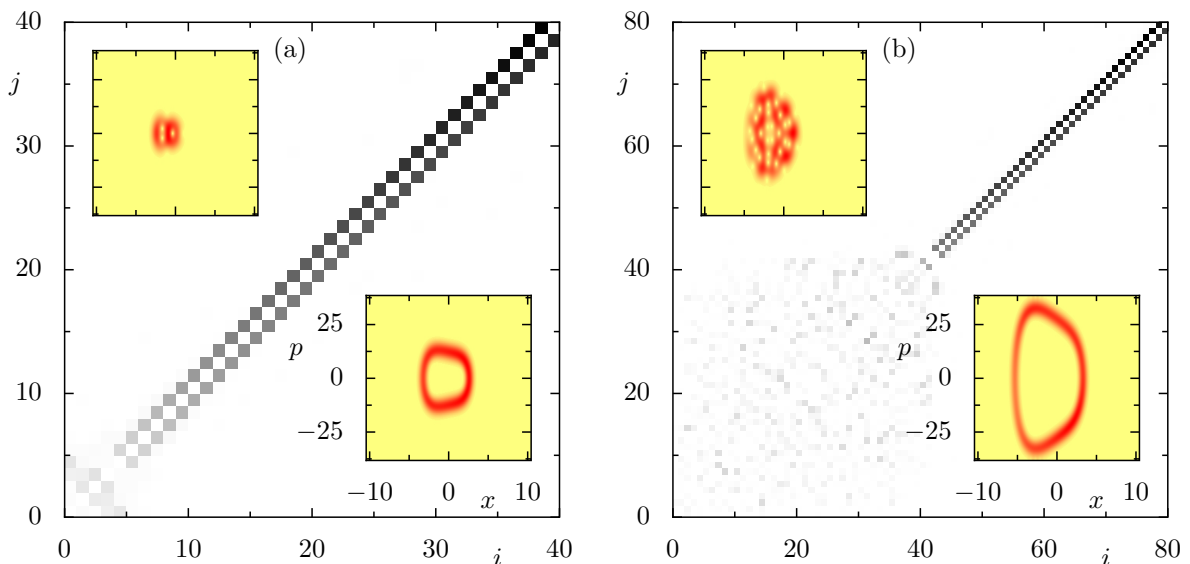


Figure 3.5.: Rates among the Floquet states of the driven quartic oscillator. The rates R_{ij} among the Floquet states ordered according to their cycle-averaged energy, Eq. (2.3), are shown [from white (zero rates) to black (maximal shown rate)]. The driving is either (a) weak ($\gamma_\omega = 8$) and or (b) strong ($\gamma_\omega = 70$). For each case, the Husimi distributions (quasiprobability phase-space distributions) of two exemplary Floquet states are shown as insets, a chaotic state (top-left) and a regular state (bottom-right) [from yellow (zero quasiprobability) to red (maximal quasiprobability)]. Since the driving angular frequency $\omega = 2.2$ is close to the lowest energy splittings of the undriven quartic oscillator ($E_1 - E_0 < \hbar\omega < E_2 - E_1$), the eigenstates of the undriven system with smallest energy get affected first by the driving. As a result, these states become chaotic first. The rates among these chaotic states show a typical all-to-all coupling [especially in panel (b)]. In contrast, the rates among regular states are approximately of nearest-neighbor type. The inverse temperature is $\beta = 0.025$. The exemplary Floquet states are (a) 3 (chaotic) and 20 (regular); (b) 10 (chaotic) and 70 (regular). The snapshots were taken at the moment when the trap reaches its maximum tilt to the left, i.e., $t = 0$.

Coupling the quartic oscillator to a thermal environment causes transitions among the Floquet states. The coupling to the thermal bath with temperature $1/\beta$ (measured in the energy V_0), shall be given by the coupling operator [cf. Eq. (2.5)]

$$\hat{A} = \hat{x}. \quad (3.10)$$

The single-particle rates [Eq. (2.38)] in the driven quartic oscillator, shown in Fig. 3.5, exhibit typical signatures of its semiclassical classification [51, 52]. While the chaotic states couple to almost all other chaotic states with random-like rates, the regular states approximately couple only to their nearest neighbor states. Only the innermost regular tori couple to the chaotic states. This hierarchy has immediate consequences on the probability distribution of the nonequilibrium steady state for a single-particle system: the chaotic states have roughly the same occupation probability while the regular states approximately obey the Boltzmann distribution with an effective temperature [51, 52].

3.4. Random-rate matrix

Other models are systems of M single-particle states with transition rates R_{ij} drawn randomly. With the help of this model, we validate generic properties of the asymptotic state not relying on specific properties of the considered system. The rates are given by independent and identically distributed random rates, which are drawn from an exponential distribution

$$P(R_{ji}) = \lambda^{-1} \exp(-\lambda R_{ji}). \quad (3.11)$$

The parameter λ controls the timescale of the relaxation but does not influence the steady state. The diagonal elements R_{ii} can be set to zero as they drop out of all relevant equations [such as Eq. (2.44)]. This choice of rates clearly models a nonequilibrium situation since condition (2.16) implying detailed balance is violated almost surely. It is motivated by the rates computed for a fully chaotic time-periodically-driven quantum system coupled to a heat bath [109]. A concrete example is given by the kicked rotor coupled to a bath whose steady states are discussed for the single-particle case in Ref. [52] and for the many-particle case in the supplemental material of our Ref. [57].

4. Equilibrium Bose condensation

Before investigating the nonequilibrium steady states of Bose gases, let us first recall fundamental properties of equilibrium states and Bose-Einstein condensation.

The equilibrium state depends on a few thermodynamic properties only. Under equilibrium conditions, the stationary state (2.40) exhibits detailed balance [Eq. (2.41)]. The latter one implies the Gibbs distribution. Thus the steady state depends on the eigenenergies E_i of the system and the temperature of the bath only and is, in particular, independent of all other details of the bath or the system-bath coupling. We are interested in the canonical ensemble of an ideal Bose gas. Approximating its mean occupation numbers (but not its occupation number fluctuations) by the ones of the grand canonical ensemble is exact in the thermodynamic limit according to the equivalence of ensembles. The occupations of the grand canonical Bose gas obey the Bose-Einstein distribution

$$\langle \hat{n}_i \rangle = \frac{1}{e^{\beta(E_i - \mu)} - 1}, \quad (4.1)$$

where $\mu = \mu(\beta, \langle \hat{N} \rangle)$ is the chemical potential, which is determined implicitly by the total particle number $\langle \hat{N} \rangle$.

Bose condensation forms when the total particle number exceeds a critical value. When the total particle number is increased (while keeping the temperature and system size fixed), also the chemical potential increases until it approaches the ground-state energy, $E_0 - \mu \ll E_1 - E_0$. This causes a saturation of the mean occupations of all excited states,

$$\langle \hat{n}_i \rangle \simeq \frac{1}{e^{\beta(E_i - E_0)} - 1}, \quad \forall i \geq 1. \quad (4.2)$$

Consequently, all the remaining particles occupy the single-particle ground state,

$$\langle \hat{n}_0 \rangle \approx N - \sum_{i \geq 1} \langle \hat{n}_i \rangle, \quad (4.3)$$

where the second term on the right-hand side is the depletion. This is illustrated for a quartic oscillator in thermal equilibrium in Fig. 1.1(a) [see also a tight-binding chain in Fig. 5.2(a) below]. This transition with respect to the particle number N (instead of temperature T) was discussed in the original work by Einstein [4].

In a finite system, Bose-Einstein condensation is a crossover [18]. This crossover occurs when the

total particle number N becomes comparable to the characteristic value N^* which is given by

$$N^* = \sum_{i \geq 1} \frac{1}{e^{\beta(E_i - E_0)} - 1}. \quad (4.4)$$

This value N^* corresponds to the depletion in the condensed regime, Eq. (4.3). In the thermodynamic limit, where the particle number N and volume V is increased to infinity under fixed particle density $n = N/V$, Bose condensation is a sharp second-order phase transition. Above the (critical) particle density n^* , the ground-state occupation becomes macroscopic, i.e., the relative occupation N_0/N is nonzero, while the occupations of all other states remain subextensive.

However, Bose condensation does not necessarily survive the thermodynamic limit [18]. For a homogeneous Bose gas of spatial dimensionality $D \leq 2$, the ratio N^*/V diverges in the thermodynamic limit due to large occupations of low-energy states, so that no phase transition exists. In this case, Bose condensation can still be observed as a crossover in systems of finite size. This is the case in the examples shown in Fig. 1.1(a) for a trapped gas [and Fig. 5.2(a) for bosons in a chain of finite extent]. One can observe a (relatively sharp) crossover: For $N > N^*$, the occupation of each excited state saturates so that all newly added particles join the condensate in the ground state.

According to the Penrose-Onsager criterion [132], the Bose-Einstein condensation is defined by a macroscopic eigenvalue of the single-particle density matrix, while all other eigenvalues remain subextensive (even though the corresponding eigenstate might not be the single-particle ground state). This concept has been extended to fragmented condensation where several condensates coexist, defined by several macroscopic eigenvalues [133]. This effect has also been termed generalized Bose-Einstein condensation [134]. One example is given by the coexistence of condensates in a degenerate ground state. This effect is unstable against slightly lifted degeneracy or smallest repulsive interactions. In the latter case, the system favors to spontaneously choose a single condensate to minimize the energy cost due to the interactions [133].

5. Bose selection

Does Bose-Einstein condensation, the macroscopic occupation in the ground state, survive in Floquet systems, where the meaning of a ground state is lost? We answer this question for general nonequilibrium steady states in this chapter with the help of numerical observations. We find that the Bose-Einstein condensation for ideal quantum gases survives far from equilibrium in a generalized form: the unambiguous *selection* of multiple states. Each selected state acquires a large occupation. In clear distinction, the occupation of any other state saturates in the limit of large total particle numbers. Furthermore, we observe that the set of selected states is independent of the bath temperature(s). We have published these findings together with their analytical explanation [see Chap. 7] in Refs. [57, 58].

Figure 5.1 shows the selection of multiple states, which is the generalization of Bose condensation

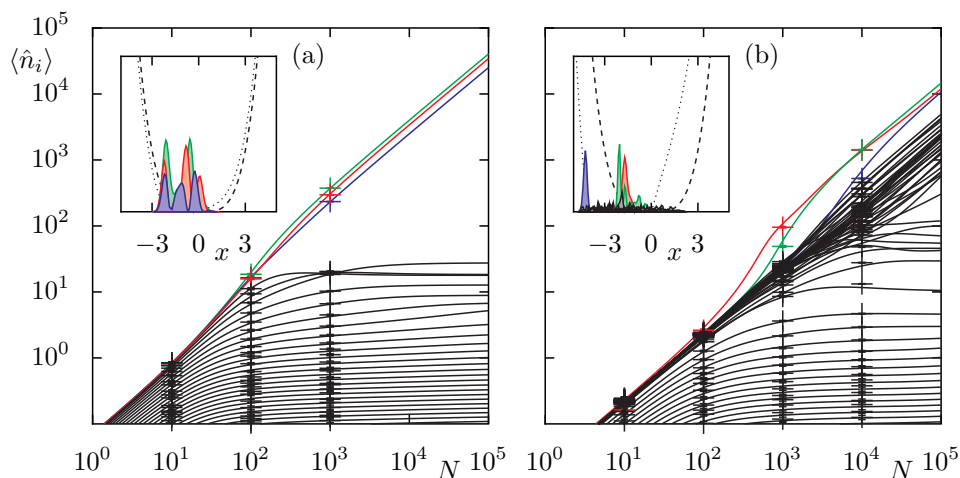


Figure 5.1.: Bose selection in quartic oscillators. The dependence of the mean occupation numbers $\langle \hat{n}_i \rangle$ on the total particle number N in a time-periodically driven quartic oscillator coupled to a heat bath for (a) weak and (b) strong driving strength are shown. The number of selected states drastically changes from three in panel (a) to 27 in panel (b). The insets show the condensate densities (shaded areas) in the asymptotic limit, $\lim_{N \rightarrow \infty} \langle \hat{n}_i \rangle |\varphi_i(x)|^2 / N$, and the quartic trap (the dashed line shows time-averaged potential, the dotted line shows the maximal tilted trap, which corresponds to the moment when the snapshot of the condensate densities was taken, i.e., $t = 0$). In panel (a), the driving strength is $\gamma_\omega = 8$ and the frequency is $\omega = 2.2$ while in panel (b) $\gamma_\omega = 70$ and $\omega = 2.0$. The energy quantum $\hbar\omega$ is of the order of the energy splitting between the first excited state and the ground state of the undriven quartic oscillator. The inverse bath temperature is $\beta = 0.025$ in both panels. The results were obtained by the mean-field method (solid lines) and Monte-Carlo simulations (crosses with error bar denoting the standard deviation).

far from equilibrium. This figure shows the mean occupation numbers $\langle \hat{n}_i \rangle$ of the Floquet states $|u_i(t)\rangle$ depending on the total particle number N for driven quartic oscillators. In the limit of large particle numbers, a group of states acquires almost all particles and the occupation of each state in this group grows proportionally to the particle number N . In contrast, the occupation of any other state saturates and remain small. In the following, we will call the first group “*Bose-selected states*” and all other states “*nonselected states*”. The phenomenon *Bose selection* refers to the case of several Bose-selected states (otherwise, it is explicitly mentioned that only a single state is Bose-selected). This observation of Bose selection is the starting point for many further investigations.

Bose selection also occurs in tight-binding chains as shown in Fig. 5.2(c, d). While panel (c) shows a Floquet system coupled to a single heat bath, panel (d) depicts a nonequilibrium situation caused by two heat baths where one is population-inverted. Apart from the quantitative differences, the phenomenon of Bose selection is generic since both different scenarios share the same qualitative behavior.

We can distinguish three regimes with respect to the particle numbers N in Fig. 5.2(c, d): First, a *classical* regime, where all occupations $\langle \hat{n}_i \rangle$ increase proportionally to the total particle number N , i.e., the relative occupations $\langle \hat{n}_i \rangle / N$ are constant and equal to the occupation probabilities of the single-particle case p_i . Since the occupations $\langle \hat{n}_i \rangle$ are below unity, the particles behave classically. Second, in the *degenerate* regime, some occupations are of the order of unity, $\langle \hat{n}_i \rangle \gtrsim 1$, and deviations from the linear increase emerge since quantum degeneracy becomes relevant. Some states benefit more from the bosonic enhancement than others. For even larger fillings, $N \gg N^*$, the system is in the *ultra-degenerate* regime, where some states are Bose-selected and acquire a large occupation.

Driving the system out of equilibrium is necessary but not sufficient to observe the Bose selection of several states. Figure 5.2(a) shows the (ground-state) Bose condensation of an undriven tight-binding chain in thermal equilibrium. Also under the nonequilibrium condition where the chain is coupled to two baths with different positive temperatures, we find Bose condensation, as shown in Fig. 5.2(b). Chapter 7 provides a necessary and sufficient condition for Bose selection (of multiple states).

Already by the presented examples, we can infer statements on how many states are Bose-selected. Firstly, one can notice that few states as well as many states can be Bose-selected. In the quartic oscillator [Fig. 5.1(a)] and in the tight-binding chains coupled to two heat baths [Fig. 5.2(c)], three states are selected. For the quartic oscillator, this means that for arbitrary shallow traps (small α) three selected states are possible when the driving frequency ω and the driving strength γ_ω are chosen accordingly [cf. Eqs. (3.6)]. In the case of the chain, the number of selected state remains three for arbitrary long chains with size $M > 5$ [not shown]. However, the number of selected states can also be large as shown in the strongly-driven quartic oscillator in Fig. 5.1(b), where 27 states are Bose-selected. The number of selected states is always found to be odd [not explicitly shown here but in Chap. 7]. Indeed, we find neither two nor any other even number of Bose-selected states when the rates are not explicitly fine-tuned.

The Bose selection may cause fragmented condensation. Fragmented condensation is defined as

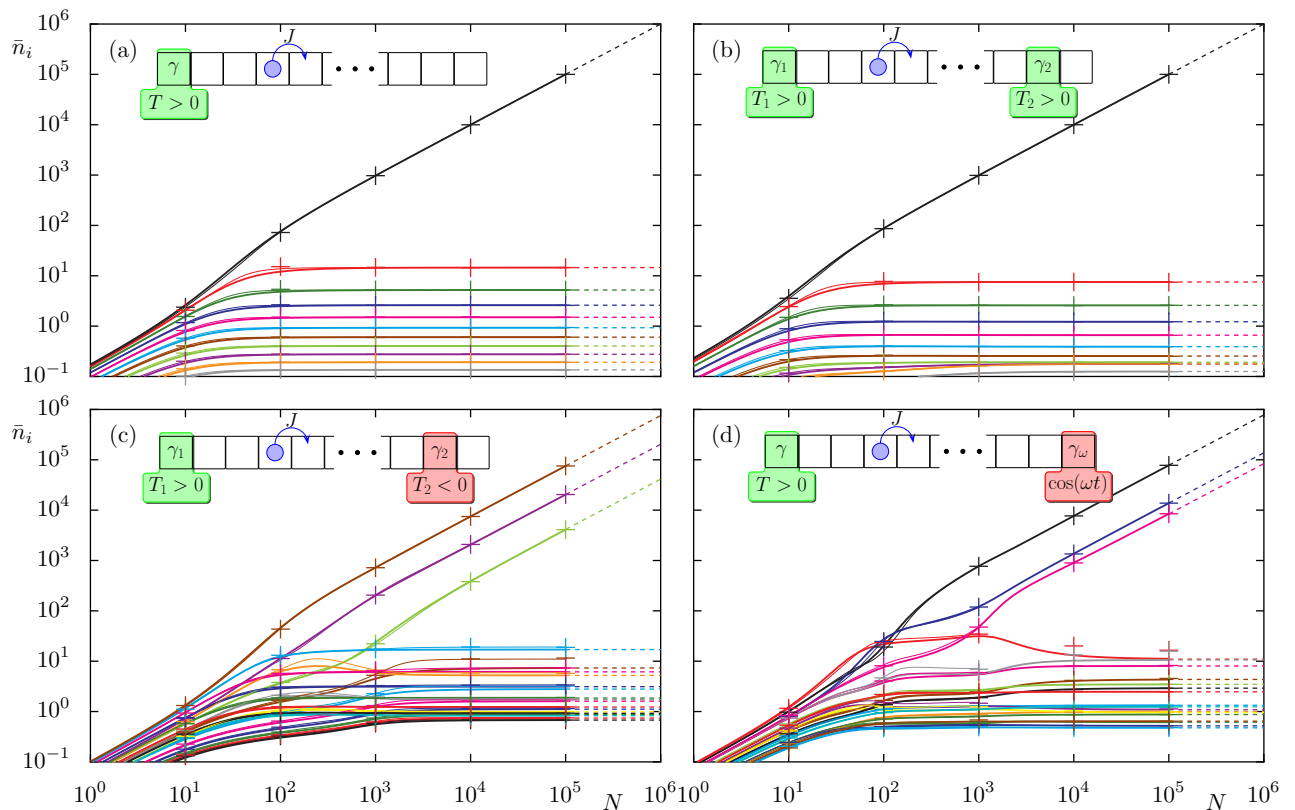


Figure 5.2.: Bose selection and Bose condensation in a tight-binding chain in equilibrium (a) and driven away from equilibrium in various ways (b-d). The dependence of the mean occupation numbers $\bar{n}_i = \langle \hat{n}_i \rangle$ on the total number of bosons N are shown in the (non)equilibrium steady state for chains of length $M = 20$. The mean occupations are obtained from the exact Monte-Carlo simulations (crosses). Furthermore the results from mean-field theory (thick solid lines), asymptotic mean-field theory (dashed lines), augmented mean-field theory (thin solid lines) [see Chap. 9] are shown. (a) Equilibrium steady state, where the chain is coupled to a single bath with temperature $T_1 = J$. (b-c) Nonequilibrium situation, where the chain is driven away from equilibrium. In (b) the system is coupled to two heat baths of different positive-temperature ($T_1 = J$ and $T_2 = J/2$), coupled to the first and the next-to-last site with $\gamma_1 = \gamma_2$. (c) Same as in (b), but with population inversion in the second heat bath, described by the negative temperature $T_2 = -J$. The color code is the same as in panels (a) and (b), where the occupations decrease with increasing energy. (d) The chain is subjected to a periodic potential modulation at the last site with amplitude $\gamma_\omega = 2.3$ and frequency $\hbar\omega = 1.5J$. The Floquet states are colored like the stationary states (a-c) from which they evolve adiabatically when the driving is switched on [see Fig. 10.2]. (This Figure was taken from Ref. [58])

several macroscopic eigenvalues of the single-particle density matrix in the thermodynamic regime, according to the Penrose-Onsager criterion [132]. In the discussed one-dimensional systems, however, no true phase transitions occur since the critical density diverges in the thermodynamic limit. Here, we observe not a phase transition but a finite-size crossover only.

The temperature $1/\beta$ affects neither the set of selected states nor their occupations in the ultra-degenerate regime. The temperature dependence of the steady states is shown in Fig. 5.3. The set of Bose-selected states is independent of temperature.¹ Even the occupations of the selected states

¹This is not true for the preasymptotic state occurring at intermediate particle numbers, which is discussed in Chap. 11.

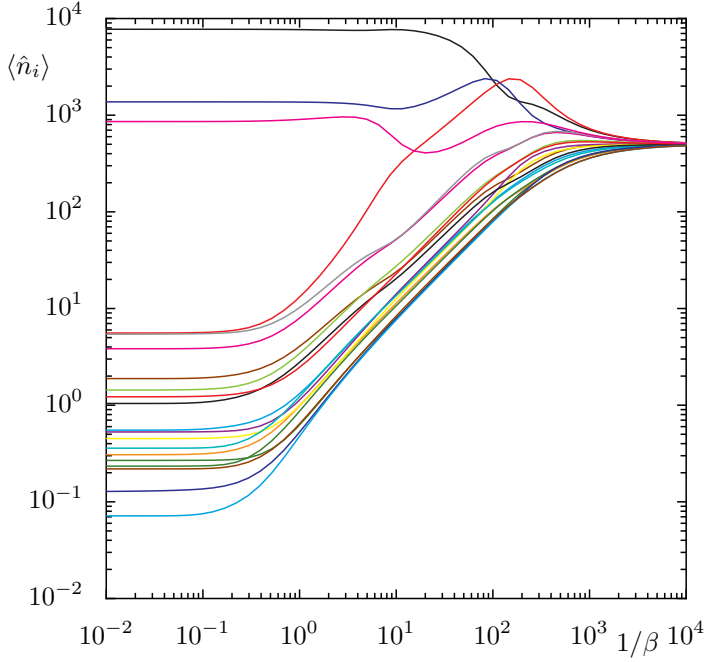


Figure 5.3: Temperature dependence of the steady state of an open Floquet gas. The mean occupation numbers $\langle \hat{n}_i \rangle$ in a tight-binding chain are shown versus the temperature $1/\beta$ of the heat bath. In the high-temperature limit, $1/\beta > 10^3$, all states approach the occupation N/M . Bose selection sets in for $1/\beta < 3$. The occupations of the selected states are temperature-independent as long as the number of particles in the nonselected states is negligible in comparison to the number of particles in the selected states. The occupations of the nonselected states decrease with decreasing temperature. However, for $1/\beta < 10^{-1}$ all occupations eventually become temperature independent and even close to zero temperature no pure state is formed. The parameters are equal to the ones in Fig. 5.2(d) except that the total particle number is fixed to $N = 1000$ (and the temperature is varied).

are temperature-independent when the temperature is low enough such that the Bose selection takes place. In other words, cooling the system enhances the Bose selection, i.e., the splitting between the occupations of the Bose-selected and nonselected states, but does not increase the occupation of some selected state at the expense of other selected states. This shows again that the set of selected states plays a role analogous to the ground state in the equilibrium Bose condensation. The occupations of the nonselected states decrease with decreasing temperature and their relative occupations depend on temperature. At very low temperatures, the system becomes temperature-independent due to the effect which was discussed in Sec. 2.4 and is unrelated to the bosonic nature.

6. Mean-field theory

So far, we have discussed Bose selection on the basis of numerical observations only. To get analytical insights and to be able to treat larger systems, we perform a mean-field approximation. Hereby, we focus on the properties of interest, the mean occupations $\langle \hat{n}_i \rangle$, only. Their equations of motion depend on higher-order correlations $\langle \hat{n}_i \hat{n}_j \rangle$. By assuming trivial two-particle correlations, $\langle \hat{n}_i \hat{n}_j \rangle \approx \langle \hat{n}_i \rangle \langle \hat{n}_j \rangle$, $\forall i \neq j$, we obtain a closed set of equations of motion and obtain the mean occupations in the steady state approximately. Exact results obtained by Monte-Carlo simulations justify this approximation. As discussed in the next chapter, this mean-field approximation helps to unveil the mechanism of Bose selection in form of an analytical asymptotic theory in the limit of large particle densities. This chapter is covered by Refs. [57, 58].

Starting from the equation of motion (2.44), the time evolution of the mean occupations is given by [see Appendix B]

$$\begin{aligned} \frac{d}{dt} \langle \hat{n}_i \rangle(t) &= \text{tr} \left(\hat{n}_i \frac{d}{dt} \hat{\rho}(t) \right) \\ &= \sum_j \left\{ R_{ij} [\langle \hat{n}_j \rangle(t) + \sigma \langle \hat{n}_i \hat{n}_j \rangle(t)] - R_{ji} [\langle \hat{n}_i \rangle(t) + \sigma \langle \hat{n}_i \hat{n}_j \rangle(t)] \right\}, \end{aligned} \quad (6.1)$$

where we consider the case of both bosons ($\sigma = 1$) and fermions ($\sigma = -1$) for illustrative purposes. Here we encounter a typical hierarchy [135, 136]: The time evolution of single-particle correlations $\langle \hat{n}_i \rangle$ (expectation values of operators that are quadratic in the field operators) are governed by two-particle correlations $\langle \hat{n}_i \hat{n}_j \rangle$ (expectation values of operators that are quartic in the field operators). The evolution of the latter will in turn be determined by three-particle correlations and so on.

A closed set of equations involving only mean occupations is obtained by assuming trivial two-particle correlations. The basic idea is a factorization approximation

$$\langle \hat{n}_i \hat{n}_j \rangle = \langle \hat{n}_i \rangle \langle \hat{n}_j \rangle + \left\langle (\hat{n}_i - \langle \hat{n}_i \rangle) (\hat{n}_j - \langle \hat{n}_j \rangle) \right\rangle \approx \langle \hat{n}_i \rangle \langle \hat{n}_j \rangle \quad \forall i \neq j. \quad (6.2)$$

Here nontrivial correlations of fluctuations are neglected so that two-particle correlations are approximated by a product of single-particle expectation values as if Wick's theorem was valid. In this way, we obtain the set of nonlinear mean-field equations

$$\frac{d}{dt} \langle \hat{n}_i \rangle(t) \approx \sum_j \left\{ R_{ij} \langle \hat{n}_j \rangle(t) [1 + \sigma \langle \hat{n}_i \rangle(t)] - R_{ji} \langle \hat{n}_i \rangle(t) [1 + \sigma \langle \hat{n}_j \rangle(t)] \right\}. \quad (6.3)$$

As we will see, the nontrivial correlations remain small at least when the state is close to the steady state.

The steady state $\frac{d}{dt}\langle\hat{n}_i\rangle(t) = 0$ is determined by

$$0 = \sum_j \left[R_{ij}\langle\hat{n}_j\rangle(1 + \sigma\langle\hat{n}_i\rangle) - R_{ji}\langle\hat{n}_i\rangle(1 + \sigma\langle\hat{n}_j\rangle) \right]. \quad (6.4)$$

The quantum degenerate regime is entered when occupations are of the order of unity or larger. Indeed if all occupations are smaller than unity, $\langle\hat{n}_i\rangle \ll 1$, we could neglect the nonlinear terms $\propto \sigma$ (the final-state stimulation for bosons and Pauli exclusion for fermions) and would recover the case of a classical gas ($\sigma = 0$). In the classical gas, the mean occupations are determined by the single-particle problem and read $\langle\hat{n}_i\rangle(t) = p_i(t)N$. However, as soon as the quantum degenerate regime is reached, where $\langle\hat{n}_i\rangle \gtrsim 1$ at least for some i , quantum statistics and with that the particle number matters. Thus, the steady state depends in a nontrivial way on the total particle number N .

Mean-field results agree well with quasiexact results from Monte-Carlo simulations [Figs. 5.1 and 5.2]. In particular, the extremely good agreement for the selected states is noticeable. For such highly occupied states, the mean-field method becomes even exact in the high-density limit [58]. However, small deviations are visible for nonselected states [Fig. 5.2] but can be resolved by higher-order expansions of the hierarchy Eq. (6.1) as discussed in Chap. 9. The mean-field method provides a good starting point for further analytical investigations.

Note that these mean-field equations of motion are compatible with the Gaussian ansatz for the density matrix,

$$\hat{\rho}_g = \frac{1}{Z} e^{-\sum_i \eta_i \hat{n}_i}, \quad (6.5)$$

with the partition function $Z = \sum_{\mathbf{n}} e^{-\sum_i \eta_i n_i}$ and parameters η_i . For bosons, the mean occupations for this Gaussian state read

$$\langle\hat{n}_i\rangle = \frac{1}{e^{\eta_i} - 1}, \quad (6.6)$$

and the correlations are given by Wick's decomposition,

$$\langle\hat{n}_i\hat{n}_j\rangle = \begin{cases} \langle\hat{n}_i\rangle\langle\hat{n}_j\rangle & \text{for } i \neq j \\ (1 + \sigma)\langle\hat{n}_i\rangle^2 + \langle\hat{n}_i\rangle & \text{for } i = j, \end{cases} \quad (6.7)$$

which includes the factorization approximation (6.2).

7. Asymptotic theory

In this chapter, we derive a transparent criterion for the Bose selection, which unveils the mechanism of Bose selection and explains all so far observed properties. We obtain this criterion from the mean-field theory in the asymptotic limit of large densities. This criterion determines both the set of states and the mean occupations of all selected and nonselected states. It provides insight into why only some states acquire large occupations but not the others. We prove that the number of selected states is odd except for fine-tuned situations. Furthermore, we show when ordinary Bose condensation breaks down in favor of Bose selection. Finally we confirm that the set of selected states are temperature-independent. All presented results are published in Refs. [57, 58]. This insight also provides a useful toolbox to quantum engineer specific asymptotic states.

7.1. Selection criterion

We start with the mean-field equations (6.4) for the bosonic case, $\sigma = 1$, which read

$$0 = \sum_j [R_{ij}\langle\hat{n}_j\rangle(1 + \langle\hat{n}_i\rangle) - R_{ji}\langle\hat{n}_i\rangle(1 + \langle\hat{n}_j\rangle)]. \quad (7.1)$$

Firstly, we focus on the selected states. In the asymptotic limit of large densities, it appears natural to neglect the spontaneous versus the stimulated processes, i.e., to keep the quadratic terms only. One then obtains the equations

$$0 = \langle\hat{n}_i\rangle \sum_j A_{ij}\langle\hat{n}_j\rangle \quad (7.2)$$

with the rate-asymmetry matrix

$$A_{ij} = R_{ij} - R_{ji}. \quad (7.3)$$

In the solution of Eq. (7.2), the occupations of some states i can vanish, $\langle\hat{n}_i\rangle \approx 0$. The subset of all other states possessing a nonzero occupation is denoted by the set of selected states \mathcal{S} . Their occupations obey the linear set of equations

$$0 = \sum_{j \in \mathcal{S}} A_{ij}\langle\hat{n}_j\rangle \quad \forall i \in \mathcal{S}, \quad (7.4)$$

which directly follows from Eqs. (7.2) with $\langle \hat{n}_i \rangle = 0$, $\forall i \notin \mathcal{S}$. This set of equations determines the occupations of the selected states, assuming that asymptotically almost all particles are in the selected states, $\sum_{i \in \mathcal{S}} \langle \hat{n}_i \rangle = N$. Thus the relative occupations of the selected states are given by this linear set of equations, which depends on the rate asymmetries only.

Secondly, the occupations of the nonselected states follow from their coupling to the selected states. For the nonselected states, we neglect all couplings to other nonselected states since their occupation is negligible compared to the selected states. Furthermore, we neglect the spontaneous processes versus the stimulated ones for transitions to selected states, $\langle \hat{n}_j \rangle + 1 \approx \langle \hat{n}_j \rangle$, $\forall j \in \mathcal{S}$. From Eqs. (7.1), we obtain the occupations of nonselected states i by

$$\langle \hat{n}_i \rangle = - \frac{\sum_{j \in \mathcal{S}} R_{ij} \langle \hat{n}_j \rangle}{\sum_{j \in \mathcal{S}} A_{ij} \langle \hat{n}_j \rangle} \quad \forall i \notin \mathcal{S}. \quad (7.5)$$

This approximation is reminiscent of the Bogoliubov approximation [137] for weakly interacting Bose gases since the dependencies of the nonselected states among each other are neglected.

Thirdly, the set of selected states \mathcal{S} is fixed by the requirement of physically meaningful occupations, i.e., nonnegative occupations. For a hypothetical set of selected states \mathcal{S} , Eq. (7.4) may not possess a solution at all or give rise to negative occupations of the selected states, Eqs. (7.4), or nonselected states, Eqs. (7.5). Note, the requirement for nonnegative occupations in the nonselected states is equivalent to the requirement that the solution is stable under the dynamics given by $d\langle \hat{n}_i \rangle / dt = \langle \hat{n}_i \rangle \sum A_{ij} \langle \hat{n}_j \rangle$ [cf. Eq. (7.2)]. However, there exists always such a set of selected states with nonnegative occupations. This set is uniquely defined except for fine-tuned situations. A proof for the existence and uniqueness is found in App. C.

Let us finally conclude the three results in a transparent criterion for the selection and the leading-order occupations. For this purpose, we introduce the parameters ν_i with $\sum_i \nu_i = 1$ and μ_i . These parameters ν_i and μ_i provide the leading-order occupations of the, respectively, selected and nonselected states via $\langle \hat{n}_i \rangle = N \nu_i \forall i \in \mathcal{S}$ and $\langle \hat{n}_i \rangle = -[\sum_{j \in \mathcal{S}} R_{ij} \langle \hat{n}_j \rangle] / \mu_i \forall i \notin \mathcal{S}$. The criterion reads

$$\mu_i = \sum_j A_{ij} \nu_j \quad \text{with} \quad \begin{cases} \nu_i \geq 0 \text{ and } \mu_i = 0 \text{ for } i \in \mathcal{S}, \\ \nu_i = 0 \text{ and } \mu_i \leq 0 \text{ for } i \notin \mathcal{S}. \end{cases} \quad (7.6)$$

Indeed this criterion is equivalent to the selection described above. We recover Eq. (7.4) for the selected states $i \in \mathcal{S}$, and Eq. (7.5) for the nonselected states. Note that in the latter case, negative parameters μ_i lead to positive occupations. The ambiguous case where

$$\nu_i = \mu_i = 0 \quad (7.7)$$

requires fine-tuning of the rates. We refer to this case as transition criterion, and we will discuss it in Chap. 8. The selection criterion (7.6) is the starting point for further analytical investigations of

the Bose selection.

7.2. Properties of Bose selection

Now, all features of Bose selection observed in Chap. 5 can be explained with the help of the selection criterion (7.6). Firstly, we explain the mechanism of the Bose selection, secondly, the minimal requirement for a Bose selection (of multiple states), thirdly, that the number of selected states is always odd except for fine-tuned situations, and, fourthly, the temperature independence.

First of all, this criterion provides insight into the selection mechanism. The relative occupations among the selected states become independent of the total particle number N since they approach the relative occupations determined by the set of linear Eqs. (7.4). The saturation of the occupations of the nonselected states follows from Eq. (7.5) together with the independence of the relative occupations of the selected states on the total particle number. This saturation explains that in the high-density limit all further added particles occupy the selected states so that their occupations grow linearly with the particle number N . Since almost all particles are distributed among the selected states, the asymptotic theory is justified.

Ordinary Bose condensation is a special case of Bose selection with a single selected states k . The occupations of all nonselected states simplify to

$$\langle \hat{n}_i \rangle = -\frac{R_{ki}}{A_{ki}} = \frac{1}{R_{ik}/R_{ki} - 1} \quad \forall i \neq k. \quad (7.8)$$

From the requirement of positive occupations follows that

$$R_{ki} > R_{ik} \quad \forall i \neq k, \quad (7.9)$$

i.e., that the state k is unique since all rates towards this state are larger than the rates in the reversed direction. Therefore we can conclude that if and only if a state k exists, which is a *ground-state-like* state k in the sense of Eq. (7.9), the state k hosts the single condensate. In equilibrium, where the rates fulfill the condition (2.30), the ground state fulfills always this condition so that the Bose-Einstein condensation is recovered. Furthermore, the expressions of the nonselected states [Eqs. (7.5)] reduce to the Bose-Einstein distribution

$$\langle \hat{n}_i \rangle = \frac{1}{e^{-\beta(E_i - E_k)} - 1}. \quad (7.10)$$

In conclusion, a necessary and sufficient condition for the Bose selection is the absence of a ground-state-like state.

We can now explain the four scenarios shown in Fig. 5.2. In the equilibrium scenario [panel (a)], the system shows Bose-Einstein condensation. In a Floquet-system [panel (d)] a ground state is not even defined, leading generally to a selection of several states. In the case of the autonomous

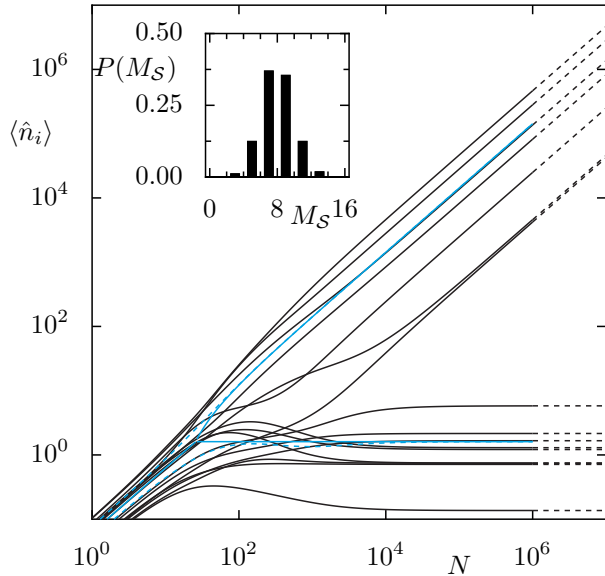


Figure 7.1: Number of Bose-selected states in the random-rate model. The mean occupation numbers $\langle \hat{n}_i \rangle$ depending on the total particle number for a random-rate model with $M = 16$ states are shown. Additionally, the average mean occupation in the selected N_S/M_S and nonselected states $N_{\bar{S}}/M_{\bar{S}}$ (dashed blue lines) are shown in comparison to the prediction given by Eq. (7.12) (solid blue lines). The separation of these predictions provides the characteristic particle number N^* [Eq. (7.13)]. The inset shows a histogram of the number of selected states M_S for an ensemble of 1000 such random-rate systems. Note, only odd numbers of selected states have been observed without exception.

system with two heat baths, the notion of the ground state becomes meaningless when one bath is population-inverted and favors higher excited states. In this case, several states are selected [panel (c)]. Note that, only breaking detailed balance, as in the nonequilibrium situation with two (positive-temperature) baths, is not sufficient to obtain several selected states since the ground state is still favored by both heat baths [panel (b)]. Also note that even in the Floquet system or in the case with a population-inverted bath, a single state can be selected by chance [cf. Fig. 10.2(a) and Fig. 10.1(a), respectively, below].

The concept of Bose selection also generalizes the definition of ground-state Bose condensation to nonequilibrium situations. The textbook derivation of Bose condensation is based on Bose-Einstein distribution, which is valid in thermal equilibrium. However, this requirement of equilibrium is too strong. The sufficient and necessary requirements are bosonic final-state stimulation and the existence of the ground-state-like state. Bose condensation is caused rather by the final-state stimulation than by equilibrium and, thus, can also occur under nonequilibrium conditions.

The number of selected states M_S is generically odd, as indicated by the inset of Fig. 7.1. Namely, without fine-tuning of the skew-symmetric matrix $A_{ij} = -A_{ji}$, the Eq. (7.4) has a solution if and only if the set of selected states \mathcal{S} contains an odd number of states (since the singularity, required to solve this equation, is guaranteed for a skew-symmetric matrix of odd but not of even dimensionality). Let us illustrate this mathematical argument. A single condensate occurs when the ground-state-like condition (7.9) is hold. An even number of two condensates $\mathcal{S} = \{k, \ell\}$ requires fine-tuning since the rates between both selected states must balance, $R_{k\ell} = R_{\ell k}$ and this condition is unstable under small variation of these rates. In contrast, three selected state $\mathcal{S} = \{k, \ell, m\}$ require, without loss of generality, $A_{k,\ell}, A_{\ell,m}, A_{m,k} > 0$. This situation, known as rock-paper-scissor configuration in game theory [138], is robust under small parameter changes. More selected states require more involved conditions. The odd number of selection states remains a surprising consequence.

We can estimate the characteristic particle number N^* at which the crossover to Bose selection occurs to be given by the depletion of the selected states,

$$N_{\bar{\mathcal{S}}} = \sum_{i \notin \mathcal{S}} \langle \hat{n}_i \rangle. \quad (7.11)$$

In order to obtain a rough estimate, we assume equal occupations in all states below the crossover and equal occupations among the selected and among the nonselected states above the crossover,

$$\langle \hat{n}_i \rangle = \begin{cases} N/M & \text{if } N < N^*, \\ N_{\bar{\mathcal{S}}}/M_{\bar{\mathcal{S}}} & \text{if } N > N^* \text{ and } i \notin \mathcal{S}, \\ N_{\mathcal{S}}/M_{\mathcal{S}} & \text{if } N > N^* \text{ and } i \in \mathcal{S}, \end{cases} \quad (7.12)$$

wherein $N_{\mathcal{S}} = N - N_{\bar{\mathcal{S}}}$ denotes the number of particles in the selected states and $M_{\bar{\mathcal{S}}} = M - M_{\mathcal{S}}$ the number of nonselected states. This ansatz is shown in Fig. 7.1. The characteristic particle number is

$$N^* = N_{\bar{\mathcal{S}}}M/M_{\bar{\mathcal{S}}}. \quad (7.13)$$

When only a few states are selected, $M_{\mathcal{S}} \ll M$, the characteristic particle number directly corresponds to the depletion of selected states in the limit of large densities,

$$N^* = N_{\bar{\mathcal{S}}}. \quad (7.14)$$

The set of selected states is independent of the temperature of the heat bath(s). This is caused by fact that the selection depends only on the rate-asymmetry matrix A_{ij} (but not on the full rate matrix R_{ij}). This rate-asymmetry matrix A_{ij} is temperature independent [Eqs. (2.32) and (2.39)] in contrast to the rate matrix. Even the relative occupations of the selected states are temperature independent¹. However since the occupations of the nonselected states depend on the temperature via the rates R_{ij} , also the characteristic particle number N^* is temperature-dependent. Cooling the system increases the characteristic particle number N^* . However, below a certain temperature, further cooling does not affect the system anymore [as discussed below Fig. 5.3] and, therefore, does not decrease the characteristic temperature anymore.

7.3. Systematic high-density expansion

The asymptotic theory is the leading order of an expansion in the inverse total particle number N^{-1} . The subleading orders provide corrections to the asymptotic theory for intermediate particle numbers. Here we derive this systematic expansion [58].

¹Note, this does not contradict our work [103] of inducing a Bose condensate via a hot bath since in this effect is a preasymptotic state at intermediate particle number N , which can occur when some rates are small [cf. Chap. 11].

We expand the mean occupations as a series in powers of the inverse particle number N^{-1} ,

$$\langle \hat{n}_i \rangle = N\nu_i + \nu_i^{(1)} + N^{-1}\nu_i^{(2)} + N^{-2}\nu_i^{(3)} + \dots \quad (7.15)$$

Since the total particle number is $N = \sum_i \langle \hat{n}_i \rangle$, we require

$$\sum_i \nu_i = 1 \text{ and } \sum_i \nu_i^{(r)} = 0 \quad \forall r \leq 1. \quad (7.16)$$

Note that this expansion is equivalent to an expansion in the inverse particle density $n^{-1} = M/N$. Applying this ansatz (7.15) into the mean-field Eqs. (6.4) gives

$$\begin{aligned} 0 = & \nu_i \sum_j A_{ij} \nu_j \\ & + \frac{1}{N} \sum_j \left[R_{ij} \nu_j - R_{ji} \nu_i + A_{ij} \left(\nu_i \nu_j^{(1)} + \nu_i^{(1)} \nu_j \right) \right] \\ & + \frac{1}{N^2} \sum_j \left[R_{ij} \nu_j^{(1)} - R_{ji} \nu_i^{(1)} + A_{ij} \left(\nu_i^{(2)} \nu_j + \nu_i^{(1)} \nu_j^{(1)} + \nu_i \nu_j^{(2)} \right) \right] \\ & + O\left(\frac{1}{N^3}\right). \end{aligned} \quad (7.17)$$

Since this expansion provides the mean occupations for all total particle numbers N , the coefficient for each power of N must vanish independently.

The leading (zeroth-order) order of Eq. (7.17) gives rise to the selection mechanism. It reads

$$0 = \nu_i \sum_j A_{ij} \nu_j \quad (7.18)$$

and correspond to Eq. (7.2) (but there we approximated $\langle \hat{n}_i \rangle \approx \nu_i, \forall i \in \mathcal{S}$). As discussed above, the solution of this equation separates all states in a group of Bose-selected states $i \in \mathcal{S}$ and a group of nonselected states $i \notin \mathcal{S}$, by [see also Eqs. 7.5]

$$0 = \begin{cases} \sum_{j \in \mathcal{S}} A_{ij} \nu_j & \forall i \in \mathcal{S}, \\ \nu_i & \forall i \notin \mathcal{S}. \end{cases} \quad (7.19)$$

The next order determines the coefficients $\nu_i^{(1)}$, which are the leading order of nonselected states and corrections for selected states. For the nonelected states, we obtain

$$\nu_i^{(1)} = -\frac{\sum_{j \in \mathcal{S}} R_{ij} \nu_j}{\sum_{j \in \mathcal{S}} A_{ij} \nu_j} \quad \forall i \notin \mathcal{S}. \quad (7.20)$$

This equation corresponds to Eq. (7.5) (where we approximated $\langle \hat{n}_i \rangle \approx \nu_i, \forall i \in \mathcal{S}$). It justifies that the occupations of the nonselected states are independent of each other in their leading order. The

leading corrections to the occupations of the selected states are given by

$$\sum_{j \in \mathcal{S}} A_{ij} \nu_j^{(1)} = \sum_{j \in \mathcal{S}} (R_{ji} \nu_i - R_{ij} \nu_j) + \nu_i \sum_{j \notin \mathcal{S}} (R_{ji} - A_{ij} \nu_j^{(1)}) \quad \forall i \in \mathcal{S}, \quad (7.21)$$

where we used Eqs. (7.17), and taking into account the requirement (7.16) for $r = 1$. This second order is also relevant for the occupations of the selected states for systems where some rates vanish as discussed in Sec. 11.2.

The two leading orders, Eqs. (7.19) and (7.20), are sufficient to recover the selection criterion (7.6) as described above. However, higher orders in the expansion (7.17) provide further corrections.

8. Transitions

The set of selected states can change in response to a parameter variation. Such a transition causes abrupt changes in the mean occupations of the states. An example is shown in Fig. 8.1: The occupations $\langle \hat{n}_i \rangle$ change abruptly when ramping up the parameter p that defines the total rate matrix $R(p)$ by an interpolation between two random rate matrices $R^{(1)}$ and $R^{(2)}$ via $R(p) = (1 - p)R^{(1)} + pR^{(2)}$. We find that two states are involved at each transition except for fine-tuning a second parameter. For finite total particle numbers, we observe that this transition is not a phase transition but a crossover with finite width. The transition (and the crossover region) corresponds to a fine-tuned situation, where the number of selected states is even. In this chapter, we provide a theoretical description of such transitions. This insight into the nature of the transition allows us to engineer a quantum switch for heat conductivity [Chap. 10] and provides an efficient algorithm for finding the set of selected states. All findings discussed in this chapter are part of Ref. [58].

At a transition, the classification (i.e., being either selected or nonselected) of two states changes. In consequence, the number of selected states is odd after the transition since it was odd before the transition [Fig. 8.1]. Approaching it from the below, the transition is triggered by a state $i^<$. This state $i^<$ can either be a selected state whose occupation drops until it becomes nonselected at the transition (case I) or a nonselected state whose occupation increases until it becomes selected at the transition (case II). Furthermore, one can observe that at the transition a second state $i^>$ becomes involved abruptly. This state changes either from being selected to nonselected (case A) or vice versa (case B). When approaching the transition from above, the states $i^<$ and $i^>$ swap their role, so that the former partner state $i^>$ plays the role of the triggering state. This classification defines four generic types of transitions that are depicted in Fig. 8.2. Type (I,A) and type (II,B), where the number M_S of selected states is lowered or raised by two, respectively, transform into each other when the transition is passed in opposite direction. Therefore, they form one class. In type (II,A) transitions, which are triggered by nonselected states from both sides, and type (I,B) transitions, which are triggered from selected states from both sides, the number M_S of selected states does not change. They cannot be transformed into each other. Transitions that involve four states are not generic as they require the fine-tuning of a second parameter.

These observations based on Fig. 8.1 can be confirmed within the asymptotic theory. Let p^* be the critical parameter at which the transition occurs and $\mathcal{S}^<$ and $\mathcal{S}^>$ be the sets of selected states below and above the transition, respectively [see Fig. 8.2]. Approaching the critical parameter from below, $p \rightarrow p^* + 0^-$, the occupation $\langle \hat{n}_{i^<} \rangle$ of the state $i^<$ either approaches (almost) zero when this

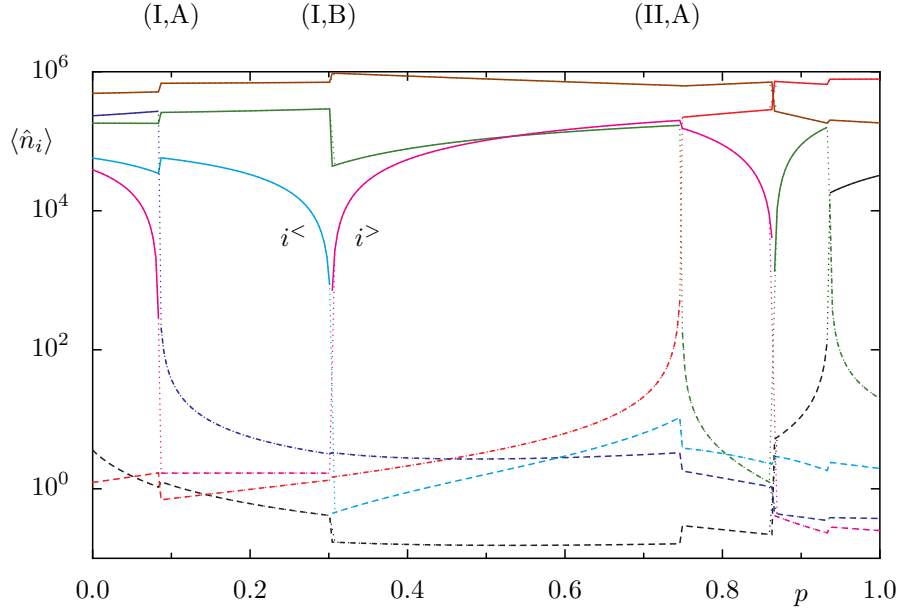


Figure 8.1.: Transitions caused by the variation of a system parameter. The dependence of the mean occupation numbers $\langle \hat{n}_i \rangle$ on a dimensionless parameter p is shown. The system of $M = 7$ states and $N = 10^6$ bosons is given by the superposition of two independently drawn random-rate matrices $R^{(1)}$ and $R^{(2)}$ with the relative weight controlled by p , $R(p) = (1 - p)R^{(1)} + pR^{(2)}$. The results are obtained using mean-field theory (dotted lines), asymptotic theory (solid lines for selected states and dashed lines for nonselected states). Each color refers to a specific state. At each transition, two states are involved each changing its classification (from selected to nonselected or vice versa). At the top, the types of three exemplary transition are given, and for the second transition the two involved states, the triggering states from below $i^<$ and above $i^>$ are labeled.

state is selected, $i^< \in \mathcal{S}^<$, or (almost) diverges when it is nonselected, $i^< \notin \mathcal{S}^<$. At the transition $p = p^*$, we encounter the transition criterion (7.7) of the asymptotic theory, $\nu_{i^<} = \mu_{i^<} = 0$. The state $i^<$ is selected (nonselected) when it was nonselected (selected) before, respectively. Thus, at this fine-tuned situation, the set of selected states contains an *even* number of states and is given by

$$\mathcal{S}^* = \begin{cases} \mathcal{S}^< \cup \{i^<\} & \text{if } i^< \notin \mathcal{S}^<, \\ \mathcal{S}^< \setminus \{i^<\} & \text{if } i^< \in \mathcal{S}^<. \end{cases} \quad (8.1)$$

As the number of Bose-selected states has to become odd after the transition, one further state $i^>$ has to be involved. The set \mathcal{S}^* can also be expressed in terms of this partner state $i^>$,

$$\mathcal{S}^* = \begin{cases} \mathcal{S}^> \cup \{i^>\} & \text{if } i^> \notin \mathcal{S}^>, \\ \mathcal{S}^> \setminus \{i^>\} & \text{if } i^> \in \mathcal{S}^>. \end{cases} \quad (8.2)$$

In the following, we describe how to determine this partner state in order to find the set $\mathcal{S}^>$ of selected states above the transition.

The behavior at the transition is determined by the rate asymmetry matrix at the transition,

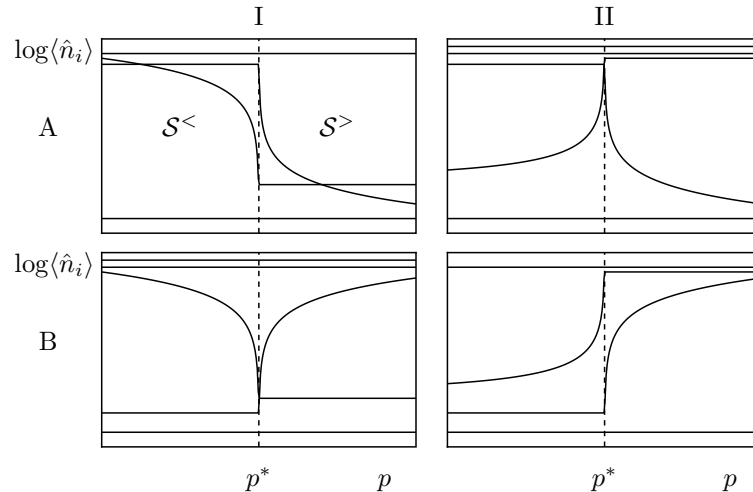


Figure 8.2.: Four generic types of transitions, where the set of selected states changes from $\mathcal{S} = \mathcal{S}^<$ to $\mathcal{S} = \mathcal{S}^>$ when a parameter p crosses a critical value p^* . In each transition, two states changed their character of being either Bose-selected or nonselected. Thus the number $M_{\mathcal{S}}$ of selected states remains odd. When approaching the transition from below, it is triggered by a state $i^<$, either a selected state whose occupation drops until it becomes nonselected at the transition (case I) or a nonselected state whose occupation increases until it becomes selected at the transition (case II). A second state $i^>$ becomes involved abruptly at the transition that changes from selected to nonselected (case A) or vice versa (case B). This state plays the role of the triggering state when the transition is approached from above. Types (I,A) and (II,B) form one class, since they transform into each other when the transition is passed in opposite direction.

$A^* = A(p^*)$. The occupations of the selected states are determined via the selection criterion (7.6) by the truncated matrix $A^{\mathcal{S}^*}$, which is obtained from A^* by removing all rows and columns corresponding to nonselected states $i \notin \mathcal{S}^*$ as in the following decomposition,

$$A = \left(\begin{array}{c|c} A^{\mathcal{S}} & A^{\mathcal{S}\bar{\mathcal{S}}} \\ \hline A^{\bar{\mathcal{S}}\mathcal{S}} & A^{\bar{\mathcal{S}}} \end{array} \right). \quad (8.3)$$

This matrix $A^{\mathcal{S}^*}$ is even dimensional and still singular by construction. As the matrix is even-dimensional and skew-symmetric, its eigenvalues are imaginary and come in pairs of opposite sign. Thus, one eigenvalue of zero, which is guaranteed since the matrix is singular, implies another one, so that generically the kernel of $A^{\mathcal{S}^*}$ is two-dimensional. One vector lying in the kernel of $A^{\mathcal{S}^*}$ is given by the limiting occupations ν_i as one approaches the transition from below, $p \rightarrow p^* + 0^-$. We denote this vector by $\boldsymbol{\nu}^<$ (note that it is now truncated to the states of \mathcal{S}^* and that $\sum_i \nu_i^< = 1$). Another (linearly independent) vector is denoted by $\boldsymbol{\nu}'$ for which we require $\sum_{i \in \mathcal{S}^*} \nu'_i = 0$. Analogously, there is a second vector $\boldsymbol{\nu}^>$ from the limiting occupations as one approaches from above, $p \rightarrow p^* + 0^+$, which also lies in the kernel and obeys $\sum_i \nu_i^> = 1$. Both limiting vectors $\boldsymbol{\nu}^<$ and $\boldsymbol{\nu}^>$ are connected via the linear interpolation

$$\boldsymbol{\nu}(a) = \boldsymbol{\nu}^< + a\boldsymbol{\nu}' \quad (8.4)$$

by $\nu^< = \nu(0)$ and $\nu^> = \nu(a^>)$. In order to obtain the occupations $\nu^>$ after the transition, we determine the missing extremal point $a^>$ in the following. The occupations of the nonselected states (and their sign) is determined by the vector μ given by the selection criterion (7.6). For the two solutions $\nu^<$ and $\nu^>$, these vectors read $\mu^< = A^{\bar{\mathcal{S}}^* \mathcal{S}^*} \nu^<$ and $\mu^> = A^{\bar{\mathcal{S}}^* \mathcal{S}^*} \nu^>$, respectively. Also these vectors are connected via the linear interpolation $\mu(a) = \mu^< + a\mu'$ with $\mu' = A^{\bar{\mathcal{S}}^* \mathcal{S}^*} \nu'$ by $\mu^< = \mu(0)$ and $\mu^> = \mu(a^<)$. Here $A^{\bar{\mathcal{S}}^* \mathcal{S}^*}$ is obtained from A^* by removing all rows i corresponding to Bose-selected states $i \in \mathcal{S}^*$ and columns j corresponding to nonselected states $j \notin \mathcal{S}^*$ [like in Eq. (8.3)]. Due to the selection criterion (7.6), we require physical solutions by $\nu_i(a) \geq 0, \forall i \in \mathcal{S}^*$ and $\mu_i(a) \leq 0, \forall i \notin \mathcal{S}^*$. Choosing the orientation of ν' conveniently such that $\nu'_{i^<} > 0$ if $i^< \in \mathcal{S}^*$ and $\mu'_{i^<} < 0$ otherwise, this is fulfilled for the finite interval $0 < a < a^>$. The extremal point $a^>$ is determined by ramping up a until an element of either $\nu(a)$ or $\mu(a)$ becomes zero. The index of this element is the second triggering state $i^>$ and the extremal point $a^>$ determines the occupations $\nu^> = \nu(a^>)$. This interpolation not only determines the transition but also provides a physical interpretation for transitions of finite width, which occur for finite particle numbers, as shown below.

The width of the transition interval $0 < a < a^>$ measures the size of the discontinuity since its extremal points describe the solutions $\nu^<$ and $\nu^>$ found when approaching the transition from below and above, respectively. The narrower the interval is, i.e., the smaller $\Delta a = a^>$ is, the more similar both solutions $\nu^<$ and $\nu^>$ are, and the smaller the discontinuity in the occupations of the states $j \notin \{i^<, i^>\}$ that are not directly involved in the transition [see also Fig. 8.1] is. The width Δa associated with a typical transition must, moreover, be expected to shrink with the system size. Namely, each of the M single-particle states of the system provides a constraint that potentially limits this interval, since the number of conditions (7.6) proliferates with size M . So under parameter variations in large systems, not only more transitions occur but also the discontinuous jumps, which the nonparticipating occupations undergo at each transition, are smaller than in small systems.

For finite particle numbers N , the sharp transition becomes a crossover of finite width. Figure 8.3 shows this crossover by five snapshots for different parameters close to or at the critical parameter p^* , where the second transition of Fig. 8.1 occurs. The first panel corresponds to a parameter well below the transition. Here three states become selected asymptotically. When closely approaching the transition but still staying below it (second panel), we can observe that a preasymptotic regime appears. Namely, at large but finite particle numbers N , the system approaches a state with two selected states, before a third state eventually becomes selected as well in the asymptotic limit $N \rightarrow \infty$. [A detailed discussion of the preasymptotic state will follow in Chap. 11.] This third state is the triggering state $i^<$. The two states that appear to be selected in this preasymptotic regime are those two states that are the only selected states at the transition (middle panel), $p = p^*$. The fourth panel corresponds to a parameter, where the transition has just been passed. Here (roughly) the same preasymptotic state is found, before a third state $i^>$ joins the set of selected states asymptotically for $N \rightarrow \infty$. The fifth panel is obtained for a parameter well above the transition finally. Here again, no preasymptotic regime is found. This crossover through the transition is described by the family of solutions of the asymptotic theory, Eq. (8.4). The emergence of a preasymptotic regime

close to the transition implies that the fine-tuned rate matrix $R(p^*)$, which gives rise to two selected states, provides an accurate description of the system within a finite interval of parameters near the transition.

The insight into the transition allows us to build a fast algorithm to find all selected states of a given rate-asymmetry matrix (the selection depends on the asymmetries A_{ij} only). This is helpful since the selection criterion (7.6) provides the set of selected states not explicitly since an inequality is involved, and a simple brute-force algorithm testing all possible sets of selected states \mathcal{S} scales exponentially with the system size. Guessing the set \mathcal{S} from the mean-field results fails often since the asymptotic limit is not numerically reachable. The basic idea of the algorithm is to start with a rate-asymmetry matrix A_{ij}^{init} whose selection is obvious, e.g., where one state fulfills the ground-state-like condition (7.9), and then changing linearly to the given asymmetry matrix A_{ij} by the parameter $0 \leq p \leq 1$ via $A_{ij}(p) = pA_{ij}^{\text{init}} + (1-p)A_{ij}$. Hereby one can track all transitions and thus end up with the selection of the given problem. We have presented this algorithm in Ref. [58]. However, I will not describe the details here since a similar algorithm is discussed in the Chap. 16.

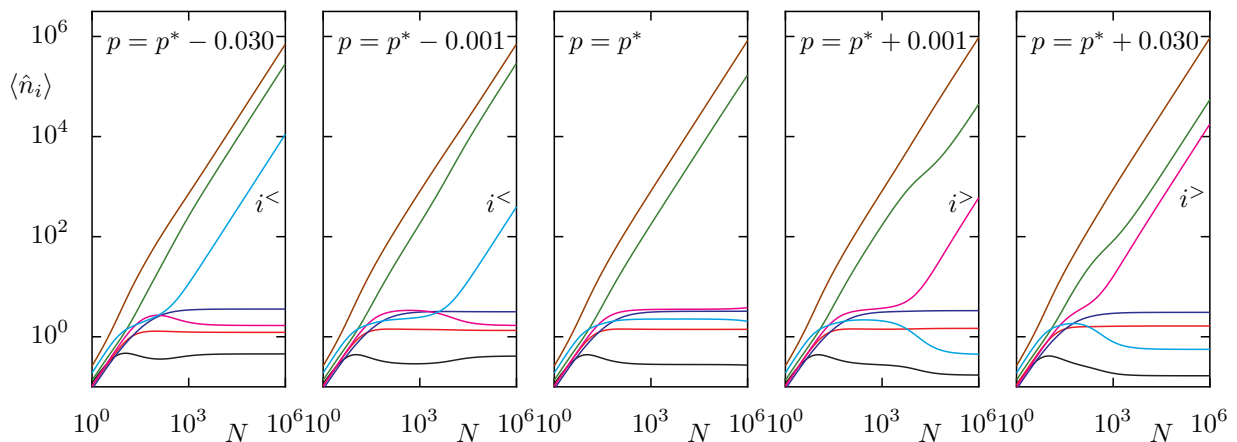


Figure 8.3.: Preasymptotic states close to a transition. The dependence of the mean occupation numbers $\langle \hat{n}_i \rangle$ on the total particle number N is shown for five successive parameters p crossing the transition at p^* . The system is described by the same rate matrix $R(p)$ as that of Fig. 8.1. The parameters p used in the different panels are chosen to be close to or at the second transition of Fig. 8.1, which is of type (I, B). The corresponding critical parameter is $p^* \approx 0.303179$. Approaching the transition from below, first the occupation of the triggering state $i^<$ (blue line) decreases. Thus a wide preasymptotic state emerges (e.g., for $10 < N < 10^4$ in the second panel), where only two states (brown and green line) appear to be selected. At the transition (middle panel), only these two (an even number) states are selected and the extend of this preasymptotic state diverges. Increasing the parameter p further, the extend of this preasymptotic state shrinks since the occupation of the newly selected state $i^>$ (pink line) increases. Above the transition, three states are selected again.

9. Beyond the mean-field approximation

Even though the particles are noninteracting, nontrivial two-particle correlations are present. These nontrivial correlations are caused by two sources: the conserved particle number and nonequilibrium effects. Although the mean-field approximation, which assumes trivial correlations, approximates the mean occupations well, deviations are visible for nonselected states [Fig. 5.2] and Wick's decomposition (6.7) for two-particle correlations and number fluctuations may not be a satisfying approximation. In this chapter, we discuss the origin of nontrivial correlations and derive an augmented mean-field approximation resolving both issues. This approach is discussed in Ref. [58].

Nontrivial correlations

$$\zeta_{ij} = \langle (\hat{n}_i - \langle \hat{n}_i \rangle)(\hat{n}_j - \langle \hat{n}_j \rangle) \rangle = \langle \hat{n}_i \hat{n}_j \rangle - \langle \hat{n}_i \rangle \langle \hat{n}_j \rangle \quad (9.1)$$

are partially caused by the conserved particle number. This is similar to the canonical ensemble, which also shows small nontrivial correlations (as long as the thermodynamic limit is not reached). The fluctuation of the total particle number

$$\Delta N^2 := \langle \hat{N}^2 \rangle - \langle \hat{N} \rangle^2 = \sum_{i,j} \left[\langle \hat{n}_i \hat{n}_j \rangle - \langle \hat{n}_i \rangle \langle \hat{n}_j \rangle \right] = \sum_i \Delta n_i^2 + \sum_{i \neq j} \zeta_{ij} \quad (9.2)$$

vanishes in the canonical ensemble, $\Delta N|_{\text{ce}} = 0$. Here $\Delta n_i^2 := \langle \hat{n}_i^2 \rangle - \langle \hat{n}_i \rangle^2$ denote the number fluctuations of individual states i . However, when the canonical ensemble is approximated by the grand canonical ensemble (or more generally by the mean-field theory), the number fluctuations are trivial [given by the Wick's decomposition (6.7)], and thus the total particle number fluctuation is nonzero,

$$\Delta N^2|_{\text{mf}} = \sum_i (\langle \hat{n}_i^2 \rangle + \langle \hat{n}_i \rangle) > 0. \quad (9.3)$$

When one is interested in mean occupations only, the mean-field approximation turns out to be very successful. In thermodynamic equilibrium, this approximation is indeed justified by the equivalence of the ensembles, which states *i.a.* that the canonical fluctuations approach the Gaussian fluctuations in the thermodynamic limit. However, there is a prominent exception known as the grand-canonical fluctuation catastrophe [139, 140]: The fluctuations of a grand-canonical Bose condensate causes large total particle number fluctuations. According to the Wick's decomposition (6.7), these fluctuations are of the order of the total particle number. This phenomenon was observed in Bose condensates

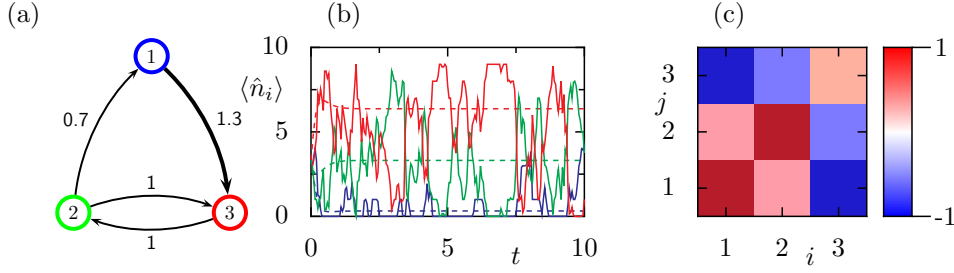


Figure 9.1.: Nontrivial correlations induced by nonequilibrium effects. (a) This sketch shows a three-state model and its rates (line widths also reflect rates). (b) The time evolutions of the occupations for a single Monte-Carlo trajectory (solid lines) are shown. Also the augmented mean-field results are shown (dashed lines), which capture the mean occupations. (c) The relative nontrivial correlations $\zeta_{ij}/\langle \hat{n}_i \rangle \langle \hat{n}_j \rangle$ are shown. The diagonal elements must be positive since they are number fluctuations. The off-diagonal elements show anticorrelated occupations (blue), $\langle \hat{n}_i \hat{n}_j \rangle < \langle \hat{n}_i \rangle \langle \hat{n}_j \rangle$, for the state pairs (1,2) and (2,3) but (positive) correlations of the occupation numbers (red) $\langle \hat{n}_1 \hat{n}_2 \rangle > \langle \hat{n}_1 \rangle \langle \hat{n}_2 \rangle$ for the other pair.

of photons, where it prevents second-order coherences in Bose condensates [141]. In contrast, in the canonical ensemble, the conserved particle number, $\Delta N^2 = 0$, restricts the fluctuations of the condensate and requires two-particle anticorrelations [according to Eq. (9.2)],

$$0 < \sum_i \Delta n_i^2|_{\text{ce}} = - \sum_{i \neq j} \zeta_{ij}|_{\text{ce}}. \quad (9.4)$$

This shows that the occupation numbers are (on average) anticorrelated, $\langle \hat{n}_i \hat{n}_j \rangle < \langle \hat{n}_i \rangle \langle \hat{n}_j \rangle$, i.e., that a larger particle number in one state i leads to smaller occupations in the other states j . As we have described in Ref. [58], these resulting nontrivial correlations can be captured by a Gaussian state which is projected onto the subspace of the sharp particle number N .

Additional to the nontrivial correlations due to the fixed particle number, correlations are also induced by nonequilibrium effects. Surprisingly, these correlations can be positive, $\langle \hat{n}_i \hat{n}_j \rangle > \langle \hat{n}_i \rangle \langle \hat{n}_j \rangle$, in contrast to equilibrium. Figure 9.1 shows a minimal example exhibiting positive correlations: The states 1 and 2 of the three-state system [panel (a)] are correlated [panel (c)], $\langle \hat{n}_1 \hat{n}_2 \rangle > \langle \hat{n}_1 \rangle \langle \hat{n}_2 \rangle$, since a large occupation in state 1 builds up only when the occupation in state 3 is small. This small occupation of state 3 causes a larger particle number in state 2 (due to conserved particle number). Thus, the occupations of the states 1 and 2 are positively correlated.

All these nontrivial two-particle correlations can be included within an augmented mean-field theory. The equations of motion for the two-particle correlations $\langle \hat{n}_k \hat{n}_i \rangle$ read

$$\begin{aligned} \frac{d}{dt} \langle \hat{n}_k \hat{n}_i \rangle = & \sum_j \{ (A_{kj} + A_{ij}) \langle \hat{n}_k \hat{n}_i \hat{n}_j \rangle + R_{kj} \langle \hat{n}_i \hat{n}_j \rangle + R_{ij} \langle \hat{n}_k \hat{n}_j \rangle - (R_{jk} + R_{ji}) \langle \hat{n}_k \hat{n}_i \rangle \\ & + \delta_{ik} [R_{kj} (\langle \hat{n}_j \rangle + \langle \hat{n}_k \hat{n}_j \rangle) + R_{jk} (\langle \hat{n}_k \rangle + \langle \hat{n}_k \hat{n}_j \rangle)] \} \\ & - R_{ik} (\langle \hat{n}_k \rangle + \langle \hat{n}_k \hat{n}_i \rangle) - R_{ki} (\langle \hat{n}_i \rangle + \langle \hat{n}_k \hat{n}_i \rangle). \end{aligned} \quad (9.5)$$

These equations still involve third-order correlations $\langle \hat{n}_k \hat{n}_i \hat{n}_j \rangle$ (according to the standard hierarchy). The equations of motion for the mean occupations (6.1) read,

$$\frac{d\langle \hat{n}_k \rangle}{dt} = \sum_j (A_{kj} \langle \hat{n}_k \hat{n}_j \rangle + R_{kj} \langle \hat{n}_j \rangle - R_{jk} \langle \hat{n}_k \rangle). \quad (9.6)$$

The set of equations is closed by assuming trivial three-particle correlations,

$$\left\langle (\hat{n}_i - \langle \hat{n}_i \rangle) (\hat{n}_j - \langle \hat{n}_j \rangle) (\hat{n}_k - \langle \hat{n}_k \rangle) \right\rangle \approx 0, \quad (9.7)$$

for all i , j , and k [except for $i = j = k$, which drops out of Eq. (9.5)]. Thus the three-particle correlations can be approximated by

$$\langle \hat{n}_k \hat{n}_i \hat{n}_j \rangle \approx \langle \hat{n}_i \rangle \langle \hat{n}_j \rangle \langle \hat{n}_k \rangle + \langle \hat{n}_i \rangle \zeta_{jk} + \langle \hat{n}_j \rangle \zeta_{ik} + \langle \hat{n}_k \rangle \zeta_{ij}. \quad (9.8)$$

The stationary state of the equation systems (9.5) and (9.6) together with Eqs. (9.8) and (9.1) provides the solution in the augmented mean-field theory. Results of this augmented theory are shown in Fig. 5.2 and agree well with the quasiexact results obtained by Monte-Carlo simulations.

Within the augmented mean-field theory, the state is not only described in terms of the mean occupations $\langle \hat{n}_i \rangle$, but also in terms of two-particle correlations $\langle \hat{n}_k \hat{n}_i \rangle$. As a consequence, we must fix not only the mean total particle number to a value N by requiring

$$\langle \hat{N} \rangle = \sum_i \langle \hat{n}_i \rangle = N \quad (9.9)$$

but also enforce vanishing total particle fluctuations

$$\Delta N^2 := \langle N^2 \rangle - \langle \hat{N} \rangle^2 = \sum_{ij} \zeta_{ij} = 0. \quad (9.10)$$

In principle, it also allows for other choices $\Delta N > 0$ characterizing possible number fluctuations of the initial state.

10. Heat current

A signature of nonequilibrium steady states is a persistent flow, e.g., heat current through the system. This flow is caused by the persistent probability flow between eigenstates (or Floquet states) of the system when detailed balance [Eq. (2.41)] is broken. In this chapter, we discuss the heat current in systems exhibiting Bose selection. We derive the heat current for both autonomous and Floquet systems and subsequently discuss one example for each of these cases. In autonomous systems, the heat current increases strongly when switching from a single condensate to Bose selection (of several states). We propose a quantum switch for heat conductivity based on this effect [57, 58].

In the autonomous system, heat flows from the hotter bath to the colder one. The heat current from the bath b into a single-particle system is given by

$$\dot{Q}^{(b)} = \sum_{ij} (E_j - E_i) R_{ji}^{(b)} p_i. \quad (10.1)$$

For an ideal Bose gas, this heat current reads

$$\dot{Q}^{(b)} = \sum_{i,j \neq i} (E_j - E_i) R_{ji}^{(b)} (\langle \hat{n}_i \hat{n}_j \rangle + \langle \hat{n}_i \rangle). \quad (10.2)$$

The energy transport is caused by transitions between all pairs $i \neq j$ of states and depends also on the occupation in the final state j due to the bosonic enhancement.

Floquet systems dissipate energy from the driving to the environment [53]. The driving provides (or absorbs) energy when the system absorbs (or emits) K photons of total energy $K\hbar\omega$. Thus the heat current from the bath (into the system) reads

$$\dot{Q} = \sum_{ijm} (\varepsilon_j - \varepsilon_i - K\hbar\omega) R_{ji}^K p_i. \quad (10.3)$$

Also pseudotransitions, which are described by rates $R_{ii}^{K \neq 0}$, contribute to the heat current [53]. These transitions transfer energy between the driving and the bath without changing the Floquet state. For an ideal Bose gas, the heat current reads

$$\dot{Q} = \sum_m \sum_{i,j \neq i} (\varepsilon_j - \varepsilon_i - K\hbar\omega) R_{ji}^K (\langle \hat{n}_i \hat{n}_j \rangle + \langle \hat{n}_i \rangle) - \sum_m \sum_i K\hbar\omega R_{ii}^K (\langle \hat{n}_i^2 \rangle + \langle \hat{n}_i \rangle). \quad (10.4)$$

Note that the pseudotransitions (the second sum) depend on the occupation number fluctuations

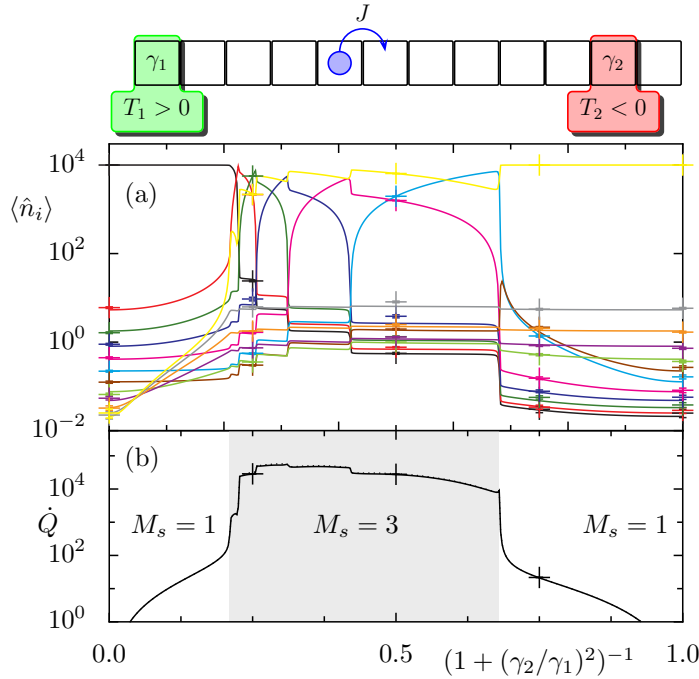


Figure 10.1: Heat current \dot{Q} through a tight-binding chain coupled to two heat baths from the hot (negative-temperature) bath to the colder one depending on the relative coupling strength $(1 + (\gamma_2/\gamma_1)^2)^{-1}$. (a) Mean occupation numbers $\langle \hat{n}_i \rangle$ obtained from mean-field theory (solid lines), and Monte-Carlo simulations (crosses). On the left-hand (right-hand) side the occupations decrease (increase) with the eigenenergies, respectively. Thus the colors are, e.g., black for the ground state and yellow for the highest-excited state. Several selected states are found since the meaning of the ground state is lost when both baths are coupled with similar coupling strength. (b) Heat current \dot{Q} through the system from the right (hotter and population-inverted) bath into the left bath obtained by mean-field theory (solid line), augmented mean-field theory (dotted line, almost perfectly on top of the mean-field results) and Monte-Carlo simulations (crosses). The heat flow increases by three orders of magnitude when several states are selected (shaded area). (a,b) The parameters are as in Fig. 5.2(c), but for (fixed) particle number $N = 10^4$ and length $M = 12$.

via $\langle \hat{n}_i^2 \rangle$, while these number fluctuations drop out in autonomous systems. The properties of these number fluctuations, which can strongly affect the heat current, are described accurately within the augmented mean-field theory only since contributions of nontrivial correlations are neglected otherwise [Chap. 9].

A chain coupled to two baths, a normal bath and a population-inverted one, exhibits Bose selection of several states when the coupling strengths to both baths are similar. Figure 10.1(a) shows the occupations of such a chain [see also Fig. 5.2(c)] depending on its relative coupling $1/(1 + (\gamma_1/\gamma_2)^2)$, where γ_1 (γ_2) denotes the coupling strength to the left (right) bath, respectively. Here the total particle number N is fixed. For $\gamma_2 = 0$ (left-hand side), only the left (positive-temperature) bath is coupled to the chain. In this case, the chain equilibrates to the temperature of the left bath T_1 . A Bose condensate is formed in the ground state (black line). For $\gamma_1 = 0$ (right-hand side), only the population-inverted bath is coupled to the chain. Here the highest excited state (yellow line) takes the role of the ground state and hosts the condensate. In the intermediate regime, neither of these states fulfills the condition (7.9), so that the notion of the ground state becomes meaningless and several states are selected.

The heat current depends strongly on the number of selected states in autonomous systems. Figure 10.1(b) shows the heat current from the hotter (population-inverted) bath to the colder one. In particular, it shows that the heat current increases drastically as soon as several states are selected (shaded area). In this case, the main contribution of the heat current is caused by transition between

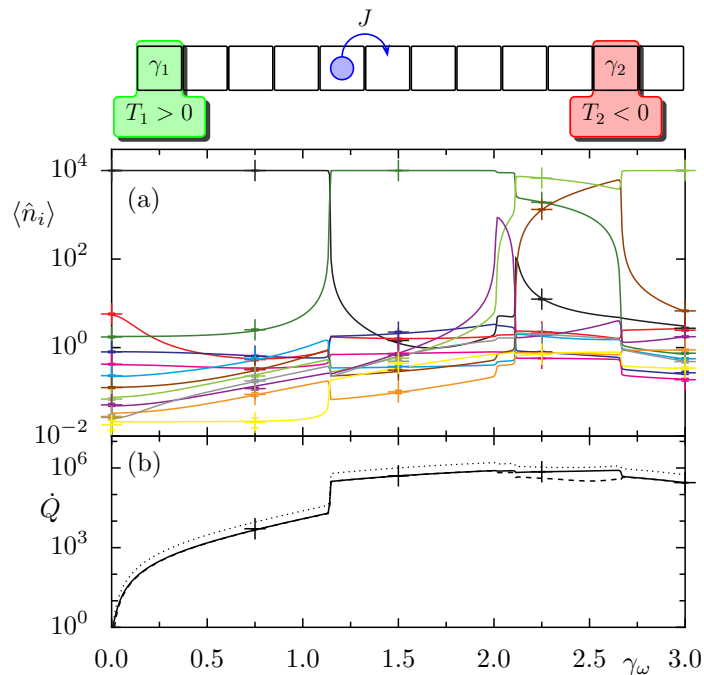


Figure 10.2: Heat current from a time-periodically-driven tight-binding chain into a heat bath depending on the driving strength γ_ω . (a) Mean occupation numbers $\langle \hat{n}_i \rangle$ obtained from mean-field theory (solid lines) and Monte-Carlo simulations (crosses). On the left-hand side, the occupations decrease with the energies of the undriven scenario. Thus, e.g., the black state is the one which connects adiabatically to the ground state when switching the driving off. (b) Heat current \dot{Q} from the driven system into the bath obtained from augmented mean-field theory (solid line), mean-field theory (dotted line), and Monte-Carlo simulations (crosses). The heat current caused by pseudotransitions (dashed line) was obtained by the augmented mean-field theory. In case of a single Floquet condensate, the pseudotransitions cause almost the entire heat current. (a,b) Parameters as in Fig. 5.2(d) but for (fixed) total particle number $N = 10^4$ and length $M = 12$.

pairs of Bose-selected states, $i, j \in \mathcal{S}$. Due to their large occupations, $\langle \hat{n}_i \rangle, \langle \hat{n}_j \rangle \propto N$, the heat current depends quadratically on the particle number N . When only a single state is selected, one involved state must be a nonselected state, which has a small occupation, so that these particle transitions are suppressed and the heat current depends only linearly on the particle number and, thus, is much smaller.

We propose to exploit the switching between one and several selected states to build a quantum switch which controls the heat current.

In a time-periodically driven chain in contact with a heat bath, transitions at which the set of Bose-selected states changes are triggered by ramping up the driving strength. Figure 10.2(a) shows the steady state of such a Floquet system for varied driving strength γ_ω and fixed total particle number N [see also Fig. 5.2(d)]. In the equilibrium situation of the undriven chain, $\gamma_\omega = 0$, (left-hand side in Fig. 10.2), a Bose-Einstein condensate is found. In the weakly driven system, $\gamma_\omega < 1.1$, that state which is adiabatically connected to the ground state remains the only state hosting the condensate. At stronger driving strength about $1.1 < \gamma_\omega < 2.0$, another state takes over the role of the ground state, i.e., hosts the single condensate. For even stronger driving, $2.0 < \gamma_\omega < 2.5$, several Floquet states are selected.

The drastic increase of the heat current when several states become selected does not occur in Floquet systems as shown in Fig. 10.2(b). Namely already for a single selected state a strong increase of the heat current can be observed. The reason is that pseudotransitions [Eq. (10.4)] allow heat transport even for single-particle transitions from the condensate state to this same state. Indeed, these pseudotransitions are the dominant contribution in the regime where only a single state is Bose-

selected. Only in the region where several states are selected, the contribution of the pseudotransitions (dashed line) is substantially smaller than the total heat current (solid line). Note also that the heat current of the pseudotransitions depends on the particle-number fluctuations $\langle n_i^2 \rangle$. Therefore, the augmented mean-field theory (solid lines) agrees much better with the exact Monte-Carlo results than the standard mean-field approximation (dotted line).

11. Small and zero rates

In this chapter, we discuss new effects, which may occur when some rates are much smaller than others: the existence of preasymptotic states at intermediate particle numbers. We show by numerical observations that this preasymptotic state is determined by the set of selected states obtained from the original rate matrix by neglecting all small rates. The existence of this preasymptotic state also justifies the cut-off of the Floquet state basis, an approximation we made so far. We generalize the selection criterion (15.8) to situations where some rates are zero. By doing this, we are able to treat the preasymptotic state and to obtain the asymptotic theory for systems where some rates are exactly zero. Hereby we find that the number of selected states can also be even in these cases.

11.1. Small rates

Small rates appear naturally when states are coupled weakly to each other since they hardly overlap either with each other or with the bath(s) [cf. Eqs. (2.29) and (2.38)]. In the following, we discuss a preasymptotic state emerging at intermediate particle numbers and justify the cut-off in the Floquet state basis.

A minimal example illustrating this preasymptotic state is an artificial three-state model. Its rates shall be given by

$$R = \begin{pmatrix} 0 & 1 & 2\varepsilon \\ 2 & 0 & 2 \\ \varepsilon & 4 & 0 \end{pmatrix}, \quad (11.1)$$

where $\varepsilon = 10^{-3}$. The rates coupling state 1 and 3 are much smaller than the others, as also sketched in the inset of Fig. 11.1(a). Moreover, this Figure shows the existence of a preasymptotic state in the regime of intermediate total particle numbers $10 < N < 10^3$. Here only state 3 acquires a large occupation, although all states are selected for $N \rightarrow \infty$. The preasymptotic state is given by the Bose selection of a rate matrix obtained by neglecting all small rates,

$$R^a = \begin{pmatrix} 0 & 1 & 0 \\ 2 & 0 & 2 \\ 0 & 4 & 0 \end{pmatrix}. \quad (11.2)$$

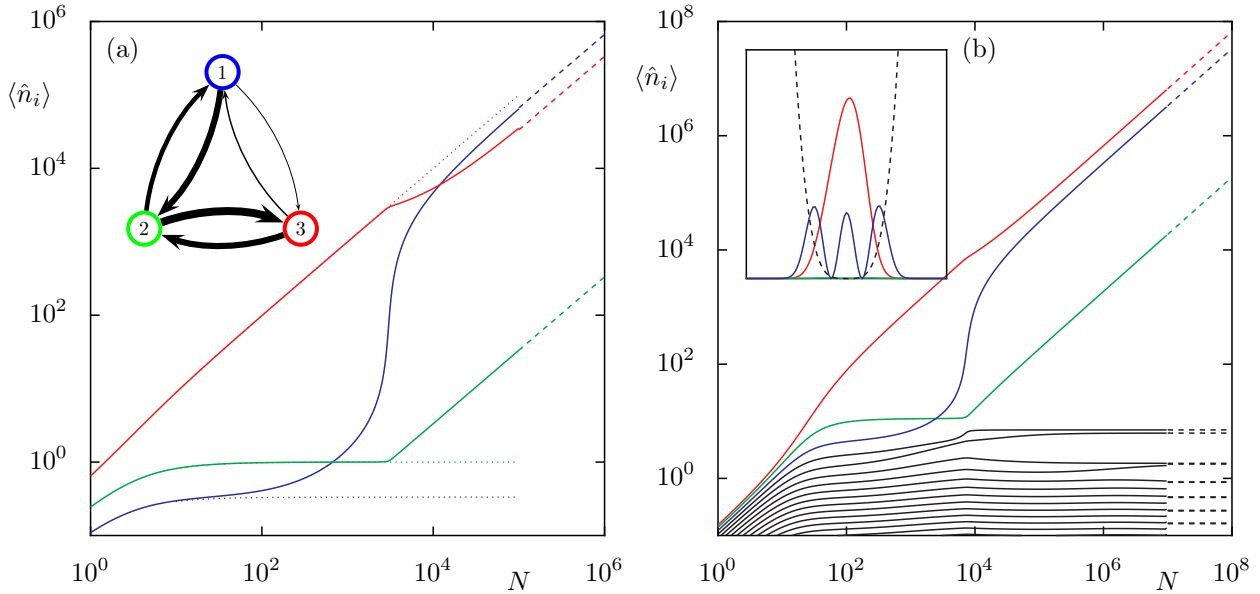


Figure 11.1.: Preasymptotic state caused by small rates. The dependence of the mean occupations $\langle \hat{n}_i \rangle$ on total particle number N are shown. These results are obtained using mean-field theory (solid lines) and asymptotic theory (dashed lines). (a) The model is given by the matrix R defined in Eq. (11.1), which is visualized in the inset (line widths reflect rates). Furthermore, the dotted lines show occupations $\langle \hat{n}_i \rangle$ obtained by the asymptotic theory for the approximate rate matrix R^a defined in Eq. (11.2), where the small rates are neglected. Blue, green, and red lines describe $\langle \hat{n}_1 \rangle$, $\langle \hat{n}_2 \rangle$, and $\langle \hat{n}_3 \rangle$, respectively. Near $N \sim 10$ the system approaches a preasymptotic state with a single selected state, described by R^a , before above $N \sim 10^3$ a crossover separates this regime from true asymptotic state, where all states are selected. (b) The similar preasymptotic state occurs in the driven quartic oscillator, given by the angular driving frequency $\omega = 6.6$, the driving strength $\gamma_\omega = 0.2$, and the inverse bath temperature $\beta = 0.05$. The colors red, green, and blue indicate the occupations $\langle \hat{n}_0 \rangle$, $\langle \hat{n}_1 \rangle$, $\langle \hat{n}_2 \rangle$ (ordered according to the cycle-averaged energy), respectively. It seems that the asymptotic results (dashed lines) of some nonselected states are missing. In fact, also these states are selected at much larger particle numbers (not shown) but with occupations much smaller than the occupations of the other selected states. The inset shows the condensate densities $\lim_{N \rightarrow \infty} \langle \hat{n}_i \rangle |\varphi_i(x)|^2 / N$.

Indeed, for this rate matrix only state 3 is selected (dotted lines). However, when increasing the particle number above $N > 10^4$, the system enters the true asymptotic regime, which has been discussed so far and where all states are selected (though state 2 still has an occupation three orders of magnitude smaller than the others).

This preasymptotic state justifies to cut-off the state space even though each state may affect the whole selection. The effect is illustrated by the results for a quartic oscillator shown in Fig. 11.1(b). While in the preasymptotic state (in the intermediate regime $10 < N < 10^4$) only the state 0 (red line) is selected, for $N > 10^4$ the states 2 (blue line) and 1 (green line) become selected as well. The selection of other states must occur (in the limit of large particle numbers) since the state 0 violates the condition (7.9) of a ground-state-like state via its coupling to state 2 (and others). However, in the preasymptotic state up to particle numbers $N < 10^4$, the state 0 is the only selected state since the coupling to state 2 is small enough. In principle, cutting-off states $i \geq 2$ would not affect the occupation in state 0 and 1 in this intermediate regime. This example demonstrates the cut-off of the basis for numerical purposes.

The decision which state can be cutted-off depends on the rate matrix. The criterion shall be that only states are cutted-off which have a small occupation *and* do not affect the occupations of other kept states significantly. We neglect all states which are coupled only with small rates to the states that are kept and states that couple only to little occupied states. In the example of the quartic oscillator, the ordering according to their cycle-average energy [Eq. (2.3)] provides a good criterion for the cut-off due to the structure of the rates [cf. Fig. 3.5]. Recall that all chaotic states, which have small cycle-averaged energies, couple to each other, while regular states, which have larger cycle-averaged energies, couple in a nearest-neighbor fashion. We can disregard all (regular) states above a certain cycle-average energy since the disregarded states have small occupations and no significant coupling to the kept states that have a large occupation (e.g., the chaotic ones). In all presented examples, states with occupation $\langle \hat{n}_i \rangle > 0.03$ are kept. However, this cut-off is valid only up to a certain particle number since for large particle numbers, small rates are eventually resolved by the system.

11.2. Zero rates

Here we generalize the selection criterion (7.6) to systems where some rates are zero. This is necessary to obtain the preasymptotic state not only for rate matrices where small rates are neglected, but also for cases where rates are exactly zero. We find the following structure: Selected states connected by nonzero rates form simple clusters. All simple clusters form a single cluster where two simple clusters are regarded as connected if they have nonzero rates to same nonselected state(s).

We exclude still cases where the rate matrices are disconnected, i.e., where it is impossible to reach every state i from every other state j in a sequence of quantum jumps (and vice versa). In this case, the steady state of the system would not be unique anymore [142] and would depend on the initial conditions.

In order to discuss the impact of zero rates, let us briefly recapitulate the derivation of the selection criterion (7.6) for the case of fully-connected rate matrices based on the systematic high-density expansion [Chap. 7.3]. Here the coefficients ν_i and $\nu_i^{(r)}$ are obtained by the zeroth and r -th order of the expansion (7.15), respectively. Since the selection criterion depends on the leading order of the selected and nonselected states, it is derived from the zeroth and first order of this expansion only. This situation contrasts the situations for zero rates, where the selected states may decompose into several (uncoupled) clusters, so that higher orders are necessary to determine the parameters ν_i .

Let us start with the zeroth-order equation of the systematic high-density expansion (7.18). As before, we conclude that the leading coefficients ν_i are nonzero only for a set of selected states \mathcal{S} ,

$$0 = \begin{cases} \sum_{j \in \mathcal{S}} A_{ij} \nu_j & \forall i \in \mathcal{S}, \\ \nu_i & \forall i \notin \mathcal{S}. \end{cases} \quad (11.3)$$

Now we have to take into account that the set of selected states \mathcal{S} may consist of K uncoupled subsets \mathcal{S}_α ,

$$\mathcal{S} = \mathcal{S}_1 \cup \mathcal{S}_2 \cup \cdots \cup \mathcal{S}_K, \quad (11.4)$$

with $R_{ij} = 0$ for all $i \in \mathcal{S}_\alpha, j \in \mathcal{S}_\beta, \alpha \neq \beta$. Each subset \mathcal{S}_α fulfills Eqs. (11.3) individually,

$$\sum_{j \in \mathcal{S}_\alpha} A_{ij} \nu_j = 0 \quad \forall i \in \mathcal{S}_\alpha. \quad (11.5)$$

Without fine-tuning, this is guaranteed as long as the number of states in each of the subsets \mathcal{S}_α is odd. Note, the total number of selected states M_S can now also be even, namely if and only if the number of subsets K is even. For $K = 1$ (including the case of fully-connected rate-matrices) the set \mathcal{S} and the normalization condition (7.16) determines ν_i . For $K > 1$, however, this is not the case anymore. Here the relative occupation of a subset \mathcal{S}_α , defined by $\nu_{\mathcal{S}_\alpha} = \sum_{i \in \mathcal{S}_\alpha} \nu_i$, is not fixed since the ratios $\nu_{\mathcal{S}_\alpha} / \nu_{\mathcal{S}_\beta}$ with $\alpha \neq \beta$ are not determined by Eqs. (11.5). The normalization condition (7.16) only requires that $\sum_{\alpha=1}^K \nu_{\mathcal{S}_\alpha} = 1$. The ratios $\nu_{\mathcal{S}_\alpha} / \nu_{\mathcal{S}_\beta}$ (corresponding to $K - 1$ parameters) remain to be determined from equations of higher orders.

We proceed with the first order ($\propto N^{-1}$) of the series expansion (7.17) to determine the relative occupations $\nu_{\mathcal{S}_\alpha}$ and the leading-order occupations of the nonselected states. We distinguish two groups of nonselected states,

$$\bar{\mathcal{S}} = \bar{\mathcal{S}}' \cup \bar{\mathcal{S}}'', \quad (11.6)$$

namely the set $\bar{\mathcal{S}}'$ of states that are directly coupled to any selected state (via nonzero rates) and the set $\bar{\mathcal{S}}''$ of all other nonselected states. The leading coefficients of all states $i \in \bar{\mathcal{S}}'$ are given by the familiar result

$$\nu_i^{(1)} = - \frac{\sum_{j \in \mathcal{S}} R_{ij} \nu_j}{\sum_{j \in \mathcal{S}} A_{ij} \nu_j} \quad \forall i \in \bar{\mathcal{S}}'. \quad (11.7)$$

Note that for states $i \in \bar{\mathcal{S}}'$ that are coupled to selected states belonging to two subsets \mathcal{S}_α and \mathcal{S}_β (or more), the right-hand side of Eq. (11.7) depends on the ratio $\nu_{\mathcal{S}_\alpha} / \nu_{\mathcal{S}_\beta}$, which is not determined yet. In this case the ratio $\nu_{\mathcal{S}_\alpha} / \nu_{\mathcal{S}_\beta}$ can be obtained from Eqs. (11.10) below. The leading coefficients of the states in set $\bar{\mathcal{S}}''$ drop out of the first-order equations and must be determined via the second order of the series expansion [see Eqs. (11.11) below]. Furthermore, we obtain the missing relative occupations $\nu_{\mathcal{S}_\alpha} / \nu_{\mathcal{S}_\beta}$ in the following way: For the selected states $i \in \mathcal{S}_\alpha$ of the subset \mathcal{S}_α , the first order of Eq. (7.17) [with Eq. (11.5)] reads

$$0 = \sum_{j \in \mathcal{S}_\alpha} \left[R_{ij} \nu_j - R_{ji} \nu_i + A_{ij} \nu_i \nu_j^{(1)} \right] + \sum_{j \in \bar{\mathcal{S}}'} \left[-R_{ji} \nu_i + A_{ij} \nu_i \nu_j^{(1)} \right] \quad \forall i \in \mathcal{S}_\alpha. \quad (11.8)$$

Summing over all these states $i \in \mathcal{S}_\alpha$, it simplifies to

$$0 = \sum_{j \in \bar{\mathcal{S}}'} \sum_{i \in \mathcal{S}_\alpha} \nu_i (R_{ji} + A_{ji} \nu_j^{(1)}). \quad (11.9)$$

Here, all nonselected states $j \in \bar{\mathcal{S}}'$ that couple only to selected states of a single subset \mathcal{S}_α do not contribute to the sum since their occupations are given by $\nu_j^{(1)} = -(\sum_{i \in \mathcal{S}_\alpha} R_{ji} \nu_i) / (\sum_{i \in \mathcal{S}_\alpha} A_{ji} \nu_i)$ according to Eq. (11.7). Thus, we obtain

$$0 = \sum_{j \in \bar{\mathcal{S}}_{\alpha+}} \sum_{i \in \mathcal{S}_\alpha} \nu_i (R_{ji} + A_{ji} \nu_j^{(1)}) \quad \forall \alpha, \quad (11.10)$$

where $\bar{\mathcal{S}}_{\alpha+}$ denotes the set of nonselected states that couple to the subset \mathcal{S}_α and at least to one more selected state of a different subset \mathcal{S}_β with $\beta \neq \alpha$. If this set $\bar{\mathcal{S}}_{\alpha+}$ is not empty, Eqs. (11.10) determine the missing relative occupations $\nu_{\mathcal{S}_\alpha} / \nu_{\mathcal{S}_\beta}$. Indeed, we will argue below that all subsets \mathcal{S}_α of selected states must form a cluster, where a subset \mathcal{S}_α is connected to another one \mathcal{S}_β via at least one nonselected state coupling to states of both subsets via nonzero rates. This guarantees that all relative occupations $\nu_{\mathcal{S}_\alpha} / \nu_{\mathcal{S}_\beta}$ can be determined from Eqs. (11.10) and (11.7) and, thus, all parameters ν_i are determined.

The leading-order occupations $\nu_i^{(1)}$ of the nonselected states that do not couple to any of the selected states, the set $\bar{\mathcal{S}}''$, are determined by the second order of the series expansion, Eqs. (7.17). For these states, this second order simplifies to

$$0 = \sum_{j \in \bar{\mathcal{S}}} \left(R_{ij} \nu_j^{(1)} - R_{ji} \nu_i^{(1)} + A_{ij} \nu_i^{(1)} \nu_j^{(1)} \right) \quad \forall i \in \bar{\mathcal{S}}'', \quad (11.11)$$

where we used that the sum runs only over nonselected states. Since in these equations the coefficients $\nu_j^{(1)}$ for the states $j \in \bar{\mathcal{S}}'$ are determined already by Eqs. (11.7), we have a well determined set of nonlinear equations.

The statement that all subsets of selected states must form a single connected cluster (in the sense described above) can now be shown by noting that the assumption of several mutually unconnected clusters A, B, C, \dots leads to a contradiction. Let us denote the set of nonselected states directly coupled to the selected states of cluster X by $\bar{\mathcal{S}}'_X$ and note that the mean particle current from one subset of nonselected states $\bar{\mathcal{S}}_1$ to another one $\bar{\mathcal{S}}_2$ is in leading order given by

$$J_{\bar{\mathcal{S}}_2 \bar{\mathcal{S}}_1} = \sum_{i \in \bar{\mathcal{S}}_2} \sum_{j \in \bar{\mathcal{S}}_1} (A_{ij} \nu_i^{(1)} \nu_j^{(1)} + R_{ij} \nu_j^{(1)} - R_{ji} \nu_i^{(1)}). \quad (11.12)$$

The total current into $\bar{\mathcal{S}}''$ then reads $J_{\bar{\mathcal{S}}''} = J_{\bar{\mathcal{S}}'' \bar{\mathcal{S}}'} = J_{\bar{\mathcal{S}}'' \bar{\mathcal{S}}_A} + J_{\bar{\mathcal{S}}'' \bar{\mathcal{S}}_B} + \dots$. It is directly given by summing the right-hand side of Eq. (11.11). Consequently, it vanishes in the steady state as it should, $J_{\bar{\mathcal{S}}''} = 0$. The total current into the cluster A reads $J_{\bar{\mathcal{S}}_A} = J_{\bar{\mathcal{S}}_A \bar{\mathcal{S}}''} + J_{\bar{\mathcal{S}}_A \bar{\mathcal{S}}_B} + J_{\bar{\mathcal{S}}_A \bar{\mathcal{S}}_C} + \dots$. Obviously, it should also vanish in the steady state. However, generically this is impossible for

more than a single cluster. Namely, (without fine-tuning) the individual terms $J_{\bar{\mathcal{S}}_A \bar{\mathcal{S}}''}$, $J_{\bar{\mathcal{S}}_A \bar{\mathcal{S}}_B}$, ..., containing the coefficients $\nu_i^{(1)}$ determined from Eqs. (11.7) and (11.11), can neither be expected to vanish individually nor to cancel each other. In contrast, for a single cluster, one has $J_{\bar{\mathcal{S}}_A} = J_{\bar{\mathcal{S}}_A \bar{\mathcal{S}}''} = -J_{\bar{\mathcal{S}}''} = 0$, as required.

We can now conclude the case of zero rates. First of all, Bose selection occurs also for rate matrices with zero rates (i.e., only a subset \mathcal{S} of the states have occupations that grow with the total particle number). Second, the asymptotic occupations of the nonselected states are still determined by the first-order coefficient $\nu_i^{(1)}$, so that their occupations saturate for large N . (In contrast, if $\nu_i^{(2)}$ would describe the leading contribution to the occupations of a state i , it would become unpopulated in the limit of large particle numbers.) This is true also for states contained in $\bar{\mathcal{S}}''$ that are not directly coupled to any selected state.

Both conclusions, Bose selection and saturation, are confirmed by the preasymptotic state that can be observed in Fig. 11.1 for $10^1 \lesssim N \lesssim 10^3$, which is approximately given by the asymptotic state of the rate matrix R^a [Eq. (11.2)]. In the approximated rate matrix R^a , the state 1 is not connected with the selected state 3 and its occupation is well determined by Eq. (11.11). Let us illustrate the above reasoning using this minimal example. The corresponding rate-asymmetry matrix reads

$$A^a = r \begin{pmatrix} 0 & -1 & 0 \\ 1 & 0 & -2 \\ 0 & 2 & 0 \end{pmatrix}. \quad (11.13)$$

Thus, applying only Eqs. (11.3) and (11.7) to this problem and requiring positive occupations, we find two subsets of selected states given by $\mathcal{S}_1 = \{1\}$ and $\mathcal{S}_2 = \{3\}$ with undetermined relative occupation $\nu_{\mathcal{S}_1}/\nu_{\mathcal{S}_2} = \nu_1/\nu_3$ and the leading occupation in the nonselected state

$$\nu_2^{(1)} = -\frac{R_{21}\nu_1 + R_{23}\nu_3}{A_{21}\nu_1 + A_{23}\nu_3} = \frac{2}{-\nu_1 + 2\nu_3}. \quad (11.14)$$

This procedure corresponds to the selection conditions (7.6), and we find a nonunique solution for $0 < \nu_1 < 2/3$ and $\nu_3 = 1 - \nu_1$. However, this is *not* the true solution. Namely since this problem also includes zero rates, Eq. (11.10) has to be applied as well. For $\mathcal{S}_\alpha = \{1\}$ this equation simplifies to $0 = \nu_1(R_{21} + A_{21}\nu_2^{(1)}) = \nu_1(2 + \nu_2^{(1)})$ and $\nu_1 = 0$ follows, contradicting that state 1 is selected. Indeed with the ansatz $\mathcal{S} = \{3\}$, we obtain from Eqs. (11.3)

$$\nu_3 = 1, \quad \nu_1 = \nu_2 = 0, \quad (11.15)$$

from Eq. (11.7)

$$\nu_2^{(1)} = -\frac{R_{23}^a}{A_{23}^a} = 1, \quad (11.16)$$

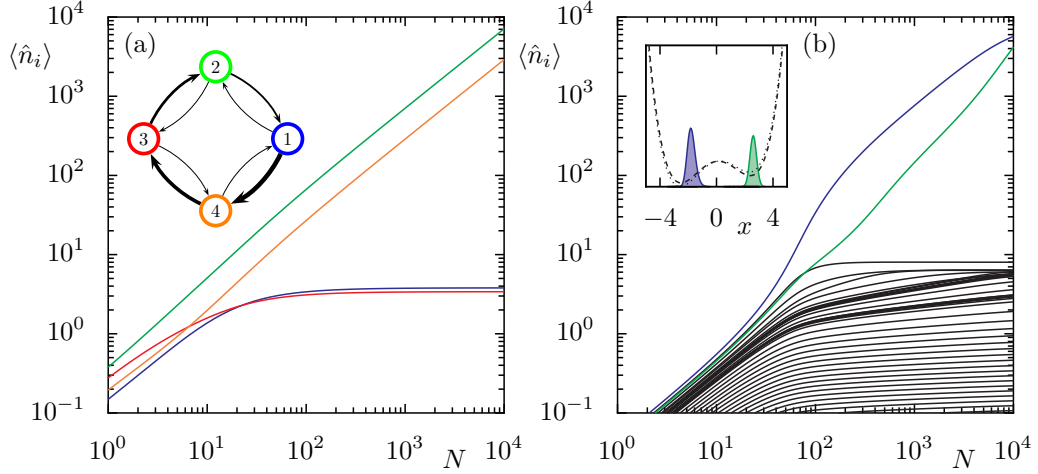


Figure 11.2.: Examples for Bose selection of two uncoupled states as a consequence of zero or small rates. (a) Mean occupation numbers $\langle \hat{n}_1 \rangle$ (blue), $\langle \hat{n}_2 \rangle$ (green), $\langle \hat{n}_3 \rangle$ (red), $\langle \hat{n}_4 \rangle$ (orange) versus the total particle number N for the rate matrix given by Eq. (11.18), which is visualized in the inset (line widths reflect rates). The two selected states 2 and 4 are not coupled directly. (b) Mean occupations $\langle \hat{n}_i \rangle$ versus the total particle number N in an asymmetric double well potential. The inset shows condensate densities (colors as in main figure) together with the time-averaged potential (dashed line) and the maximal tilted potential (dotted line). Small rates cause a preasymptotic regime (the end of this preasymptotic regime is not visible here). The Floquet state space is cutted-off for the 45 Floquet states with lowest cycle-average energy. The potential is given by $V(x, t) = x^4 - 12x^2 + 3x + 3x \cos(7t)$ and the inverse temperature is $\beta = 0.025$ both given in the dimensionless quantities [Sec. 3.3]. (a, b) All results are obtained by the mean-field theory.

and from Eq. (11.11)

$$\nu_1^{(1)} = \frac{R_{12}^a \nu_2^{(1)}}{R_{21}^a - A_{12}^a \nu_2^{(1)}} = \frac{1}{3}. \quad (11.17)$$

Equation (11.10) is trivially fulfilled for the single subset $\mathcal{S}_1 = \mathcal{S}$ since $\bar{\mathcal{S}}_{\alpha+}$ is empty. We can see that the initial assumption $\mathcal{S} = \{3\}$ is confirmed by the fact that we obtain meaningful positive occupation numbers. The just-obtained asymptotic occupations for the rate matrix R^a are plotted as dotted lines in Fig. 11.1 and provide a good description of the preasymptotic state.

For completeness, we will finally present a simple example for a situation where the set of selected states consists of two uncoupled subsets. It is given by a model of four states with the rate matrix

$$R = r \begin{pmatrix} 0 & 2 & 0 & 1 \\ 1 & 0 & 3 & 0 \\ 0 & 1 & 0 & 4 \\ 5 & 0 & 1 & 0 \end{pmatrix}. \quad (11.18)$$

The occupations plotted in Fig. 11.2(a) show that the set of selected states contains two uncoupled states 2 and 4, i.e., $\mathcal{S} = \mathcal{S}_1 \cup \mathcal{S}_2$ with $\mathcal{S}_1 = \{2\}$ and $\mathcal{S}_2 = \{4\}$.

Figure 11.2(b) shows Bose selection in a driven asymmetric double well. Here two condensates, one in each well, emerge. The even number indicates that this is a preasymptotic selection. Indeed, since both states localize in different wells, they overlap hardly and couple via small rates only. Note that the driving is so weak that the right well is always above the left one.

While we could find the Bose-selected states in the two examples directly, an efficient algorithm would be helpful for larger systems. However, we cannot apply the efficient algorithm presented in Chap. 16 in order to find the set of selected states since the selected states \mathcal{S} are no longer determined by the conditions (7.6) anymore. (Neither one can apply the algorithm of Ref. [143], which is based on the same conditions). It seems likely that the set of selected states of the mean-field equations are still unique and determined by the requirement of having positive occupations, as the full many-body master equation possesses a unique steady state. However, unlike in the case of fully connected rate matrices, we have no proof for this statement.

12. Lotka-Volterra systems and evolutionary game theory

In this chapter, we discuss a link between, on the one hand, Bose selection and, on the other hand, phenomena in evolutionary game theory and population dynamics. This connection, first discussed by Knebel *et al.* [143], relies on the similarities of our asymptotic theory and Lotka-Volterra equations. The latter ones describe the population dynamics under predator-prey interactions. The mechanism of Bose selection is equivalent to the survival of a group of species. In the following, we discuss this connection and point out important differences [58].

The link between Bose selection and population dynamics is established by the similarities between the leading order of the asymptotic theory, Eq. (7.2), and the conservative antisymmetric Lotka-Volterra equations for M species,

$$\dot{N}_i(t) = N_i(t) \sum_j A_{ij} N_j(t). \quad (12.1)$$

The latter equations describe the time evolution of the average populations $N_i(t)$ under the predator-prey interaction given by the skew-symmetric rate matrix A_{ij} . When $A_{ij} > 0$, species i is the predator of the prey j . For each captured prey, the predator creates one offspring. This standard model for the population dynamics in mathematical biology is a special case of the replicator equation [100].

For fully-connected rate matrices, the selection of species is given by the selection criterion (7.6). However there are important differences caused by the underlying mean-field equations. While the Lotka-Volterra equation (12.1) does not include a linear term, such a linear term is present in the mean-field equation (6.3) in form of spontaneous processes. This has various consequences: An extinct species will not revive. Since this extinction can also be caused by strong fluctuations, the group of surviving species is not deterministic. This contrasts the case of Bose gases. Here bosons can also occupy a previously empty state. This causes the general difference that while in the Bose-gas case the nonselected states retain a small but nonzero occupation, they die out completely in the population-dynamics case. Moreover, without the linear term, there is no damping of oscillations in the Lotka-Volterra system. This oscillatory behavior has been observed in the reproduction strategies of lizards [138]. In contrast, the Bose gas reaches a steady state.¹ An extension to include a damping factor in form of spontaneous processes was discussed in Ref. [143].

¹Note, that strong fluctuation in a single realization can still lead to permanent stochastic fluctuations.

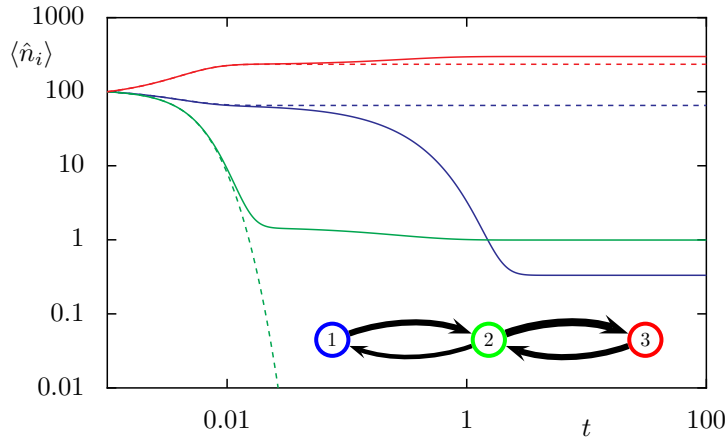


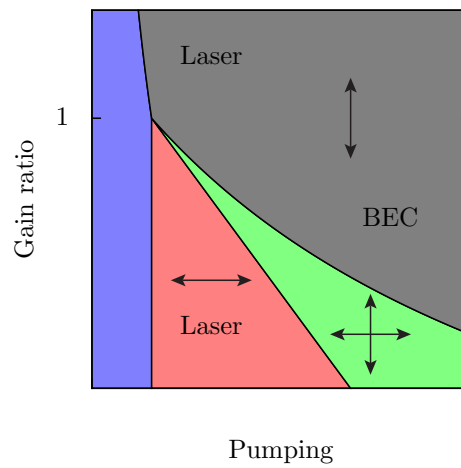
Figure 12.1: Comparison between the dynamics of the mean-field equations (6.3) [solid lines] and the Lotka-Volterra equations (12.1) [dashed lines] for the rate matrix given by Eq. (11.2), which is visualized in the inset (line widths reflect rates). The $N = 300$ particles are initially uniformly distributed. While in both cases the population in state 2 (green) decays on an intermediate timescale, the population in state 1 (blue) decays on a longer timescale in the mean-field equations only leading to a single condensate in state 3 (red). In the Lotka-Volterra system, the two species 1 and 3 survive.

In the case of nonfully-connected rate matrices, the selection criterion (7.6) still determines the surviving species of the Lotka-Volterra system (12.1) [143] but not the selected states in a Bose gas [58]. In the latter case, however, on short timescales the spontaneous processes are irrelevant, so that the selection criterion provides the states which seem to be selected on intermediate timescales (not to be confused with the preasymptotic state for intermediate particle numbers). This is illustrated in Fig. 12.1 by comparing the time evolution governed by the Lotka-Volterra equations (dashed lines) and the mean-field equations (solid lines) for the rates matrix (11.2), which is also sketched in the inset. In both cases, the population of state 2 decays on an intermediate timescale because the condition (7.6) predicts an extinction of occupation n_2 on the level of the Lotka-Volterra equations [see Eq. (11.14)]. For the case of Bose gases, however, this second state saturates at a nonzero occupation, so that on longer timescales the occupation of the first state can slowly decrease. This difference is caused by higher-order terms, which become relevant in the full mean-field equations of motion. Eventually only the third state is selected as predicted by Eq. (11.15). In contrast, in the Lotka-Volterra system, species 1 and 3 survive since there is no direct interaction between these two species.

This difference of the selection in the Lotka-Volterra system and the Bose gas has two consequences: In the Lotka-Volterra system groups of surviving species can survive, which are neither connected directly by a nonzero rate nor indirectly via a species with nonzero rates to species in both groups. Second, the relative number of species in these two groups is determined by the initial conditions.

Part II.

Open Systems



13. Framework

13.1. Introduction

Open systems¹ exchange particles with their environment. In the nonequilibrium steady state, these systems establish a permanent flow of particles through the system. Electron transport in solids is one of the most prominent examples of such a steady-state current. In recent years, this transport has been mimicked in cold-atom experiments by separating a cloud of atoms with a barrier and connecting the both formed reservoirs via a small channel [144, 145].

Other systems are intrinsically driven away from equilibrium by pumping and particle loss, such as photonic systems. Here, the loss of photons caused by imperfect cavities is compensated via an externally-pumped reservoir or a gain medium. The balance between loss and pumping determines the steady state. Examples of these nonequilibrium steady states are lasers.

Many new effects arise when gain and loss compete with intermode kinetics. These scenarios have been realized with exciton-polaritons in microcavities [61], photons in dye-filled microcavities [13], and bimodal microlasers [102] and have attracted huge interest [73, 76]. The steady states of these systems are determined by the interplay of, on the one hand, the intermode kinetics and, on the other hand, the loss and pumping. The demarcation between lasing and Bose condensation constitutes a subtle issue in these systems. For a detailed discussion, let me refer the reader to the introduction in Chap. 1.

This second part of the thesis focuses on the relation between lasing and Bose condensation. More generally, it connects Bose condensation and Bose selection found in closed systems with Bose condensation and lasing in open systems. The canonical and the grand canonical ensemble (the state of closed and open systems in thermal equilibrium, respectively) become equivalent in the thermodynamic limit. However, away from equilibrium, the details of the system, the environment, and their coupling affect the steady state. Nevertheless, we find commonalities between the steady state in open and closed systems far from equilibrium.

We investigate the steady state for a large class of open systems. Our theory presented in Chap. 15 provides a criterion for multi-mode lasing and condensation. We find a remnant of the equivalence of ensembles far from equilibrium between closed and open systems in the limit of strong pumping.

¹In this thesis, we use the definition from statistical physics: In contrast to closed systems, which only exchange energy with their environment, open systems also exchange particles with their environment. [cf. Chap. 1]

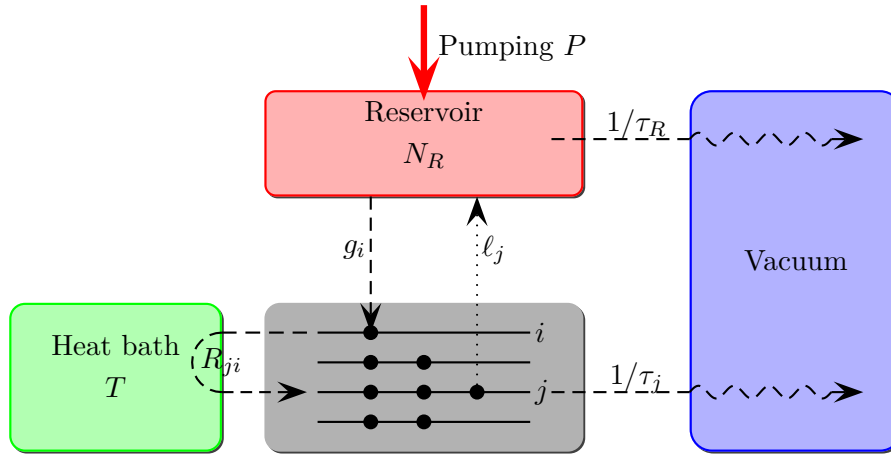


Figure 13.1.: Sketch of open ideal Bose gases driven far away from equilibrium via pumping and loss. The system of interest (gray) is a gas of particles occupying the states $i \in \{0, \dots, M-1\}$. These particles exchange energy with an thermal heat bath (green) at temperature T . Moreover, the particles have a finite lifetime τ_i . The loss is compensated by new particles from the reservoir (red), which is pumped at rate P . In particular, particles are transferred from the reservoir to state i at gain rate g_i but can also be reabsorbed at rate l_j . Reservoir excitations have the finite lifetime τ_R due to decay processes in modes other than the ones considered as system. The interplay of the intermode kinetics with the pumping and loss determines the nonequilibrium dynamics of the system.

We find good agreement between our theory and experimental results for an exciton-polariton gas [101] covered in Chap. 14 and 16 and a bimodal microcavity [102] covered in Chap. 17. In the bimodal cavity, we observe a switching of the mode emitting light coherently from one polarization direction to the other one when ramping up the pumping. We argue that the dominance of the intermode kinetics justifies describing this mode switching as a transition from lasing to Bose-Einstein condensation. Thus this bimodal microcavity could be seen as a minimal instance of a Bose-Einstein condensate of photons.

13.2. Kinetic equations

We consider ideal Bose gases which exchange energy and particles with their environment and suffer from particle loss. Such a scenario is sketched in Fig. 13.1: The heat bath triggers transitions of particles among the single-particle states by providing or absorbing energy. Furthermore, the particles have finite lifetimes caused by the loss. This loss is compensated by new particles from a reservoir so that a persistent particle flow through the system is established. The reservoir is externally pumped.

The dynamics of the mean occupations $\langle \hat{n}_i \rangle$ in each state $i \in \{0, \dots, M-1\}$ are given within the mean-field approximation by the kinetic equations

$$\frac{d}{dt} \langle \hat{n}_i \rangle = D_i^{\text{inter}}(\langle \hat{n}_0 \rangle, \dots, \langle \hat{n}_{M-1} \rangle) + D_i^{\text{open}}(\langle \hat{n}_0 \rangle, \dots, \langle \hat{n}_{M-1} \rangle). \quad (13.1)$$

The first term D^{inter} comprises the intermode kinetics caused by the exchange of energy with its environment and the second part comprises gain and loss processes.

The intermode kinetics reads

$$D_i^{\text{inter}}(\langle \hat{n}_0 \rangle, \dots, \langle \hat{n}_{M-1} \rangle) = \sum_{j=0}^{M-1} [R_{ij} \langle \hat{n}_j \rangle (\langle \hat{n}_i \rangle + 1) - R_{ji} \langle \hat{n}_i \rangle (\langle \hat{n}_j \rangle + 1)]. \quad (13.2)$$

The rates R_{ij} correspond to processes where a single particle is transferred from mode j to mode i via the heat bath which provides or absorbs the energy difference $E_j - E_i$. This kinetics is identical to the one in closed systems of massive bosons [Eq. (6.3)]. Due to the exchange of particles with the environment, which is the second contribution D^{open} discussed below, the system is driven out of equilibrium even when the rates R_{ij} (as in the sketch of Fig. 13.1) are thermal, i.e., fulfill the condition (2.30). This contrasts closed systems.

The dynamics caused by the loss and the influx of new particles is given by

$$D_i^{\text{open}}(\langle \hat{n}_0 \rangle, \dots, \langle \hat{n}_{M-1} \rangle) = G_i (\langle \hat{n}_i \rangle + 1) - L_i \langle \hat{n}_i \rangle. \quad (13.3)$$

Here $L_i = \ell_i + 1/\tau_i$ denotes the total loss rate for particles in the single-particle state i either by its decay with the lifetime τ_i or by reabsorption into the reservoir at rate ℓ_i . The loss is compensated by new particles from the reservoir. The rate for new particles jumping into state i is the gain G_i . The factor $(\langle \hat{n}_i \rangle + 1)$ reflects the final-state stimulation due to bosonic quantum enhancement.

The equation of motion (13.1) is valid under the assumption of weak-coupling. Its derivation within the Born-Markov framework is analog to closed systems [Chap. 2.3] and can be found (for fermions) in Ref. [146].

The reservoir provides new particles to the system. The number of particles in the reservoir affects directly the gain rate of the system. The gain rate is

$$G_i = g_i \langle \hat{N}_R \rangle, \quad (13.4)$$

where g_i is the rate that one of the N_R reservoir particles jumps into state i . The dynamics of the mean reservoir occupation number $\langle \hat{N}_R \rangle$ reads

$$\frac{d}{dt} \langle \hat{N}_R \rangle = P - \frac{\langle \hat{N}_R \rangle}{\tau_R} + \sum_{i=0}^{M-1} [\ell_i \langle \hat{n}_i \rangle - \langle \hat{N}_R \rangle g_i (\langle \hat{n}_i \rangle + 1)]. \quad (13.5)$$

Herein τ_R denotes the lifetime of particles in the reservoir and P denotes the pumping power, the rate at which new reservoir excitations are generated. Particles can also be absorbed from state i by the reservoir at rate ℓ_i . The reservoir is treated classically, namely the loss ℓ_i does not depend on the reservoir occupation $\langle \hat{N}_R \rangle$. By doing so, we assume that all these excitations are distributed over a continuum of states so that each reservoir state possesses an occupation much smaller than unity so

that stimulated process can be neglected in comparison to spontaneous processes.

We are interested in the steady state of this system given by

$$0 = G_i(\langle \hat{n}_i \rangle + 1) - L_i \langle \hat{n}_i \rangle + \sum_{j=0}^{M-1} [R_{ij} \langle \hat{n}_j \rangle (\langle \hat{n}_i \rangle + 1) - R_{ji} \langle \hat{n}_i \rangle (\langle \hat{n}_j \rangle + 1)] \quad (13.6)$$

$$0 = P - \frac{\langle \hat{N}_R \rangle}{\tau_R} + \sum_{i=0}^{M-1} [\ell_i \langle \hat{n}_i \rangle - \langle \hat{N}_R \rangle g_i (\langle \hat{n}_i \rangle + 1)]. \quad (13.7)$$

Before investigating this steady state, we discuss the relaxation kinetics of exciton-polariton systems, which can be described by such equations.

14. Exciton-polaritons in a micro-cavity

This chapter describes exciton-polariton systems [7, 60, 76], which are prime examples for Bose condensations of photonic particles. First, we summarize a few properties of exciton-polariton systems. Then, we recapitulate a recent experiment by Galbiati *et al.* [101], which exemplifies our general findings.

Exciton polaritons are quasiparticles formed by excitons and photons inside a semiconductor heterostructure [75]. The excitons, electron-hole pairs, are trapped in quantum wells and the photons are confined in a microcavity. The electric field of the photons couples to the dipole moment of the excitons such that a photon and an exciton hybridize to a quasiparticle called polariton (in the strong-coupling regime). Figure 14.1 shows the bare photons and excitons (upper and lower dashed line, respectively) as well as the lower-energy and upper-energy polaritons (solid lines) as a result of the hybridization. Polaritons inherit small effective masses and finite lifetimes from the photons which have small effective masses due to their confinement. The excitonic nature causes repulsive interactions among the polaritons and interactions between the polaritons and phonons. These interactions provide a relaxation kinetics.

The experimental realization of polariton condensates [7, 8] has facilitated the investigation of a novel type of condensates. The novelty lies in the intrinsic nonequilibrium nature of the condensate caused by the finite polariton lifetime and the need to balance the loss by external pumping. Furthermore, the extremely light masses of the polaritons allow Bose condensation even at room temperature [147]; and direct observations of the polariton gas is possible due to the photons leaving the cavity.

The major challenge in creating a Bose condensate is to provide a sufficiently fast relaxation compared to the short particle lifetime [60, 61]. The relaxation is slowed down in a region in the

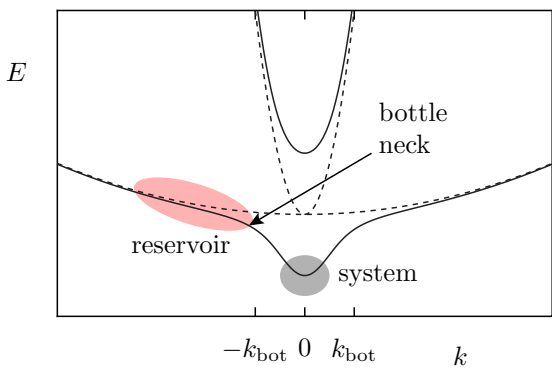


Figure 14.1: Dispersion relation of upper and lower polaritons (upper and lower solid line), cavity photons (upper dashed line), and excitons (lower dashed line) with respect to the in-plane momentum k . The degeneracy of the cavity photons and excitons (at $k = 0$) is lifted by the Rabi splitting in the strong-coupling regime. The lower-energy and upper-energy polaritons result from this coupling. Dividing the lower polariton branch into a reservoir and a system is sketched and motivated by the bottle neck separating both parts.

dispersion relation called bottle neck [Fig. 14.1]. While the lower polaritons are mainly excitons for large in-plane wave numbers $|k| > k_{\text{bot}}$, they have a large photonic contribution for small in-plane wave numbers $|k| < k_{\text{bot}}$. Furthermore, the density of states decreases drastically for small in-plane wave numbers [Fig. 14.1]. As a result, cooling (i.e., scattering to smaller wave numbers) is slowed down before the bottleneck at the in-plane wave number $k \approx k_{\text{bot}}$ and polaritons accumulate incoherently in this bottleneck region [148]. However, when the lifetime of the polaritons at $|k| \approx 0$ is long enough, polaritons can also reach this region since stimulated processes increase the scattering rate. Recently, an almost equilibrated condensation obeying the Bose-Einstein distribution has been observed by extending the lifetimes of the polaritons [73]. The bottle neck allows to separate the dispersion relation into two parts, the reservoir in the bottleneck region and the system around in-plane wave numbers $k \approx 0$ as shown in Fig. 14.1.

A vivid example of polariton condensation in a double-pillar structure has been performed experimentally and simulated numerically by Galbiati *et al.* [101]. The authors observed condensation of polaritons in two coupled micropillars [cf. inset of Fig. 14.2]. In one scenario, this system was pumped asymmetrically, i.e., only in one pillar. The authors observed that while for small pumping the condensate forms in the pumped pillar, it switches to the ground state, which is localized in the unpumped pillar, in the limit of strong pumping. The numerical model, described in Ref. [101], is almost of the form discussed in Chap. 13.2. We will use this example in the following to illustrate our findings. First, we recapitulate the findings in Ref. [101] in a minimalistic numerical model.

The single-particle modes of the polaritons are approximately given by the modes in a two-dimensional asymmetric potential [inset of Fig. 14.2]. The eigenmodes $|\psi_i\rangle$ are solutions of the single-particle Schrödinger equation,

$$E_i \psi_i(x, y) = -\frac{\hbar^2}{2m} \Delta \psi_i(x, y) + V_{\text{dp}}(x, y) + V_{\text{mf}}(x, y). \quad (14.1)$$

Here V_{mf} denotes a mean-field potential caused by the repulsive interaction and

$$V_{\text{dp}}(x, y) = \begin{cases} 0 & \text{when } (x \pm d_{\text{cc}}/2)^2 + y^2 < d^2, \\ \infty & \text{else.} \end{cases} \quad (14.2)$$

denotes the potential of the double pillar (two overlapping disks in top view) of diameter d and with the center-to-center distance $d_{\text{cc}} < d$ [inset of Fig. 14.2].

Interactions are inherently present due to exciton-exciton repulsions. To obtain the equation of motion for the mean occupations (the diagonal elements of the single-particle density operator) from a full microscopic description, one can trace out one of the two particles of the term which describes two-particle collisions. One obtains two contributions, a coherent part, which can be taken into account by an additional (mean-field) potential to the single-particle Hamiltonian, and an incoherent part, which describes nonunitary, dissipative time evolution of Lindblad type. The latter one can be interpreted such that the system forms its own bath as discussed below.

The coherent part is treated by the mean-field potential $V_{\text{mf}}(x, y)$. The repulsive interactions with the reservoir excitations cause a blue shift. Since the left pillar is pumped only, the reservoir excitations are localized in this pillar and the mean-field potential V_{mf} is asymmetric,

$$V_{\text{mf}}(x, y) = \begin{cases} E_{\text{left}} & \text{for } x \leq 0, \\ 0 & \text{for } x > 0. \end{cases} \quad (14.3)$$

Here we take into account only the contribution of the reservoir polaritons and neglect the dependency of the blue shift E_{left} on the reservoir occupation. Despite this approximation, we can reproduce the main features of the system.

The single-particle eigenmodes of the (isolated) system are shown in the inset of Fig. 14.2. Due to the (two-dimensional) asymmetric double-well, low-energy states are localized in either pillar. In particular, the ground state (black) is localized in the right pillar.

The relaxation kinetics is an interplay of, on the one hand, the intermode kinetics and, on the other hand, the gain and loss. The intermode kinetics is caused by the dissipative part of both polariton-polariton and polariton-phonon interactions. We model this contribution by a heat bath. The loss due to the finite lifetime is compensated by new polaritons from the bottle-neck region. The full derivation of the kinetics and the parameters used in Ref. [101] are reproduced and discussed in App. D. The resulting relaxation kinetics is of the form given by Eq. (13.1).

The mode characteristics for ramping up the pumping is shown in Fig. 14.2. For small pumping,

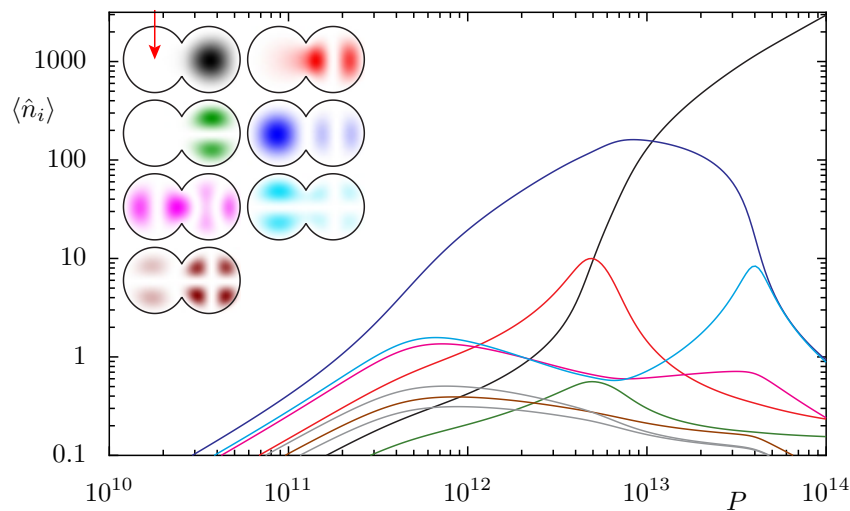


Figure 14.2.: Input-output characteristics of polaritons in an asymmetrically-pumped double-pillar structure. The dependence of the mean polariton occupations $\langle \hat{n}_i \rangle$ on the pumping power P is shown. The inset shows the wave functions $|\psi_i(x, y)|^2$ in the respective colors. The boundary of the double-pillar system in top view looks like two overlapping disks. The system is pumped only in the left pillar (see exemplary red arrow), giving rise to an blue-shift of this pillar resulting in an asymmetric potential. The states are ordered in increasing energies in reading direction ($i = 0, 1, \dots, 6$ are black, red, green, blue, magenta, turquoise, and brown, respectively)

all states are weakly occupied, $\langle \hat{n}_i \rangle \lesssim 1$. Above a threshold, a condensate forms in the third excited state (the fourth state). This state (blue) is the lowest state that is localized in the left pillar so that it significantly overlaps with the reservoir. When further ramping up the pumping, other states acquire significant occupation in certain regimes like the first excited state (red). Eventually, a polariton condensate in the ground state (black) emerges and all other condensates disappear in the limit of strong pumping. This observation in our model reproduces central features observed in Ref. [101]. Here, first a condensate emerges in the third excited state (localized in the left pillar) and, finally, the condensate switches to the ground-state in the limit of strong pumping.

15. Multi-mode condensation

We investigate the mechanism for multi-mode condensation in terms of Bose selection in open driven-dissipative ideal Bose gases. This mechanism separates clearly highly occupied (Bose-selected) modes from all other (nonselected) modes. We also discuss its relation to the Bose selection in closed systems [Chap. 5]. In particular, we find that also an even number of modes can be selected due to the particle exchange. We illustrate our findings by numerical simulations of the polariton system discussed in the previous Chap. 14.

The dynamics of the system is determined by an interplay of, on the one hand, the relaxation due to the intermode kinetics and, on the other hand, the pumping and loss. Let us first recapitulate the asymptotic theory for closed systems, where only intermode kinetics is present [Chap. 7]. Here a group of states is selected in the limit of large particle numbers, $N \rightarrow \infty$, i.e., each selected state but no nonselected state acquires a large occupation. In contrast to closed systems, the total particle number is not conserved and given by a initial condition but it is determined by the balance between pumping and loss. Since the particle number N is not fixed anymore, we focus on the limit where intermode rates are much smaller than gain and loss rates, $L_i, G_i \gg R_{ij}$. To achieve this limit, we scale the term D_i^{open} by a factor $\alpha \gg 1$ so that the equation of motion (13.1) for the occupation of state i reads

$$\frac{d}{dt} \langle \hat{n}_i \rangle = D_i^{\text{inter}}(\langle \hat{n}_0 \rangle, \dots, \langle \hat{n}_{M-1} \rangle) + \alpha D_i^{\text{open}}(\langle \hat{n}_0 \rangle, \dots, \langle \hat{n}_{M-1} \rangle). \quad (15.1)$$

We observe Bose selection in the limit of weak intermode kinetics (i.e., large $\alpha \gg 1$) in Fig. 15.1(a). The occupations of one group of states, the *Bose-selected* states, grow linearly with α . The occupation of each state from the other group, the *nonselected* states, saturates at much smaller values of the order of unity. This behavior is similar to the Bose selection in closed systems taking place in the limit of large total particle numbers. In this section, we will investigate under which condition a single state or several states become selected in an open system and acquire a (macroscopic) occupation.

Motivated by this observation, we expand the mean occupations in series expansions in α^{-1} ,

$$\langle \hat{n}_i \rangle = \nu_i \alpha + \nu_i^1 + \nu_i^2 / \alpha + \dots \quad (15.2)$$

The parameter ν_i is by definition nonzero if and only if the state i is Bose-selected. Within this

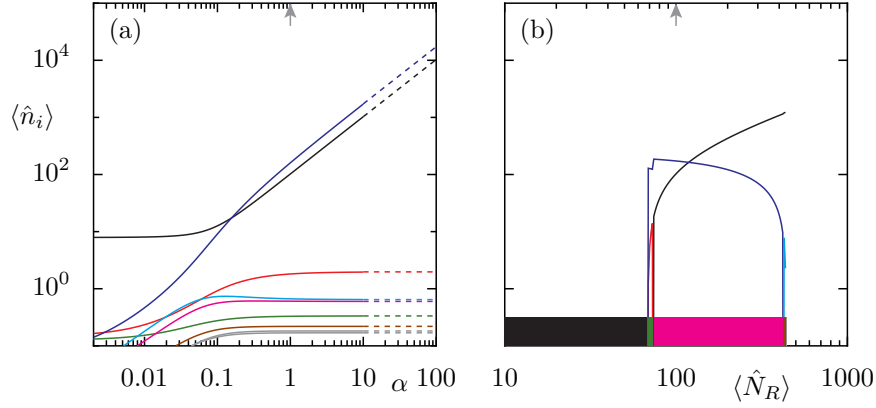


Figure 15.1: Bose selection in the double-pillar system. (a) Mean occupation numbers $\langle \hat{n}_i \rangle$ versus the factor α tuning the system from strong intermode kinetics (left) to weak intermode kinetics (right) [α scales gain and loss as $G_i \rightarrow \alpha G_i$ and $L_i \rightarrow \alpha L_i$, see Eq. (15.1)] for the fixed reservoir occupation $\langle \hat{N}_R \rangle = 100$. For large parameter α , the ground state (black line) and the third state (blue line) acquire large occupations proportionally to α , while the occupation of any other state saturates. The mean-field results (solid lines) are well described by the asymptotic theory (dashed lines) in this limit. (b) Mean occupation numbers $\langle \hat{n}_i \rangle$ of the selected states obtained by the asymptotic theory versus reservoir occupation $\langle \hat{N}_R \rangle$ for $\alpha = 1$. Increasing the reservoir occupation $\langle \hat{N}_R \rangle$ triggers transitions between different sets of Bose-selected states, indicated by different colors in the bottom (black: $\mathcal{S} = \{\}$, green $\mathcal{S} = \{1, 3\}$, pink: $\mathcal{S} = \{0, 3\}$). The steady state exists for reservoir occupations up to $\langle \hat{N}_R \rangle \approx 400$ only.

ansatz, Eqs. (13.6) read:

$$\begin{aligned}
0 = & \alpha^2 \left[\sum_j (R_{ij} - R_{ji}) \nu_i \nu_j + (G_i - L_i) \nu_i \right] \\
& + \alpha \left[\sum_j (R_{ij} \nu_j - R_{ji} \nu_i + (R_{ij} - R_{ji})(\nu_j \nu_i^1 + \nu_j^1 \nu_i)) + (G_i - L_i) \nu_i^1 + G_i \right] \\
& + O(\alpha^{-2}) \quad \forall i.
\end{aligned} \tag{15.3}$$

In a Bogoliubov-like approximation where the effects of nonselected states onto each other and onto selected states are neglected, we obtain the occupations of all states. The leading order of Eq. (15.3) reads

$$0 = \nu_i \left(\sum_j A_{ij} \nu_j + W_i \right) \tag{15.4}$$

with the short-hand notations for the rate asymmetries

$$A_{ij} = R_{ij} - R_{ji} \quad \text{and} \quad W_i = G_i - L_i. \tag{15.5}$$

The solution of Eq. (15.4) is of the form

$$0 = \begin{cases} \sum_{j \in \mathcal{S}} A_{ij} \nu_j + W_i & \forall i \in \mathcal{S}, \\ \nu_i & \forall i \notin \mathcal{S}. \end{cases} \quad (15.6)$$

This provides two disjoint sets of states, namely selected states $i \in \mathcal{S}$ with occupations $\langle \hat{n}_i \rangle \approx \nu_i \alpha$ and nonselected states $i \notin \mathcal{S}$ with saturated occupations, $\nu_i = 0$.

The number of selected states is even except for fine-tuned situations. The existence of a solution of the inhomogeneous set of linear equations (15.6) is guaranteed when the number of selected states \mathcal{S} is even since the matrix \mathbf{A} is (generally) nonsingular in this case. In contrast, for an odd number of selected states, the matrix \mathbf{A} is singular (since it is skew-symmetric) and a (family of) solution exists for fine-tuned inhomogeneities \mathbf{W} only.

The next order of the expansion (15.3) provides the occupations of the nonselected states (in leading order),

$$\langle \hat{n}_i \rangle \approx \nu_i^1 = -\frac{\sum_{j \in \mathcal{S}} R_{ij} \nu_j + G_i}{\sum_{j \in \mathcal{S}} A_{ij} \nu_j + W_i} \quad \forall i \notin \mathcal{S}. \quad (15.7)$$

This equation corresponds to Eq. (7.20) for closed systems.

The set of selected states \mathcal{S} is fixed by the physical requirement that the leading occupations of all states must be nonnegative, i.e., $\nu_i \geq 0 \forall i \in \mathcal{S}$ and $\nu_i^1 \geq 0 \forall i \notin \mathcal{S}$. When such a steady state exists, it is unique as proven in App. C. However, above a certain gain, there exists no steady state but the occupations would grow infinite with time.

In conclusion, we obtain the following selection criterion

$$\sum_j A_{ij} \nu_j + W_i = \mu_i \text{ with } \begin{cases} \nu_i \geq 0 \text{ and } \mu_i = 0, & \text{for } i \in \mathcal{S}, \\ \nu_i = 0 \text{ and } \mu_i \leq 0, & \text{for } i \notin \mathcal{S}, \end{cases} \quad (15.8)$$

with the shorthand notation

$$\mu_i = \sum_{j \in \mathcal{S}} A_{ij} \nu_j + W_i. \quad (15.9)$$

This criterion provides the (unique) set of selected states \mathcal{S} , the occupations of all selected states $\langle \hat{n}_i \rangle \approx \alpha \nu_i \forall i \in \mathcal{S}$ by Eq. (15.6) and the occupations of all nonselected states $\langle \hat{n}_i \rangle \approx \nu_i^1 \forall i \notin \mathcal{S}$ by Eq. (15.7) for a fixed asymmetry \mathbf{W} , i.e., a fixed gain \mathbf{G} and thus a fixed reservoir occupation $\langle \hat{N}_R \rangle$. Figure 15.1(b) shows the set of Bose-selected states and their occupations depending on the reservoir occupation $\langle \hat{N}_R \rangle$. While for small reservoir occupations, no state is selected, several phases where two states are selected appear for larger reservoir occupations. When the reservoir occupation is too large, the steady state does not exist anymore.

The reservoir occupation $\langle \hat{N}_R \rangle$ determines the gain rates via Eq. (13.4) and depends on the pumping

$$P = \frac{\langle \hat{N}_R \rangle}{\tau_R} - \sum_{i \in \mathcal{S}} (\ell_i - \langle \hat{N}_R \rangle g_i) \nu_i. \quad (15.10)$$

If no state is selected, this approximation may fail since our approximation of neglecting subleading contributions ν_i^1 with respect to ν_i^0 is violated. Thus this approximation fails when the contribution due to spontaneous processes in the cavity modes is larger or of the order of the spontaneous loss to all other modes¹.

It turns out that the reservoir favors fine-tuned situations where an odd number of states are Bose-selected. These fine-tuned situations are the transition points in Fig. 15.1(b). In the next chapter, we will see that these transition points become whole intervals of the pumping power P such that also an odd number of selected states can occur.

¹This is exactly the same circumstances which make it necessary to use another definition than the kink in the double-logarithmic input-output curve for the lasing threshold in high- β lasers [149].

16. Transitions

The variation of a system parameter, such as pumping power, can trigger transitions where the occupations change abruptly. These transitions are caused by changes in the set of selected states. Illustrated by the example of exciton polaritons in a double-pillar system [see Fig. 16.1], we discuss the behavior when ramping up the pump power.

We find the following generic behavior: For sufficiently small pumping, no state is selected. The first state is selected by the ordinary laser criterion [62] that the gain exceeds the loss in this mode. Subsequently, several phases follow, which are determined by the interplay of the gain, loss and intermode kinetics. At each transition, a single condensate either emerges or disappears. Eventually, in the limit of strong pumping, the set of selected states is found to be determined by the intermode kinetics alone. This sequence of transitions provides new insights for the discussion on photonic Bose condensations.

Remarkably, the limit of strong pumping is equivalent to the situations in closed systems. Namely, the selection in this limit is determined only by the intermode kinetics (the only kinetics present in closed systems), while the gain and loss determine only the total particle number. Thus this selection resembles the (nonequilibrium) condensation of massive bosons. This shows that there is a leftover from the equivalence of ensembles even far away from equilibrium. This similarity is exploited in an algorithm to find the selected states in closed systems.

If the intermode kinetics is caused by a thermal reservoir, the condensation resembles equilibrium condensation, i.e., a single condensate in the ground state. When the lifetimes of the particles are much longer than the single-particle relaxation timescale, the gas thermalizes to a Bose condensate and a Bose-Einstein distribution in the excited states.

In the following, we discuss the mechanism of the transitions and unveil the generic behavior of the sequence of sets of selected states when increasing the pumping.

16.1. Phase diagram of a photonic system

The phase diagram shown in Fig. 16.1(b) has a simple structure and describes the transitions. This phase diagram shows the dependence of the set of selected states \mathcal{S} on the reservoir occupation $\langle \hat{N}_R \rangle$ and the parameter ℓ . While the reservoir occupation $\langle \hat{N}_R \rangle$ scales the gain rates via $G_i = \langle \hat{N}_R \rangle g_i$, the parameter ℓ shall scale all loss rates via $\ell L_i \rightarrow L_i$ where L_i are the original loss rates. The

radial structure of this phase diagram reflects that the phase depends on the ratio $\alpha = \langle \hat{N}_R \rangle / \ell$ only. Indeed, Fig. 15.1(a) is a radial cut through this phase diagram (within the pink colored phase). When ramping up the reservoir occupation $\langle \hat{N}_R \rangle$ at the fixed loss ℓ (white dashed line), the system passes a sequence of phases: no selected state (gray area), then several phases [the (thin) green, pink, and brown area], where two states are selected in each phase. No steady states exist in the white region. This sequence was shown in Fig. 15.1(a) in detail. In all these phases, the number of selected states is even.

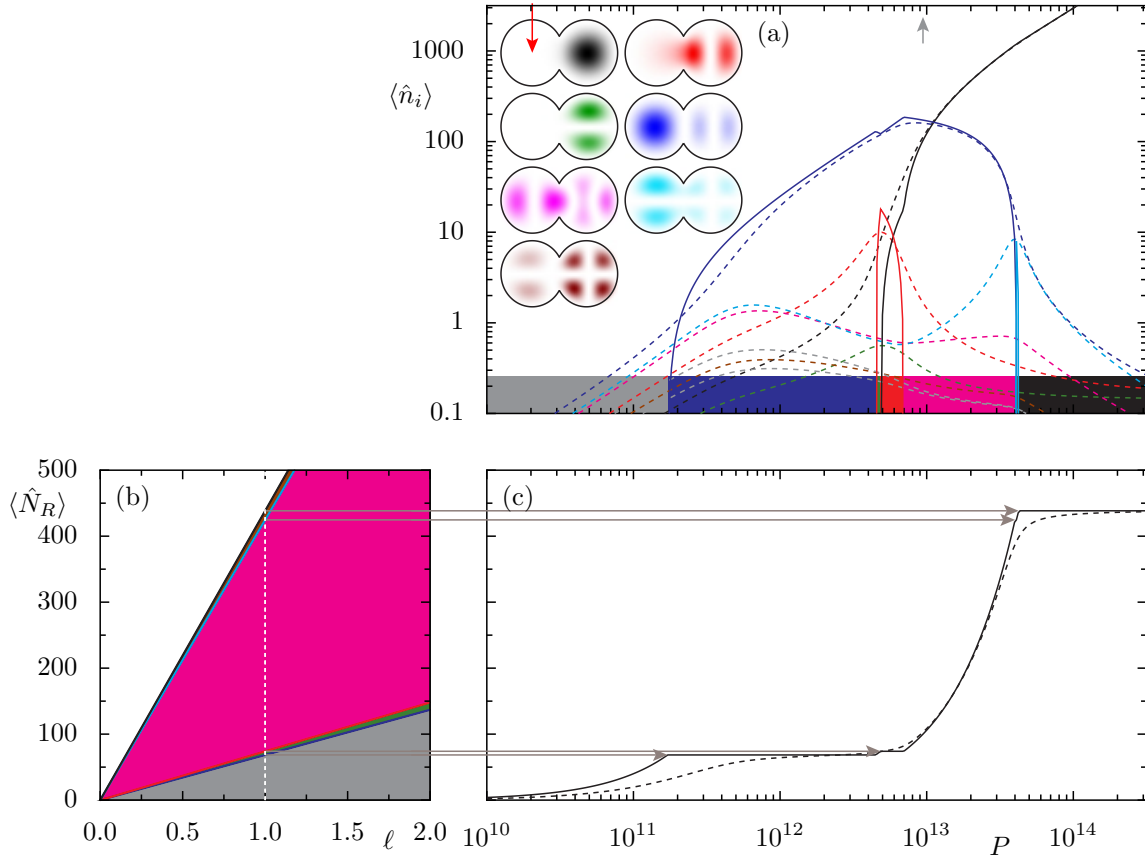


Figure 16.1.: Transitions triggered by ramping up the pumping in the asymmetrically-pumped double-pillar system. (a) The dependence of the mean occupation numbers $\langle \hat{n}_i \rangle$ on the pumping P is shown. At transitions, the occupation of the selected states given by the asymptotic theory (solid lines) vanishes. The mean-field results for all states (dashed lines) are shown as a comparison [see Fig. 14.2]. At the bottom, each phase (set of selected states) is colored uniquely. The inset is the same as in Fig. 14.2. (b) Phase diagram: depending on the reservoir occupation $\langle \hat{N}_R \rangle$ and the inverse lifetime ℓ , the steady state of the system has different sets of selected states (green, pink, and brown). The colors are identical to the one at the bottom of panel (a). Phases with an odd number of selected states collapse to a line (for increasing $\langle \hat{N}_R \rangle$): dark blue, red, light blue, and black.) For small reservoir occupations $\langle \hat{N}_R \rangle$ or large losses ℓ , none of the states is selected (gray). For sufficient large values $\langle \hat{N}_R \rangle / \tau$, no steady state exists (white). (c) Reservoir occupation $\langle \hat{N}_R \rangle$ depending on the pumping P . The asymptotic theory (dashed line) explains the plateaus seen in the mean-field result (solid line) for phases with an odd number of selected states. The pumping in Fig. 15.1 is denoted by the arrow at the top of panel (a).

At the transitions where the reservoir occupation $\langle \hat{N}_R \rangle$ is fine-tuned, an odd number of states is selected [dark blue, red, light blue, and black line in Fig. 16.1(b)]. However, these fine-tuned situations are whole regions with respect to the pumping P as shown in Fig. 16.1(c). For a whole interval of the pumping P , the reservoir occupation $\langle \hat{N}_R \rangle$ is clamped at these fine-tuned situations [62]. A consequence is that at transitions with respect to the pumping a *single* state becomes selected or nonselected [Fig. 16.1(a)]. This contrasts the transitions in closed systems, where two states are involved at each transition [Chap. 8].

Figure 16.1(a) shows that the asymptotic theory (solid lines) can explain the mean-field results (dashed lines). The condensate in the third excited state (dark blue) as well as the ground-state condensate (black) is captured by the asymptotic theory. Furthermore, the first excited state (red) and the fifth excited state (light blue) are selected in a narrow interval but with much smaller occupations. This explains the maxima in the mean-field results of these states and may indicate weak condensates in these states. Their selection would be more visible if the intermode kinetics were slower. Furthermore, one can see that the number of selected states is odd whenever the reservoir occupation has a plateau.

For sufficiently strong pumping, the reservoir occupation saturates at its maximal value. This is the phase where the selection is determined only by the intermode kinetics corresponding to the selection in closed systems as discussed below and shown in Fig. 16.1(a). Here only the ground state (black) is selected. This phase is just a single line separating the region with no steady state from the regime that has a steady state in the phase diagram 16.1(b).

Let us now determine this structure with the help of the asymptotic theory.

16.2. Theoretical description by the asymptotic theory

For sufficiently small pumping, none of the states is selected, $\mathcal{S}_0 = \{\}$. The reservoir occupation increases linearly with the pumping as $\langle \hat{N}_R \rangle = P\tau_R$ [see Eq. (15.10)]. According to Eqs. (15.8), the first state k is selected when the gain balances the loss, $W_k = N_R^* g_k - L_k = 0$, while the loss still prevails for all other states. This is the laser criterion [62]. The state k is thus determined by the largest gain-loss ratio g_k/L_k while it is independent of the intermode kinetics given by intermode rates R_{ij} .

Increasing the pumping further may result in a sequence of various sets of selected states. Even and odd numbers of selected states alternate since only a single condensate emerges or disappears at each transition. Due to the distinct properties of phases with an even or an odd number of Bose-selected states, we discuss both cases separately.

We start with the case of an odd number $M_{\mathcal{S}}$ of selected states $i \in \mathcal{S}$, which includes also the case of the single selected state after the first transition. The state which triggered the preceding transition shall be denoted by k . Since the number of selected states is odd, the matrix $A_{\mathcal{S}}$ [see

Eq. (8.3)] is odd-dimensional and thus singular (since it is skew-symmetric). As a consequence, the selection criterion (15.8) has infinite many solutions given by

$$\nu_i(q) = \nu_i^A + q\nu_i^B \quad \forall i \in \mathcal{S}, \quad (16.1)$$

where ν_i^A denotes the occupations at the preceding transition (with $\nu_k^A = 0$ if $k \in \mathcal{S}$) and ν_i^B is given by the homogeneous solution of Eq. (15.8),

$$\sum_i A_{ij} \nu_i^B = 0 \quad \forall i \in \mathcal{S}, \quad (16.2)$$

under the condition $\sum_{i \in \mathcal{S}} \nu_i^B = s$, where we describe the convention for choosing the sign $s = \pm 1$ later. The occupations of the nonselected states are determined via Eq. (15.7) by

$$\mu_i(q) = \sum_j A_{ij} (\nu_j^A + q\nu_j^B) + W_i(\langle \hat{N}_R \rangle) =: \mu_i^A + q\mu_i^B \quad \forall i \notin \mathcal{S}. \quad (16.3)$$

We choose the above introduced sign s in such a way that the occupation of the state k is positive for $q > 0$ by requiring $\nu_k^B > 0$ if $k \in \mathcal{S}$ and $\mu_k^B < 0$ otherwise. When increasing the pumping P , the reservoir occupation remains constant while the parameter q is [according to Eqs. (15.10)]

$$q = \frac{P - \langle \hat{N}_R \rangle / \tau_R - \sum_i \nu_i^A (\langle \hat{N}_R \rangle g_i - \ell_i)}{\sum_i \nu_i^B (\langle \hat{N}_R \rangle g_i - \ell_i)} \quad (16.4)$$

so that q and, thus, also the occupations of the selected states increase linearly with the pumping P .

The next transition is triggered by a selected (nonselected) state m which becomes nonselected (selected) since its occupation vanishes (diverges) at the smallest parameter $q^* > 0$, respectively. Here the transition criterion,

$$\nu_m(q^*) = \mu_m(q^*) = 0, \quad (16.5)$$

holds. This parameter q^* is given [according to Eqs. (16.1) and (16.3)] by

$$q^* = \min\{q_i | q_i > 0\} \text{ with } q_i = \begin{cases} -\nu_i^A / \nu_i^B & \text{if } i \in \mathcal{S}, \\ -\mu_i^A / \mu_i^B & \text{else.} \end{cases} \quad (16.6)$$

The case where none of the q_i is positive and, thus, no further transition occurs is discussed below.

Otherwise, the new phase has an even number of selected states $i \in \mathcal{S}$. The occupations of the

selected states are [according to Eq. (15.8)]

$$\begin{aligned}\nu_i(\langle \hat{N}_R \rangle) &= \sum_{j \in \mathcal{S}} (A_{\mathcal{S}}^{-1})_{ij} L_j - \langle \hat{N}_R \rangle \sum_{j \in \mathcal{S}} (A_{\mathcal{S}}^{-1})_{ij} g_j \\ &=: \nu_i^A + \langle \hat{N}_R \rangle \nu_i^B \quad \forall i \in \mathcal{S},\end{aligned}\tag{16.7}$$

and increase linearly with the reservoir occupation $\langle \hat{N}_R \rangle$. Here $A_{\mathcal{S}}^{-1}$ denotes the inverse of $A_{\mathcal{S}}$ and all indices are elements of the new set of selected states \mathcal{S} . (Since the matrix $A_{\mathcal{S}}$ is even-dimensional and skew-symmetric, it is generally invertible). The occupations of the nonselected states are given by Eq. (15.7) with the parameters [according to Eq. (15.8)]

$$\begin{aligned}\mu_i(\langle \hat{N}_R \rangle) &= \sum_j A_{ij} \nu_j^A - L_i - \frac{1}{\tau_i} + \langle \hat{N}_R \rangle (g_i + \sum_j A_{ij} \nu_j^B) \\ &=: \mu_i^A + \langle \hat{N}_R \rangle \mu_i^B.\end{aligned}\tag{16.8}$$

The reservoir occupation increases [according to Eqs. (13.5)] linearly with the pumping as

$$\langle \hat{N}_R \rangle = \frac{P + \sum_i \nu_i \ell_i}{1/\tau_R + \sum_i \nu_i g_i}\tag{16.9}$$

and, thus, also the occupations of the selected states.

Again, a transition is triggered by a state m which fulfills the transition criterion (16.5) when the reservoir occupation is ramped up until $\langle \hat{N}_R \rangle$ reaches N_R^* . Ensuing from Eqs. (16.7) and (16.8), this reservoir occupation is

$$N_R^* = \min\{N_i | N_i > N'_R\}, \quad N_i = \begin{cases} -\nu_i^A/\nu_i^B & \text{if } i \in \mathcal{S}, \\ -\mu_i^A/\mu_i^B & \text{else.} \end{cases}\tag{16.10}$$

The lower boundary N'_R denotes the (constant) reservoir occupation of the preceding phase or is zero when no states are selected. A phase with an odd number of selected states follows.

Eventually, a final phase $\mathcal{S}_{\text{final}}$ with an odd number of selected states is reached where no further transition occurs. As mentioned above, this is the case when $q_i^* < 0 \forall i$ in Eq. (16.6). Since the occupations [given by Eqs. (16.1) and (16.3)] fulfill the selection condition (15.8) for all $q > 0$, the homogeneous solution fulfills

$$\nu_i^B > 0 \quad \forall i \in \mathcal{S}_{\text{final}} \quad \text{and} \quad \mu_i^B < 0 \quad \forall i \notin \mathcal{S}_{\text{final}}.\tag{16.11}$$

These conditions give rise to the behavior, which is equivalent to closed systems as discussed below.

This equivalence is exploited to design an algorithm to find the set of selected states for closed systems [cf. Chap. 8]. The algorithm works as follows. The rates of the closed system of interest are taken as intermode rates of an artificial open system. The lifetimes can be chosen like $\tau_i = \tau_R = 1 \forall i$,

while reabsorption of excitations by the reservoir are disallowed, $\ell_i = 0 \forall i$. The gain rates $g_i > 0$ are chosen for each state i randomly to avoid fine-tuned situations. The pumping P is ramped from zero, where no state is selected, up until the final set of selected states is reached. This final set is equivalent to the set of selected states in the system of interest. Thus we can find this set by following to above discussed sequence of transitions. The number of transition scales polynomial with the number of states. Hence this algorithm enables to find the selected states also for large closed systems.

16.3. Bose selection in open and closed systems

The Bose selection of open systems in the limit of strong pumping resembles the Bose selection of closed systems. I.e., the set of finally Bose-selected states $\mathcal{S}_{\text{final}}$ in the strong-pumping limit is given by the set of selected states in the corresponding closed system. This is so because Eq. (16.2) under the condition (16.11) for the final set of Bose-selected states is equivalent to the selection condition in closed systems (7.6). Therefore, the set $\mathcal{S}_{\text{final}}$ is determined only by the intermode kinetics via the intermode rates R_{ij} and is independent of the individual gain and loss rates. The result that in the limit of strong pumping the intermode kinetics plays the major role seems counterintuitive. It is a consequence of the fact that the dependence on the occupations numbers of the intermode kinetics [Eq. (13.2)] is quadratically while the one of the gain and loss processes [Eq. (13.3)] is linearly. Thus the intermode kinetics dominates for large occupations. Furthermore, the occupations of the Bose-selected states (more precisely their relative occupations) are given by the intermode kinetics alone. This follows from the dominant contribution $q\nu_i^B$ in Eq. (16.1) for strong pumping (and thus large q) since the homogeneous solution ν_i^B is determined by the intermode rates R_{ij} only. This final phase resembles therefore the (nonequilibrium) Bose condensation of closed systems [Chap. 7].

Figure 16.2 shows this equivalence of the Bose selection of open systems in the strong-pumping limit and closed system in the high-density limit. Panel (a) shows the occupations in the nonequilibrium steady state of a random-rate model [for details see figure caption]. When increasing the pumping, several abrupt changes of the occupations $\langle \hat{n}_i \rangle$ caused by transitions occur. The Bose selection of that closed system which has the same intermode kinetics, i.e., the same rates R_{ij} , is shown as well (dashed lines). The occupations in the limit of strong pumping P of the open system approach the occupations of the closed system in the limit of large particle numbers N . Hereby, we compare the open system with pumping P with that closed system that has the same total particle number N (which is $N = LP$ since $L_i = L \forall i$).

When the rates are thermal, i.e., fulfill condition (2.30), the ground state is the only selected state for strong pumping. Furthermore, the occupation of all (nonselected) states approach the Bose-Einstein distribution. Namely, the terms describing the intermode kinetics in Eq. (15.7) prevail in the limit of large condensate occupations $\langle \hat{n}_0 \rangle > G_i/R_{i0} \forall i$, so that the occupations of the nonselected

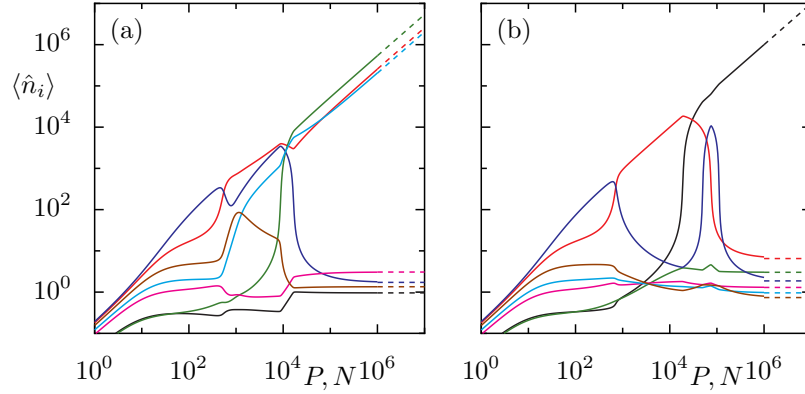


Figure 16.2.: Comparison of Bose selection in open and closed systems. The mean occupation numbers $\langle \hat{n}_i \rangle$ for an open system with random rates are shown depending on the pumping P (solid lines). Moreover, the mean occupation numbers of a *closed* system are shown (dashed lines) depending on the total particle number N in the limit $N \rightarrow \infty$ [obtained by the selection criterion (7.6) for closed systems]. The rates of the closed system and the intermode rates of the open system are the same. (a) The rates R_{ij}^a are drawn randomly from a uniform distribution with $0 < R_{ij} < 0.001$. Since the condition (2.30) is violated, this situation mimics nonequilibrium conditions similar to Floquet systems. The mean occupation numbers $\langle \hat{n}_i \rangle$ of the open and closed system approach each other in the limit of strong pumping P and large total particle numbers N , respectively. Thus, the same set of states is Bose-selected. (b) The rates are obtained by Eq. (16.13), so that these rates are thermal, i.e., fulfill condition (2.30). In the limit of strong pumping P for the open system and large total particle numbers N of the closed system, only the ground state (black line) is selected. (a,b) The loss is state-independent, $L_i = 1 \forall i$, and the gain rates G_i are drawn uniformly from the interval $[0, 1]$.

states read approximately

$$\langle \hat{n}_i \rangle = \frac{1}{R_{0i}/R_{i0} - 1} = \frac{1}{e^{\beta(E_i - E_0)} - 1}. \quad (16.12)$$

This scenario is shown in Fig. 16.2(b), which shows the occupations $\langle \hat{n}_i \rangle$ similar to panel (a) but for a system with thermal rates. These rates R_{ij}^b are thermal since they are obtained from the rates R_{ij}^a used in panel (a) by

$$R_{ij}^b = \begin{cases} R_{ij}^a & \text{for } i \leq j, \\ R_{ji}^a e^{-\beta(E_i - E_j)} & \text{for } i > j, \end{cases} \quad (16.13)$$

where $\beta = 1$ denotes the inverse temperature and $E_i = i/M$ the eigenenergies.

The intermode kinetics in the discussed polariton gas in the double pillar is thermal. Thus, we also find ground-state condensation in the strong-pumping limit there [Fig. 16.1].

In conclusion, the asymptotic theory provides a clear distinction between lasing, Bose condensation, and Bose selection. Bose condensation is caused by the intermode kinetics [Eq. (13.2)]: The condensation is formed by *stimulated cooling*, where the environment absorbs energy. Here, ground-state condensation is found when this intermode kinetics is given by thermal rates. More generally, when the intermode kinetics does not favor such a ground-state-like state [Eq. (7.9)], Bose selection

of closed systems is found, where the intermode kinetics selects multiple states. Lasing is caused by the competition between gain and loss [Eq. (13.3)]: The *stimulated emission* from the gain medium causes lasing when this emission exceeds the loss. When intermode kinetics, gain, and loss compete with each other, the Bose selection of open systems is found. For strong pumping, however, this is akin to Bose selection to closed systems since the intermode kinetics becomes dominant. This can be interpreted as a leftover from the equivalence of ensembles.

17. Mode-switching in a microcavity

We investigate the switching of the mode that emits light coherently triggered by ramping up the pumping power in a bimodal microcavity. A switching of the lasing mode [150–154] shows potential technical applications, such as optical flip-flop memories, tunable sensitive switches [155, 156], and simple realizations of nonequilibrium phase transitions [157, 158]. Starting from the equations for the steady state of our photonic model (13.6) and (13.7), the switching is inferred in the framework of transitions discussed in Chap. 16. We find that the switching by increasing the pump power is a minimal instance of the Bose selection mechanism: First, above a threshold, the mode with the largest effective gain starts lasing. Then, the competition between effective gain and intermode kinetics leads to a selection of both modes. Eventually, the intermode kinetics dominates and determines the Bose-selected mode at strong pumping. A comparison to experimental results, measured in the group of Reitzenstein [102], shows excellent agreement. This chapter covers parts of Ref. [102], namely the experimental results and an analytical part which I have contributed, which is the application of the Bose selection. A fruitful discussion on the fluctuations and correlations, which is also covered by this reference, will not be discussed here.

The device is a bimodal quantum-dot micropillar cavity [159]. This vertical-cavity surface-emitting laser [160, 161] consists of a λ -cavity with Bragg reflectors and a central active layer of quantum-dots pumped electrically via the injection current I . The diameter of the micropillar is $3.0\ \mu\text{m}$. The two fundamental modes $\text{HE}_{1,1}$ are orthogonal, linearly polarized. Although the modes are ideally degenerate, the degeneracy is lifted by, e.g., the birefringence caused via the elasto-optic effect by anisotropic strain [162] since the manufacturing process induces an asymmetry. The resulting splitting in the sample is $(41.6 \pm 1.6)\ \mu\text{eV}$. Due to the different shapes also both quality factor and both emission rates differ. The quality factors are (14000 ± 1500) and (12500 ± 1500) for the modes l and h , respectively. Although the structure of the vertical-cavity surface-emitting lasers is similar to that of the exciton-polariton systems, both systems fundamentally differ by the absence of the strong coupling in the microcavity, i.e., photons and excitons do not form polaritons.

The switching in the input-output characteristics is shown in Fig. 17.1(a). This characteristics exhibits four regions. Below the laser threshold of about $13\ \mu\text{A}$, the output emissions of both modes remain small (*region A*). Above the laser threshold, the mode h starts lasing accomplished by a strong increase of its output while mode l remains nonlasing (*region B*). However, at the injection current of about $36\ \mu\text{A}$ (*region C*) up until $50\ \mu\text{A}$, the modes switch their character. Namely, while the output of mode l increases strongly, the output of mode h decreases until it saturates at a small value. Above $50\ \mu\text{A}$ (*region D*), only mode l is highly occupied and emits light coherently.

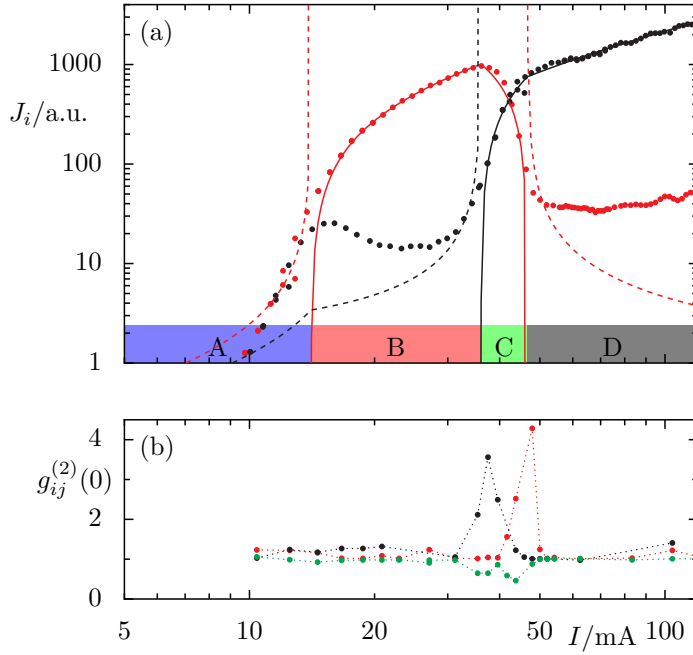


Figure 17.1: Measured and calculated input-output characteristics for a bimodal quantum-dot micropillar cavity. (a) Input-output characteristics J_i of the emitted photons from the high-effective-gain mode (red) and the low-effective-gain mode (black) depending on the injection current I . The figure shows both the experimental data (points) and the asymptotic theory (line, which is solid or dashed when the mode is selected or nonselected, respectively.) At the bottom, four regions are labeled, namely A, B, C, and D, where, respectively, neither mode, the high-effective-gain mode, both modes, and the low-effective-gain mode are selected. The selection of a mode corresponds to a large occupation. (b) Measured autocorrelations $g_{hh}^{(2)}(0)$ [red], $g_{ll}^{(2)}(0)$ [black] and cross-correlation $g_{hl}^{(2)}(0)$ [green]. In the analytic model, the effective-gain ratio was extracted as $G = 0.77$. The other parameters are in units of τ^{-1} : $g_h = 1.6 \cdot 10^{-3}$, $g_l = 2.1 \cdot 10^{-3}$, $\ell_h = 2.2 \cdot 10^{-2}$, $\ell_l = 3.8 \cdot 10^{-2}$, $A_{h \rightarrow l} = 8.5 \cdot 10^{-6}$, $R_{l \rightarrow h} = 1.7 \cdot 10^{-4}$.

Figure 17.1(b) also shows the equal-time autocorrelations $g_{ii}^{(2)}(\tau = 0)$ and cross-correlation $g_{hl}^{(2)}(\tau = 0)$ with zero delay time for the emission. These correlations were measured via a fiber-coupled Hanbury-Brown and Twiss setup. These equal-time correlations are defined by

$$g_{ij}^{(2)}(\tau = 0) = \frac{\langle \hat{b}_i^\dagger \hat{b}_j^\dagger \hat{b}_i \hat{b}_j \rangle}{\langle \hat{b}_i^\dagger \hat{b}_i \rangle \langle \hat{b}_j^\dagger \hat{b}_j \rangle}, \quad (17.1)$$

where \hat{b}_i denotes the annihilation operator of mode i . Note that the autocorrelations $g_{ll}^{(2)}(0)$ in region B and $g_{hh}^{(2)}(0)$ in region D are not resolved due to the finite temporal resolution of the Hanbury-Brown and Twiss setup and the low coherence time of the light [163]. The maximum in the measured autocorrelation indicates that in region C first mode l starts emitting light coherently and then mode h ceases to emit light coherently. This is consistent with its high occupations corresponding to its selection.

17.1. Theoretical description

Let us apply the theory of transitions in open system [Chap. 16] to the bimodal microcavity. Figure 17.1 shows together with the measured data the results of this analysis. For this comparison, however, it is necessary to extract the experimental parameters which are otherwise inaccessible and to relate the photon numbers in the cavity to the measured emitted photons, as discussed in App. F.

The kinetics of the bimodal cavity is sketched in Fig. 17.2. This kinetics is given by the interplay

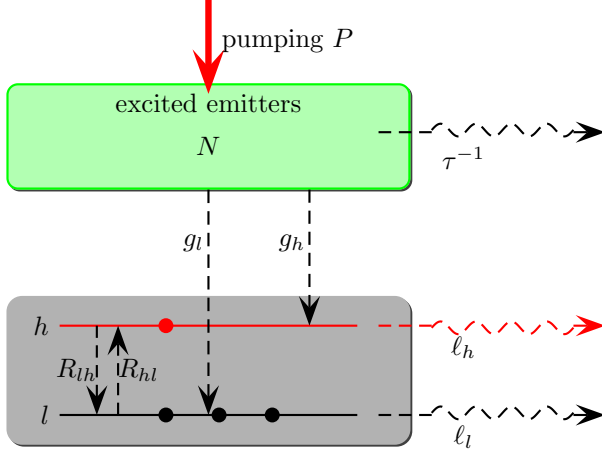


Figure 17.2: Phenomenological model of the bimodal cavity. The system has two modes $i \in \{l, h\}$. The rate R_{lh} and R_{hl} transfer photons directly from state h to state l and vice versa, respectively. The lifetime and thus the loss rates ℓ_i of the photon is mode-dependent. The losses are compensated by excitations from the emitters (i.e., quantum dots) via rates g_i . These quantum dots are excited by the pumping P and the quantum-dot excitations decay to nonlasing modes with rate τ^{-1} .

of, on the one hand, the effective gain, which is the ratio between gain from the emitters and the loss of the cavity, and, on the other hand, the intermode kinetics. The modes are labeled according to their higher (h) or lower (l) effective gain. The kinetic equations for the photon number in both modes $\langle \hat{n}_h \rangle$ and $\langle \hat{n}_l \rangle$ and the number of excited emitters $\langle \hat{N} \rangle$ are given by Eqs. (13.1)-(13.5). For bimodal cavities, they simplify to

$$\frac{d}{dt} \langle \hat{n}_i \rangle = D_i^{\text{inter}}(\langle \hat{n}_l \rangle, \langle \hat{n}_h \rangle) + D_i^{\text{open}}(\langle \hat{n}_l \rangle, \langle \hat{n}_h \rangle) \quad \forall i \in \{l, h\} \quad (17.2)$$

with the intermode kinetics

$$D_i^{\text{inter}}(\langle \hat{n}_l \rangle, \langle \hat{n}_h \rangle) = [R_{ij} \langle \hat{n}_j \rangle (\langle \hat{n}_i \rangle + 1) - R_{ji} \langle \hat{n}_i \rangle (\langle \hat{n}_j \rangle + 1)] \quad \forall (i, j) \in \{(l, h), (h, l)\}, \quad (17.3)$$

and the dynamics caused by the loss and the influx of new particles

$$D_i^{\text{open}}(\langle \hat{n}_l \rangle, \langle \hat{n}_h \rangle) = g_i \langle \hat{N} \rangle (\langle \hat{n}_i \rangle + 1) - \ell_i \langle \hat{n}_i \rangle \quad \forall i \in \{l, h\}. \quad (17.4)$$

The term D^{open} captures all processes which are necessary to model a single-mode lasing in mode h [164]. The dynamics of the reservoir is given by

$$\frac{d}{dt} \langle \hat{N} \rangle = P - \frac{\langle \hat{N} \rangle}{\tau} - \langle \hat{N} \rangle \sum_{i \in \{h, l\}} g_i (\langle \hat{n}_i \rangle + 1). \quad (17.5)$$

The two modes h and l are defined by the higher and lower effective gain g_i/ℓ_i . The effective-gain ratio

$$G = \frac{g_l/\ell_l}{g_h/\ell_h} < 1 \quad (17.6)$$

is the central parameter comprising the loss and the coupling to the emitters. We will now apply the theory of transitions to this microcavity device.

In *region A*, neither mode is selected, $\mathcal{S} = \{\}$. The occupation of both modes $i \in \{l, h\}$ are $\langle \hat{n}_i \rangle_A = (\ell_i / (g_i \langle \hat{N} \rangle) - 1)^{-1}$, according to Eq. (15.7). The number of excited emitters increases linearly with the pumping, $\langle \hat{N} \rangle_A = \tau P$, according to Eq. (15.10). The occupation of the high-effective-gain mode h diverges at the laser threshold $P_{AB} = \ell_h / g_h \tau$ so that this mode starts lasing.

In *region B*, only the high-effective-gain mode is selected, $\mathcal{S} = \{h\}$. The number of excited emitters is clamped at the threshold value $\langle \hat{N} \rangle_B = \ell_h / g_h$ since the new excitations are coherently transferred to the lasing mode [62]. Thus the occupation of the mode h increases as [see Eq. (16.9)]

$$\langle \hat{n}_h \rangle_B = \frac{P}{\ell_h} - \frac{1}{\tau g_h} \quad (17.7)$$

while the occupation of the nonselected mode l is [see Eq. (15.7)]

$$\langle \hat{n}_l \rangle_B = \frac{g_l \langle \hat{N} \rangle_B}{\ell_l - g_l \langle \hat{N} \rangle_B - A_{lh} \langle \hat{n}_h \rangle_B}. \quad (17.8)$$

In the case where the mode-coupling process favors this high-effective-gain mode, $A_{lh} < 0$, the occupation of mode l would remain small. In the opposite case $A_{lh} > 0$, which is realized in our sample, the occupation of mode l diverges at

$$P_{BC} = \frac{\ell_l}{g_h} \left[\frac{1}{\tau} + \frac{g_h \ell_l - g_l \ell_h}{A_{lh}} \right] \quad (17.9)$$

and this mode l becomes selected.

Thus, in *region C*, both modes are selected, $\mathcal{S} = \{h, l\}$. The number of excited emitters $\langle \hat{N} \rangle$ increases again with the pumping P ,

$$\langle \hat{N} \rangle_C = P \left[\frac{1}{\tau} + \frac{g_h \ell_l - g_l \ell_h}{A_{lh}} \right]^{-1} \quad (17.10)$$

While the occupation of the low-effective-gain mode l increases, the occupation of the other mode h decreases linearly with the number of excited emitters $\langle \hat{N} \rangle$ and thus with the pumping P ,

$$\langle \hat{n}_h \rangle_C = - \frac{g_l \langle \hat{N} \rangle_C(P) - \ell_l}{A_{lh}}, \quad (17.11)$$

$$\langle \hat{n}_l \rangle_C = \frac{g_h \langle \hat{N} \rangle_C(P) - \ell_h}{A_{lh}}. \quad (17.12)$$

The occupation of mode h (almost) vanishes when the number of excited emitters reaches $\langle \hat{N} \rangle_D = \ell_l / g_l$. The corresponding pump power P_{CD} is given by

$$P_{CD} = \frac{P_{BC}}{G}. \quad (17.13)$$

Interestingly, this ratio provides the effective-gain ratio G [Eq. (17.6)] by measuring the width of

region C from the input-output characteristics since this ratio is independent of the intermode rates.

Eventually, in *region D*, only the low-effective-gain mode l is lasing, $\mathcal{S} = \{l\}$, and both modes have switched their roles in comparison to region B. The number of excited emitters is clamped at the higher value $\langle \hat{N} \rangle_D$ [see above] to compensate the higher loss rate of mode l . The occupation of this selected mode l reads

$$\langle \hat{n}_l \rangle_D = \frac{P}{\ell_l} - \frac{1}{\tau g_l} \quad (17.14)$$

while the occupation of the nonselected mode h reads

$$\langle \hat{n}_h \rangle_D = \frac{g_h \langle \hat{N} \rangle_D}{\ell_h - g_h \langle \hat{N} \rangle_D - A_{hl} \langle \hat{n}_h \rangle_D}. \quad (17.15)$$

Both equations are analog to Eqs. (17.7) and (17.8), respectively. A further transition is impossible since the denominator remains larger than zero due to $A_{hl} < 0$. (Further transitions would require a change of the model parameters due to, e.g., heating or externally induced strain [162].)

17.2. Phase diagram

The generic phase diagram shown in Fig. 17.3 summarizes all possible scenarios. It shows the selected modes [neither mode, either horizontal (\leftrightarrow) or vertical (\updownarrow) polarized mode, or both modes] depending on the pumping power P and the effective-gain ratio $G = g_{\updownarrow} \ell_{\leftrightarrow} / g_{\leftrightarrow} \ell_{\updownarrow}$. For pumping below threshold (region A), none of the modes is lasing. Above the lasing threshold, the high-effective-gain mode h starts lasing (i.e., $h = \leftrightarrow$ for $G < 1$ and $h = \updownarrow$ for $G > 1$). For sufficient strong pumping, the only selected mode is the mode that is favored by the mode-coupling rates, i.e., the vertical polarized

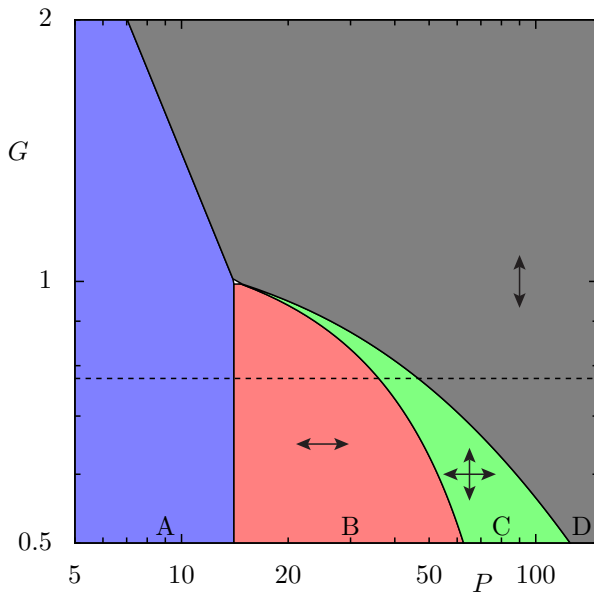


Figure 17.3: Phase diagram of the bimodal microcavity depending on the pump power P and the effective gain ratio $G = g_{\updownarrow} \ell_{\leftrightarrow} / g_{\leftrightarrow} \ell_{\updownarrow}$ (where $g_{\leftrightarrow}, \ell_{\leftrightarrow}, \ell_{\updownarrow}$ are kept constant) showing which of the two (horizontal and vertical polarized) modes are Bose-selected. Below the laser threshold, no state is lasing (region A). Above the lasing threshold, the high-effective-gain mode h starts lasing (region B with mode $h = \leftrightarrow$ and region D with mode $h = \updownarrow$). For sufficient strong pump power, only the mode \updownarrow which is favored by the intermode-kinetic rates, $R_{\updownarrow\leftrightarrow} > R_{\leftrightarrow\updownarrow}$, is selected (region D). For $G < 1$, the high-effective-gain mode and the mode favored by the intermode kinetics are different. Thus a transition occurs via the intermediate region C where both modes are selected. This is the case for the cut along the dashed line, which is shown in Fig. 17.1 and was observed in the experiment.

mode (\uparrow) since $R_{\uparrow\leftrightarrow} > R_{\leftrightarrow\uparrow}$. For $G < 1$, the high-effective-gain mode (\leftrightarrow) is different from the mode favored by the intermode kinetics (\uparrow). Thus a transition occurs in between (region C), where both modes are selected. For $G \geq 1$, the high-effective-gain mode is already the favored mode, and no switching occurs like in a regular laser. Actually, this is the case for most samples of bimodal micropillar cavities [not shown].

The selection in region D is determined by the intermode kinetics only akin to a condensation of massive bosons. This implies that the mechanism for selecting the mode in this limit is the same as the one responsible for Bose-Einstein condensation. Thus this bimodal microcavity can be seen as a minimal instance of a Bose condensate of photons.

18. Conclusion

My initial motivation for this research was the investigation of the fate of Bose-Einstein condensation in periodically-driven open quantum systems. Bose-Einstein condensation, the macroscopic collection of bosons occupying the ground state, is an exotic quantum effect. This collective behavior allows quantum phenomena to arise even on macroscopic scales, such as the interference of whole atom clouds or superconductivity. However, driving such systems time-periodically (e.g., shaking the system) threatens the existence of the condensate. This threat is a consequence of the absence of the definition of a ground state for Floquet systems, where Floquet states generalize the energy eigenstates. This loss of a ground state, which hosts the ordinary Bose condensation, led to the initial question “Does the Bose condensate survive in open Floquet systems?” and then, step by step, to problems of nonequilibrium Bose condensation in more general driven-dissipative quantum systems.

18.1. Summary

We have shown that Bose condensation generalizes far from equilibrium to the unambiguous selection of a group of states each acquiring a large mean occupation number. This group of Bose-selected states takes over the role of the ground state in ordinary Bose condensation. Various examples [Chap. 3], including an open time-periodically-driven quartic oscillator, serve to illustrate this phenomenon [Chap. 5]. The condensate breaks up into several Bose-selected states, which acquire a large occupation each. In contrast, each nonselected state has a small occupation. Analogously to the equilibrium condition, the occupations of nonselected states are bounded when increasing the total particle number. Thus additional particles must be acquired by the selected states, whose occupation numbers increase proportionally to the total particle number [Fig. 1.1].

We showed several properties of Bose selection, which were observed numerically [Chap. 5] and explained analytically within an asymptotic theory for large densities [Chap. 7]. A Bose selection forms a fragmented condensate when several selected states acquire a macroscopic fraction of all particles. The selection criterion (7.6) determines the selected states and the occupations in the high-density limit. The number of selected states is odd except for fine-tuned situations. By introducing the concept of a ground-state-like state (7.9), we can distinguish between the Bose selection of several states (when no such state exist) and the situation of a single Bose-selected state (e.g., ordinary Bose condensation). This criterion provides the minimal requirement for Bose selection of multiple states

and shows that nonequilibrium conditions (i.e., breaking the detailed balance) are necessary but not sufficient. Finally we found that the set of selected states is independent of the bath temperature(s).

Varying a system parameter can trigger transitions where the set of selected states changes. For large but finite densities, these transitions are narrow crossovers where an even number of states are Bose-selected [Chap. 8]. In situations of an autonomous system coupled to two heat baths, where one is population-inverted, the heat current depends sensitively on whether a single state or multiple states are selected. We proposed to exploit this effect to control the heat flow through a chain by switching between a single selected state and three selected states [Chap. 10].

In the case where some rates are much smaller than others, a preasymptotic regime can occur where a preasymptotic selection takes place at intermediate particle numbers [Chap. 11]. Its description made a careful discussion of the situations with zero rates necessary. This discussion also provides a criterion regarding the cut-off of the Floquet state space, which is necessary for numerical simulations. Furthermore, this situation is relevant for other systems described by equations similar to the mean-field equations, like Lotka-Volterra systems [Chap. 12]

Bose selection is not a special case in Floquet systems but occurs generically in driven dissipative systems. One example is the scenario of the coupling to two heat baths. Roughly speaking, Bose selection relies on the loss of a meaningful ground state [Chap. 7]. While this is an intrinsic consequence in Floquet systems, it can be realized via population-inverted baths in autonomous systems as well.

Open driven-dissipative ideal Bose gases, which are driven by particle injection, offer another scenario exhibiting Bose selection [Chap. 15]. Generalizing the concept of Bose selection of closed systems to open systems provides new perspectives on the recent discussion how to define the demarcation between lasing and Bose condensation. This discussion was triggered by progress in photonic many-body systems. In particular, the selection criterion can clearly distinguish between the selection of states by stimulated emission (caused by the gain medium), by stimulated cooling (caused by the intermode kinetics), and by the interplay of both. By doing so, we recover lasing in the limit of small pumping but above a threshold and Bose condensation in the ground state in the limit of strong pumping [Chap. 16]. At intermediate pumping, several phases with excited-state condensation or fragmented condensation (multi-mode condensation) emerge.

The mode switching in a bimodal quantum-dot micro-pillar cavity is a minimal instance exhibiting lasing and Bose condensation of photons [Chap. 17]. Above the lasing threshold, the system lases in a mode selected by its higher effective-gain rate. When the intermode kinetics favors the other mode, ramping up the pump power triggers a switching to its selection. This selection is a Bose condensation of photons since stimulated cooling (the intermode kinetic) is responsible for it. This switching occurs via a phase where both modes are selected.

A second example, where we applied the Bose-selection theory, is a polariton gas in a “photonic molecule” (i.e., a double-pillar system) [Chap. 14]. Here a similar behavior is observed – a switching

from an excited-state condensate to a ground-state condensate. Furthermore, our results indicate that more phases are found in between.

18.2. Outlook

Many fascinating effects in condensates rely on interactions. Among them are superconductivity and superfluidity. Even very small interactions among the particles can have a large impact, such as the change of the condensate profile described by the Thomas-Fermi approximation in trapped atomic gases [165]. In equilibrium, small repulsive interactions can also destroy fragmented Bose condensation when the states overlap spatially since a single condensate minimizes the energy cost [133]. This motivates the investigation of the impact of interactions on the presented Bose selection and address questions like: Is this effect stable against small interactions? How do different condensates interact with each other? My intuition concerning the first question is that the Bose selection remains stable at least under weak interactions since the Bose selection is caused by strong particle flows among the selected states. This contrasts the mentioned case of fragile fragmented condensation in a degenerate ground state, which requires fine-tuning.

Another interesting question addresses the dimensionality. For closed systems, we have considered finite one-dimensional systems only. In equilibrium, true Bose-condensation occurs in three-dimensional systems only, according to the Mermin-Wagner-Theorem [17]. In one- and two-dimensional systems, Bose condensation exists only in the form of its finite-size version [18] or for sufficient strong confinement [166]. It would be interesting to study whether the restriction of the Mermin-Wagner theorem can be surpassed away from equilibrium. Also the study of phase transitions between different Bose selections requires three-dimensional systems.

In my opinion, one of the most interesting questions is whether the equivalence of ensembles has a counterpart under nonequilibrium conditions, i.e., the connection between the properties of open, closed, and isolated systems. Under equilibrium conditions, the ensembles become equivalent in the thermodynamic limit. This is exploited, i.a., to apply results obtained in the grand canonical ensemble to the canonical ensemble. Under nonequilibrium conditions, however, the dependence on the details of the environment shows that changing the scenario affects steady-state properties. Among others, the discussed Bose selection shows that, nevertheless, closed and open systems share generic properties and effects, and that open systems approach the closed ones in the strong pumping limit. It would be interesting to investigate the relations to isolated interacting Floquet gases [95, 96].

Cold atoms in optical traps are a successful approach to study many-body quantum physics. I would find it fascinating to see an experimental realization of Bose selection. A realization could be a Floquet gas that is cooled by immersing it into an external heat bath. One might also think of a scenario where a Bose selection is created in an interacting Floquet gas by evaporative cooling. Evaporative cooling is a technique to cool a cloud of atoms by permanently removing the particles with highest energy so that the average energy per remaining particle decreases. The interactions

among the particles redistribute the energy such that the system thermalizes. For an interacting Floquet gas, this setup might be a technique to cool the system or, at least, to prevent it from heating up (due to the driving). The cooling is necessary to form a Bose selection in such Floquet systems. This selection would, however, be a preasymptotic state on intermediate timescales only since eventually all particles are lost or the system heats up.

Last but not least, I would be interested in where else the mechanism of Bose selection might occur. Many classical systems show effects akin to Bose condensation, e.g., classical light condensation [167], condensation in complex networks [168], economics [169], or zero-range processes describing traffic [170, 171]. Some of their descriptions allow even a mapping to the theory of Bose-Einstein condensation. The relationship to evolutionary game theory [143] was discussed in Chap. 12. I expect further interesting connections to others of these examples.

Appendix

A. Many-body rate equation

We derive the equations of motion for the many-body occupation probabilities $p_{\mathbf{n}} = \langle \mathbf{n} | \rho | \mathbf{n} \rangle$, ensuing from the master equation (2.23) in Lindblad form. We replace the single-particle operators $\hat{L}_{ij} = |i\rangle\langle j|$ by their representation in the Fock space $\hat{L}_{ij} = \hat{a}_i^\dagger \hat{a}_j$. The equations of motion for the diagonal elements of the density operator read

$$\begin{aligned} \dot{p}_{\mathbf{n}}(t) &= \langle \mathbf{n} | \dot{\rho}(t) | \mathbf{n} \rangle \\ &= \sum_{i,j} R_{ij} \left(\langle \mathbf{n} | \hat{a}_i^\dagger \hat{a}_j \hat{\rho}(t) \hat{a}_j^\dagger \hat{a}_i | \mathbf{n} \rangle - \frac{1}{2} \langle \mathbf{n} | \{ \hat{\rho}(t), \hat{a}_j^\dagger \hat{a}_i \hat{a}_i^\dagger \hat{a}_j \} | \mathbf{n} \rangle \right). \end{aligned}$$

For $i = j$, both terms inside the bracket cancel each other. For $i \neq j$, we have $\hat{a}_j^\dagger \hat{a}_i | \mathbf{n} \rangle = \sqrt{n_i(1 \pm n_j)} | \mathbf{n}_{ji} \rangle$ and $\hat{a}_j^\dagger \hat{a}_i \hat{a}_i^\dagger \hat{a}_j | \mathbf{n} \rangle = n_j(1 \pm n_i) | \mathbf{n} \rangle$, where the upper (lower) sign applies to bosons (fermions) and $\mathbf{n}_{ji} = (n_1, \dots, n_i - 1, \dots, n_j + 1, \dots)$ denotes the occupation numbers obtained from \mathbf{n} by transferring one particle from i to j . Thus, the master equation simplifies to

$$\begin{aligned} \dot{p}_{\mathbf{n}}(t) &= \sum_{i,j} R_{ij} [n_i(1 \pm n_j) p_{\mathbf{n}_{ji}}(t) - n_j(1 \pm n_i) p_{\mathbf{n}}(t)], \\ &= \sum_{i,j} (1 \pm n_j) n_i [R_{ij} p_{\mathbf{n}_{ji}}(t) - R_{ji} p_{\mathbf{n}}(t)]. \end{aligned} \quad (\text{A.1})$$

We have not explicitly excluded the terms with $i = j$ since they still cancel. The second line was obtained by exchanging i and j in the second term.

B. Equations of motion for mean occupations

In this appendix, we derive the equations of motion (6.1) for the mean occupation numbers $\langle \hat{n}_i \rangle$ from the master equation (2.23) in Lindblad form.

The equations of motion for the mean occupations $\langle \hat{n}_i \rangle$ reads

$$\frac{d}{dt} \langle \hat{n}_k \rangle(t) = \text{tr} \left(\hat{n}_k \frac{d}{dt} \hat{\rho}(t) \right). \quad (\text{B.1})$$

By employing the master equation (2.23) with the many-body jump operators [Eq. (2.43)], we obtain

$$\frac{d}{dt}\langle\hat{n}_k\rangle(t)=\sum_{i,j}R_{ij}\mathrm{tr}\left(\hat{n}_k\hat{a}_i^\dagger\hat{a}_j\hat{\rho}(t)\hat{a}_j^\dagger\hat{a}_i-\frac{1}{2}\hat{n}_k\left\{\hat{a}_j^\dagger\hat{a}_i\hat{a}_i^\dagger\hat{a}_j,\hat{\rho}(t)\right\}\right). \quad (\text{B.2})$$

We rewrite the first term of the sum as

$$\mathrm{tr}\left(\hat{n}_k\hat{a}_i^\dagger\hat{a}_j\hat{\rho}(t)\hat{a}_j^\dagger\hat{a}_i\right)=\mathrm{tr}\left(\hat{n}_k\hat{a}_j^\dagger\hat{a}_i\hat{a}_i^\dagger\hat{a}_j\hat{\rho}(t)\right)+(\delta_{ik}-\delta_{jk})\mathrm{tr}\left(\hat{a}_j^\dagger\hat{a}_i\hat{a}_i^\dagger\hat{a}_j\hat{\rho}(t)\right). \quad (\text{B.3})$$

This can be done since the trace is invariant under cyclic permutations and the relation

$$\left[\hat{a}_j^\dagger\hat{a}_i,\hat{n}_k\right]=\hat{a}_j^\dagger\hat{a}_i(\delta_{ik}-\delta_{jk}) \quad (\text{B.4})$$

holds. This commutator relation is valid for either statistics since it is a consequence of the commutation relation $[\hat{a}_i,\hat{a}_j^\dagger]=\delta_{ij}$ for bosons as well as the anticommutation relation $\{\hat{a}_i,\hat{a}_j^\dagger\}=\delta_{ij}$ for fermions.

Furthermore, we employ the relation

$$\hat{a}_j^\dagger\hat{a}_i\hat{a}_i^\dagger\hat{a}_j=\hat{n}_j(1\pm\hat{n}_i)\mp\delta_{ij}\hat{n}_i, \quad (\text{B.5})$$

with the upper (lower) sign referring to bosons (fermions) into Eq. (B.3). By doing so, we obtain

$$\begin{aligned} \frac{d}{dt}\langle\hat{n}_k\rangle(t) &= \sum_{i,j}R_{ij}(\delta_{ik}-\delta_{jk})\mathrm{tr}(\hat{n}_j(1\pm\hat{n}_i)\hat{\rho}(t)) \\ &= \sum_j\left\{R_{kj}[\langle\hat{n}_j\rangle(t)\pm\langle\hat{n}_k\hat{n}_j\rangle(t)]-R_{jk}[\langle\hat{n}_k\rangle(t)\pm\langle\hat{n}_k\hat{n}_j\rangle(t)]\right\}, \end{aligned} \quad (\text{B.6})$$

which is identical to Eq. (6.1).

C. Existence and uniqueness of the set of selected states

In this subsection, we prove first the uniqueness and existence of the set of selected states for fully connected rate matrices in closed systems and second the uniqueness of it in open systems (here the existence is not guaranteed). We have published the proof for closed systems in the supplement material of Ref. [57] and I thank Henning Schomerus for contributing this proof.

In closed systems, the set of selected states \mathcal{S} is defined by the selection condition (7.6) for a given rate-asymmetry matrix A with elements A_{ij} . A solution of this selection condition is given by the set of selected state \mathcal{S} and the two vectors $\boldsymbol{\nu}=(\nu_0,\dots,\nu_{M-1})^T$ and $\boldsymbol{\mu}=(\mu_0,\dots,\mu_{M-1})^T$. The selection condition (7.6) requires that the elements of $\boldsymbol{\nu}$ are nonnegative for selected states and otherwise zero, while the elements of $\boldsymbol{\mu}=A\boldsymbol{\nu}$ are zero for selected states and nonpositive otherwise. We first prove the uniqueness of such a solution and then its existence.

The uniqueness of the set \mathcal{S} is proven by contradiction. For this, we assume the existence of two different sets \mathcal{S}_1 and \mathcal{S}_2 , both fulfilling the selection criterion (7.6) for some vectors ν_i and $\mu_i = A\nu_i$ with $i \in \{1, 2\}$. Using the equation

$$\nu_2^T \mu_1 = \nu_2^T A\nu_1 = (\nu_2^T A\nu_1)^T = \nu_1^T A^T \nu_2 = -\nu_1^T A\nu_2 = -\nu_1^T \mu_2, \quad (\text{C.1})$$

and the inequalities $\nu_2^T \mu_1, \nu_1^T \mu_2 > 0$ [due to the selection condition (7.6)] it follows that

$$0 \geq \nu_2^T \mu_1 = -\nu_1^T \mu_2 \geq 0. \quad (\text{C.2})$$

Consequently, both expressions must vanish, $\nu_2^T \mu_1 = 0$ and $\nu_1^T \mu_2 = 0$, and thus $\mathcal{S}_2 \subset \mathcal{S}_1$ and $\mathcal{S}_1 \subset \mathcal{S}_2$. Therefore, both sets are equivalent, $\mathcal{S}_1 = \mathcal{S}_2 \equiv \mathcal{S}$, the initial assumption is contradicted, and we have proven the uniqueness of the set \mathcal{S} of selected states. Furthermore, the homogeneous linear system for ν generically has a single solution only, so that also both vectors ν and μ are unique.

The existence of the set \mathcal{S} is proven by a combinatoric argument as follows. Let \mathcal{S} be any set with an odd number of states. We denote by $\nu_{\mathcal{S}}$ and $\mu_{\mathcal{S}} = A\nu_{\mathcal{S}}$ the solution of the selection criterion (7.6), where we release the requirement of positivity and negativity, i.e., that the solutions are physical. The vector of signs $\sigma_{\mathcal{S}} = (\sigma_0, \dots, \sigma_{M-1})$ with

$$\begin{cases} \sigma_i = \text{sign}(\nu_i) & \text{for } i \in \mathcal{S}, \\ \sigma_i = -\text{sign}(\mu_i) & \text{for } i \notin \mathcal{S}, \end{cases} \quad (\text{C.3})$$

distinguishes the physical solution ($\sigma_i = 1 \forall i$) from nonphysical solutions. Here, we fix an overall sign due to the orientation of the vector $\nu_{\mathcal{S}}$ by the convention for its first element $\sigma_0 = 1$. Now we observe: (i) Each vector $\sigma_{\mathcal{S}}$ occurs at most for one (odd-numbered) set \mathcal{S} . This can be proven by contradiction, assuming the existence of two different sets \mathcal{S}_1 and \mathcal{S}_2 such that $\sigma_{\mathcal{S}_1} = \sigma_{\mathcal{S}_2}$. Then the modified rate-asymmetry matrix $\tilde{A} = \sigma_{\mathcal{S}_1} \otimes A \otimes \sigma_{\mathcal{S}_1}^T = \sigma_{\mathcal{S}_2} \otimes A \otimes \sigma_{\mathcal{S}_2}^T$ has (physical) solutions for both sets, \mathcal{S}_1 and \mathcal{S}_2 . This contradicts the previously established uniqueness of the set of selected states. (ii) The number 2^{M-1} of possible vectors σ equals the number $\sum_{M_{\mathcal{S}}=1,3,\dots} \binom{M}{M_{\mathcal{S}}} = 2^{M-1}$ of possible sets \mathcal{S} . Therefore, for each vector σ exist one set of selected states $\mathcal{S}(\sigma)$. In particular, the set $\mathcal{S}(\sigma)$ for the vector $\sigma = (1, \dots, 1)$ is the (physical) solution of the rate-asymmetry matrix A . Thus its existence is guaranteed.

The proof for uniqueness in open systems is similar to that of closed systems. We start from the selection criterion for open systems (15.8) in vector notation

$$A\nu + \mathbf{W} = \mu, \quad (\text{C.4})$$

where $\mathbf{W} = (G_0 - L_0, \dots, G_{M-1} - L_{M-1})$ denotes the vector of gain-loss differences. Again, we prove by contradiction, where we assume the existence of two different sets of selected states \mathcal{S}_1 and \mathcal{S}_2 .

We find that

$$\begin{aligned}\boldsymbol{\nu}_2^T \boldsymbol{\mu}_1 &= \boldsymbol{\nu}_2^T (A\boldsymbol{\nu}_1 + W) = [\boldsymbol{\nu}_2^T (A\boldsymbol{\nu}_1 + W)]^T = \boldsymbol{\nu}_1^T A^T \boldsymbol{\nu}_2 + W^T \boldsymbol{\nu}_2 = -\boldsymbol{\nu}_1^T A \boldsymbol{\nu}_2 + \boldsymbol{\nu}_2^T W \\ &= -\boldsymbol{\nu}_1^T \boldsymbol{\mu}_2 + \boldsymbol{\nu}_2^T W + \boldsymbol{\nu}_2^T W.\end{aligned}\quad (\text{C.5})$$

The two last terms vanish since these are the net particle flow in the steady state in leading order. This can be also seen when summing over all indices i in Eq. (15.4)

$$0 = \boldsymbol{\nu}^T (A\boldsymbol{\nu} + W) = \boldsymbol{\nu}^T A\boldsymbol{\nu} + \boldsymbol{\nu}^T W = \boldsymbol{\nu}^T W, \quad (\text{C.6})$$

where we have used the skew-symmetry in the last step. Thus Eq. (C.5) equals Eq. (C.2) and the same reasoning as below Eq. (C.2) applies so that the uniqueness is proven.

However, such a solution is not guaranteed. A simple counter example is a case with $W_i > 0 \forall i$, e.g. a system without loss. No steady state exists since each occupation increases without limit.

D. Relaxation dynamics of a double-pillar polariton system

In the following, we describe the relaxation kinetics of the polariton model in Chap. 14. This derivation is motivated by the experiment published in Ref. [101] and follows mostly the numerical simulation discussed in its supplemental material. The approximative kinetic equations are of the form given by Eq. (13.1). This chapter provides the rates for gain, loss, and the intermode kinetics. All scattering processes are assisted by either reservoir excitons or phonons. We discuss first the gain rates, then the loss rates and finally the intermode kinetics.

The processes where two reservoir excitations at energies E and E' (both larger than the bottle-neck energy E_R) scatter into the mode i and a reservoir excitation at the higher energy $E'' = E + E' - E_i$ gives the following contribution to the dynamics,

$$\begin{aligned}W_x \int dx dy \int dE dE' D(E) \rho_R(x, y) n(E) \cdot D(E') \rho_R(x, y) n(E') \cdot |\psi_i|^2 (n_i + 1) \\ D(E'') (1 + \rho_R(x, y) n(E'')) \\ \approx W_x D_x \langle \hat{N}_R \rangle^2 (\langle \hat{n}_i \rangle + 1) \int dx dy \rho_R^2(x, y) |\psi_i(x, y)|^2 \\ = \langle \hat{N}_R \rangle^2 (\langle \hat{n}_i \rangle + 1) g_i^x \quad \text{with} \quad g_i^x = W_x D_x \int dx dy \rho_R^2(x, y) |\psi_i(x, y)|^2,\end{aligned}\quad (\text{D.1})$$

where $n(E) = n(0)e^{-\beta E}$ is the exciton distribution, which is Boltzmann-distributed since we assume small occupations in the reservoir only [$n(E) \ll 1$ for all energies $E > E_R$ in the reservoir above the bottleneck energy E_R] and $D(E) = D_x$ denotes the exciton's density of states, which is constant since the system is two-dimensional. We assume that the spatial distribution of the reservoir occupation is given by a Gaussian profile $\rho_R(x, y)$ of width w , which is normalized, $\int dx dy \rho_R(x, y) = 1$. In the

second step in Eq. (D.1), we used $\langle \hat{N}_R \rangle = \int dx dy dE D(E) \rho_R(x, y) n(E) = \int dE D(E) n(E)$. Here and henceforth, we neglect, furthermore, the final-state stimulation in the reservoir, $1 + n(E) \approx 1 \forall E > E_R$.

A scattering can also be assisted by phonons. The process where a reservoir exciton at energy E scatters to the mode at energy E_i while creating a phonon of energy $E - E_i$ reads

$$\begin{aligned} & W_p \int dx dy dE D(E) \rho_R(x, y) n(E) \cdot |\psi_i|^2 (n_i + 1) \cdot D_p(E - E_i) (1 + n(E - E_i)) \\ & \approx (\langle \hat{n}_i \rangle + 1) W_p \int dx dy \rho_R(x, y) |\psi_i(x, y)|^2 = g_i^p (\langle \hat{n}_i \rangle + 1), \end{aligned} \quad (\text{D.2})$$

where $D_p(E) = D_p$ is the density of states of the phonons. The total gain is given by

$$g_i = g_i^x + g_i^p = W_x D_x N_x \int dx dy \rho_R^2(x, y) |\psi_i(x, y)|^2 + W_p D_p \int dx dy \rho_R(x, y) |\psi_i(x, y)|^2 \quad (\text{D.3})$$

with the parameters $W_x D_x = 2 \times 10^4 \text{ s}^{-1}$, $W_p D_p = 1 \times 10^9 \text{ s}^{-1}$, $w = 3.0 \mu\text{m}$, and $N_x = 100$.

The backward processes from the system to the reservoir are again either exciton- or phonon-assisted. The rate of the process where a polariton from mode i and a reservoir excitation at energy $E'' = E + E' - E_i$ scatters to two reservoir excitations at energies E and E' are

$$\begin{aligned} & W_x \int dx dy dE dE' |\psi_i|^2 \langle \hat{n}_i \rangle \cdot D(E'') \rho_R n(E'') \cdot D(E) (1 + \rho_R n(E)) \cdot D(E') (1 + \rho_R n(E')) \\ & \approx W_x \int dx dy dE dE' |\psi_i|^2 \langle \hat{n}_i \rangle \cdot D(E'') \rho_R n(E') e^{\beta E_i} e^{-\beta E} \cdot D(E) \cdot D(E') \\ & \approx \langle \hat{N}_R \rangle \frac{D}{\beta} \langle \hat{n}_i \rangle W_x \int dx dy \rho_R(x, y) |\psi_i(x, y)|^2 = \langle \hat{n}_i \rangle \ell_i^x. \end{aligned} \quad (\text{D.4})$$

The backward process for a phonon assisted scattering from the mode i to the reservoir at energy E by absorption a phonon of energy $E - E_i$ is

$$\begin{aligned} & W_p \int dx dy dE |\psi_i|^2 n_i \cdot D_p(E - E_i) n_p(E - E_i) \cdot D(E) (1 + \rho_R n(E)) \\ & \approx \langle \hat{n}_i \rangle W_p D e^{-\beta E_i} \int dx dy \rho_R(x, y) |\psi_i(x, y)|^2 = \langle \hat{n}_i \rangle \ell_i^p. \end{aligned} \quad (\text{D.5})$$

The total loss rates are

$$\ell_i = \ell_i^x + \ell_i^p = N_x \frac{D}{\beta} W_x \int dx dy \rho_R(x, y) |\psi_i(x, y)|^2 + W_p D e^{-\beta E_i} \int dx dy \rho_R(x, y) |\psi_i(x, y)|^2. \quad (\text{D.6})$$

The intermode kinetics, where a polariton in a state j scatters into the state i , is caused either by

another polariton or a phonon. The rate R_{ij} for this process is

$$R_{ij} = \left[W_x N_x \int dx dy |\langle i|j\rangle|^2 \rho_R^2(x, y) + \int dx dy W_p S |\langle i|j\rangle|^2 \right] \begin{cases} e^{\beta(E_k - E_i)} & \text{for } k < i, \\ 1 & \text{else.} \end{cases} \quad (\text{D.7})$$

Here the first (second) term describes the scattering with an exciton (phonon), respectively.

Furthermore, we assumed the lifetimes [see Eq. (13.1)] to be $\tau_R = 400$ ps and $\tau_i = 20$ ps.

E. Augmented mean-field equation

In this appendix, we derive the equations of motion for the two-particle correlations $\langle \hat{n}_k \hat{n}_i \rangle(t)$ [Eqs. (9.5)]. Together with the equations of motion for the mean occupations $\langle \hat{n}_i \rangle(t)$ [Eqs. (9.6)] they build the set of equations for the augmented mean-field theory described in Chap. 9. Hereby we close the hierarchy of equations by assuming trivial three-particle correlations. For brevity, we will suppress the time argument in the following.

The exact equations of motion for the two-particle correlations $\langle \hat{n}_k \hat{n}_i \rangle$ are obtained from the many-body master equation (2.23) in Lindblad form. We multiply this equation by $\hat{n}_k \hat{n}_i$ from the left and take the trace,

$$\frac{d}{dt} \langle \hat{n}_k \hat{n}_i \rangle = \text{tr} \left(\hat{n}_k \hat{n}_i \dot{\hat{\rho}} \right) = \sum_{j,l} R_{lj} \text{tr} \left(\hat{n}_k \hat{n}_i \hat{a}_l^\dagger \hat{a}_j \hat{\rho} \hat{a}_j^\dagger \hat{a}_l - \frac{1}{2} \hat{n}_k \hat{n}_i \left\{ \hat{\rho}, \hat{a}_j^\dagger \hat{a}_l \hat{a}_l^\dagger \hat{a}_j \right\} \right). \quad (\text{E.1})$$

Invoking cyclic permutation under the trace and using Eq. (B.4), we regroup the operators as

$$\hat{a}_j^\dagger \hat{a}_l \hat{n}_k \hat{n}_i = \hat{n}_k \hat{n}_i \hat{a}_j^\dagger \hat{a}_l + [(\delta_{li} - \delta_{ji}) \hat{n}_k + (\delta_{lk} - \delta_{jk}) \hat{n}_i + (\delta_{li} - \delta_{ji})(\delta_{lk} - \delta_{jk})] \hat{a}_j^\dagger \hat{a}_l. \quad (\text{E.2})$$

Here, the first term and the anticommutator in Eq. (E.1) form a commutator, which vanishes under the trace, $\text{tr}(\rho[\hat{n}_k \hat{n}_i, \hat{a}_j^\dagger \hat{a}_l \hat{a}_l^\dagger \hat{a}_j]) = 0$. Applying also the operator relation Eq. (B.5), we arrive at

$$\frac{d}{dt} \langle \hat{n}_k \hat{n}_i \rangle = \sum_{j,l} R_{lj} \text{tr} \left\{ [(\delta_{li} - \delta_{ji}) \hat{n}_k + (\delta_{lk} - \delta_{jk}) \hat{n}_i + (\delta_{li} - \delta_{ji})(\delta_{lk} - \delta_{jk})] [\hat{n}_j (1 \pm \hat{n}_l) \mp \delta_{jl} \hat{n}_j] \hat{\rho} \right\}. \quad (\text{E.3})$$

The term $\delta_{jl} \hat{n}_j$ vanishes in combination with each of the δ -prefactors, leaving

$$\begin{aligned} \frac{d}{dt} \langle \hat{n}_k \hat{n}_i \rangle = \sum_{j,l} R_{lj} & \left[(\delta_{li} - \delta_{ji}) (\langle \hat{n}_k \hat{n}_j \rangle \pm \langle \hat{n}_k \hat{n}_j \hat{n}_l \rangle) \right. \\ & \left. + (\delta_{lk} - \delta_{jk}) [(\langle \hat{n}_i \hat{n}_j \rangle \pm \langle \hat{n}_i \hat{n}_j \hat{n}_l \rangle) + (\delta_{li} - \delta_{ji}) (\langle \hat{n}_j \rangle \pm \langle \hat{n}_j \hat{n}_l \rangle)] \right]. \end{aligned} \quad (\text{E.4})$$

Evaluating one of the two sums, we arrive at

$$\begin{aligned}
\frac{d}{dt}\langle\hat{n}_k\hat{n}_i\rangle &= \pm\sum_j(A_{kj}+A_{ij})\langle\hat{n}_k\hat{n}_i\hat{n}_j\rangle \\
&+ \sum_j(R_{kj}\langle\hat{n}_i\hat{n}_j\rangle - R_{jk}\langle\hat{n}_i\hat{n}_k\rangle + R_{ij}\langle\hat{n}_k\hat{n}_j\rangle - R_{ji}\langle\hat{n}_k\hat{n}_i\rangle) \\
&+ \delta_{ik}\sum_j(R_{kj}(\langle\hat{n}_j\rangle \pm \langle\hat{n}_j\hat{n}_k\rangle) + R_{jk}(\langle\hat{n}_k\rangle \pm \langle\hat{n}_k\hat{n}_j\rangle)) \\
&- R_{ik}(\langle\hat{n}_k\rangle \pm \langle\hat{n}_k\hat{n}_i\rangle) - R_{ki}(\langle\hat{n}_i\rangle \pm \langle\hat{n}_i\hat{n}_k\rangle),
\end{aligned} \tag{E.5}$$

which is identical to Eq. (9.5).

F. Extracting parameters of a bimodal laser

The asymptotic theory describes the generic form of the mode switching. Thus, their analytic expressions can be used to obtain the experimental parameters. However, the model parameters cannot be related directly to the experimental parameters since the proportionality factor a_i between the intensity of the emitted light J_i and the occupation of modes, $\langle\hat{n}_i\rangle = a_i J_i$, and the excitation efficiency b of the pumping with respect to the injection current, $P = bI$, is unknown.

The main properties of the switching are captured by the effective-gain ratio $G = \frac{P_{BC}}{P_{CD}}$ [see Eq. (17.13)]. This ratio can be obtained in the following way: We apply a linear fit for the intensities of the selected modes i in each of the regions $R \in \{B, C, D\}$,

$$J_i(I)|_R = A_{iR}I + B_{iR}. \tag{F.1}$$

The ratio $\frac{P_{CD}}{P_{BC}} = \frac{I_{CD}}{I_{BC}}$ is determined by either both intersections $J_h|_B(I_{BC}) = J_h|_C(I_{BC})$ and $J_l|_C(I_{CD}) = J_l|_D(I_{CD})$ or both currents where the occupation of a mode approaches zero, $J_h|_C(I_{CD}) = 0$ and $J_l|_C(I_{BC}) = 0$. Both procedures give similar values for the effective-gain ratio G via Eq. (17.13), namely 1.22 and 1.27, respectively. Obtaining the effective-gain ratio G is possible since it requires neither the knowledge of the excitation efficiency b nor the absolute number of cavity photons via a_i .

The parameters $A_{h \rightarrow l}$, g_h , g_l , ℓ_h , ℓ_l , are extracted for comparison between theory and experiment via the least-squares method for all experimental data with $I < 80 \mu A$ and are listed in the caption of Fig. 17.1. Since the timescale does not affect steady-state properties, all parameters are measured in units of the lifetime τ . The individual rates $R_{l \rightarrow h}$ and $R_{h \rightarrow l}$ do not affect the asymptotic theory, only the rate asymmetry $A_{l \rightarrow h}$ does. However, the correlation function $g_{ll}^{(2)}$ (not discussed in this thesis) depends on the individual rates, so that $R_{l \rightarrow h}$ can be chosen to reproduce this correlation function. A discussion of this correlation function can be found in Ref. [102].

List of Figures

1.1. Bose condensation versus Bose selection	3
2.1. Two scenarios of driven-dissipative ideal Bose gases	13
2.2. Monto-Carlo simulation for a quartic oscillator	24
3.1. Tight-binding chain coupled to two heat baths	27
3.2. Rates in the tight-binding chain coupled to two heat baths	28
3.3. Time-periodically driven chain in contact with a heat bath	29
3.4. Rates in the time-periodically driven chain coupled to a thermal bath	30
3.5. Rates among the Floquet states of the quartic oscillator	31
5.1. Bose selection in a quartic oscillator	35
5.2. Bose selection and Bose condensation in a tight-binding chain	37
5.3. Temperature dependence of the steady state of an open Floquet gas.	38
7.1. Number of selected states in the random-rate model	44
8.1. Transitions caused by the variation of a system parameter	50
8.2. Four generic types of transitions	51
8.3. Preasymptotic state close to a transition	53
9.1. Nontrivial correlations induced by nonequilibrium effects	56
10.1. Heat current through a chain coupled to two heat baths	60
10.2. Heat current in a bath coupled to periodically-driven chain	61
11.1. Preasymptotic state caused by small rates	64
11.2. Two uncoupled Bose-selected states	69
12.1. Comparison between ideal bosons and population dynamics	72
13.1. Sketch of open driven-dissipative ideal Bose gases	76
14.1. Sketch of the exciton-polariton dispersion relation	79
14.2. Input-output characteristics of an asymmetrically-pumped double-pillar structure	81
15.1. Bose selection in open ideal Bose gases	84

16.1. Bose selection for the asymmetrically-pumped double-pillar polariton gas	88
16.2. Bose selection in the limit of strong pumping	93
17.1. Switching in a bimodal micropillar cavity	96
17.2. Phenomenological model of bimodal cavities	97
17.3. Phase diagram of bimodal cavities	99

Bibliography

- [1] L. Pitaevskii and S. Stringari, *Bose-Einstein Condensation and Superfluidity*, volume 164, Oxford University Press (2016). Cited on page 1.
- [2] T. Schumm, S. Hofferberth, L. M. Andersson, S. Wildermuth, S. Groth, I. Bar-Joseph, J. Schmiedmayer, and P. Krüger, “Matter-wave interferometry in a double well on an atom chip”, *Nature Phys.* **1**, 57 (2005). Cited on page 1.
- [3] S. N. Bose, “Wärmegleichgewicht im Strahlungsfeld bei Anwesenheit von Materie”, *Z. Phys.* **27**, 384 (1924). Cited on page 1.
- [4] A. Einstein, “Quantentheorie des einatomigen idealen Gases – Zweite Abhandlung”, *Sitzungsber. Kgl. Preuss. Akad. Wiss.* **I**, 3 (1925). Cited on pages 1 and 33.
- [5] M. H. Anderson, J. R. Ensher, M. R. Matthews, C. E. Wieman, and E. A. Cornell, “Observation of Bose-Einstein condensation in a dilute atomic vapor”, *Science* **269**, 198 (1995). Cited on page 1.
- [6] K. B. Davis, M. O. Mewes, M. R. Andrews, N. J. Van Druten, D. S. Durfee, D. M. Kurn, and W. Ketterle, “Bose-Einstein condensation in a gas of sodium atoms”, *Phys. Rev. Lett.* **75**, 3969 (1995). Cited on page 1.
- [7] J. Kasprzak, M. Richard, S. Kundermann, A. Baas, P. Jeambrun, J. M. J. Keeling, F. M. Marchetti, M. H. Szymanska, R. André, J. L. Staehli, V. Savona, P. B. Littlewood, B. Deveaud, and L. S. Dang, “Bose-Einstein condensation of exciton polaritons”, *Nature* **443**, 409 (2006). Cited on pages 1 and 79.
- [8] R. Balili, V. Hartwell, D. Snoke, L. Pfeiffer, and K. West, “Bose-Einstein condensation of microcavity polaritons in a trap”, *Science* **316**, 1007 (2007). Cited on pages 1 and 79.
- [9] S. O. Demokritov, V. E. Demidov, O. Dzyapko, G. A. Melkov, A. A. Serga, B. Hillebrands, and A. N. Slavin, “Bose-Einstein condensation of quasi-equilibrium magnons at room temperature under pumping”, *Nature* **443**, 430 (2006). Cited on page 1.
- [10] T. Nikuni, M. Oshikawa, A. Oosawa, and H. Tanaka, “Bose-Einstein condensation of dilute magnons in TlCuCl_3 ”, *Phys. Rev. Lett.* **84**, 5868 (2000). Cited on page 1.
- [11] M. Greiner, C. A. Regal, and D. S. Jin, “Emergence of a molecular Bose-Einstein condensate from a Fermi gas”, *Nature* **426**, 537 (2003). Cited on page 1.

-
- [12] J. Klaers, J. Schmitt, F. Vewinger, and M. Weitz, “Bose-Einstein condensation of photons in an optical microcavity”, *Nature* **468**, 545 (2010). Cited on pages 1 and 4.
- [13] J. Klaers, F. Vewinger, and M. Weitz, “Thermalization of a two-dimensional photonic gas in a ‘white wall’ photon box”, *Nature Phys.* **6**, 512 (2010). Cited on pages 1, 4, and 75.
- [14] F. London, “On the Bose-Einstein condensation”, *Phys. Rev.* **54**, 947 (1938). Cited on page 1.
- [15] J. Bardeen, L. N. Cooper, and J. R. Schrieffer, “Theory of superconductivity”, *Phys. Rev.* **108**, 1175 (1957). Cited on page 1.
- [16] E. T. Jaynes, “Information theory and statistical mechanics”, *Phys. Rev.* **106**, 620 (1957). Cited on page 1.
- [17] N. D. Mermin and H. Wagner, “Absence of ferromagnetism or antiferromagnetism in one- or two-dimensional isotropic Heisenberg models”, *Phys. Rev. Lett.* **17**, 1133 (1966). Cited on pages 2 and 103.
- [18] W. Ketterle and N. J. van Druten, “Bose-Einstein condensation of a finite number of particles trapped in one or three dimensions”, *Phys. Rev. A* **54**, 656 (1996). Cited on pages 2, 33, 34, and 103.
- [19] A. Dhar, “Heat transport in low-dimensional systems”, *Adv. Phys.* **57**, 457 (2008). Cited on page 2.
- [20] A. Asadian, D. Manzano, M. Tiersch, and H. J. Briegel, “Heat transport through lattices of quantum harmonic oscillators in arbitrary dimensions”, *Phys. Rev. E* **87**, 012109 (2013). Cited on page 2.
- [21] D. Manzano, M. Tiersch, A. Asadian, and H. J. Briegel, “Quantum transport efficiency and Fourier’s law”, *Phys. Rev. E* **86**, 061118 (2012). Cited on page 2.
- [22] P. H. Guimarães, G. T. Landi, and M. J. de Oliveira, “Nonequilibrium quantum chains under multisite Lindblad baths”, *Phys. Rev. E* **94**, 032139 (2016). Cited on page 2.
- [23] J. Weber, “Fluctuation dissipation theorem”, *Phys. Rev.* **101**, 1620 (1956). Cited on page 2.
- [24] U. M. B. Marconi, A. Puglisi, L. Rondoni, and A. Vulpiani, “Fluctuation–dissipation: response theory in statistical physics”, *Phys. Rep.* **461**, 111 (2008). Cited on page 2.
- [25] T. W. Kibble, “Topology of cosmic domains and strings”, *J. Phys. A* **9**, 1387 (1976). Cited on page 2.
- [26] L. M. Sieberer, S. D. Huber, E. Altman, and S. Diehl, “Dynamical critical phenomena in driven-dissipative systems”, *Phys. Rev. Lett.* **110**, 195301 (2013). Cited on page 2.
- [27] A. Polkovnikov, K. Sengupta, A. Silva, and M. Vengalattore, “Colloquium: Nonequilibrium dynamics of closed interacting quantum systems”, *Rev. Mod. Phys.* **83**, 863 (2011). Cited on pages 2 and 5.

- [28] B. Kraus, H. P. Büchler, S. Diehl, A. Kantian, A. Micheli, and P. Zoller, “Preparation of entangled states by quantum Markov processes”, *Phys. Rev. A* **78**, 042307 (2008). Cited on page 2.
- [29] K. W. Murch, U. Vool, D. Zhou, S. J. Weber, S. M. Girvin, and I. Siddiqi, “Cavity-assisted quantum bath engineering”, *Phys. Rev. Lett.* **109**, 183602 (2012). Cited on page 2.
- [30] T. Iadecola, T. Neupert, and C. Chamon, “Occupation of topological Floquet bands in open systems”, *Phys. Rev. B* **91**, 235133 (2015). Cited on page 2.
- [31] K. I. Seetharam, C.-E. Bardyn, N. H. Lindner, M. S. Rudner, and G. Refael, “Controlled population of Floquet-Bloch states via coupling to Bose and Fermi baths”, *Phys. Rev. X* **5**, 041050 (2015). Cited on page 2.
- [32] A. Griessner, A. J. Daley, S. R. Clark, D. Jaksch, and P. Zoller, “Dark-state cooling of atoms by superfluid immersion”, *Phys. Rev. Lett.* **97**, 220403 (2006). Cited on pages 2 and 27.
- [33] S. Diehl, A. Micheli, A. Kantian, B. Kraus, H. P. Büchler, and P. Zoller, “Quantum states and phases in driven open quantum systems with cold atoms”, *Nature Phys.* **4**, 878 (2008). Cited on pages 2 and 27.
- [34] S. Diehl, E. Rico, M. A. Baranov, and P. Zoller, “Topology by dissipation in atomic quantum wires”, *Nature Phys.* **7**, 971 (2011). Cited on page 2.
- [35] J. C. Budich, P. Zoller, and S. Diehl, “Dissipative preparation of Chern insulators”, *Phys. Rev. A* **91**, 042117 (2015). Cited on page 2.
- [36] J. H. Shirley, “Solution of the Schrödinger equation with a Hamiltonian periodic in time”, *Phys. Rev.* **138**, B979 (1965). Cited on pages 2 and 14.
- [37] H. Sambe, “Steady states and quasienergies of a quantum-mechanical system in an oscillating field”, *Phys. Rev. A* **7**, 2203 (1973). Cited on pages 2 and 14.
- [38] A. Eckardt, “Atomic quantum gases in periodically driven optical lattices”, *Rev. Mod. Phys.* **89**, 011004 (2017). Cited on page 2.
- [39] J. Struck, C. Ölschläger, M. Weinberg, P. Hauke, J. Simonet, A. Eckardt, M. Lewenstein, K. Sengstock, and P. Windpassinger, “Tunable gauge potential for neutral and spinless particles in driven optical lattices”, *Phys. Rev. Lett.* **108**, 225304 (2012). Cited on page 2.
- [40] J. Struck, M. Weinberg, C. Ölschläger, P. Windpassinger, J. Simonet, K. Sengstock, R. Höppner, P. Hauke, A. Eckardt, M. Lewenstein, and L. Mathey, “Engineering Ising-XY spin-models in a triangular lattice using tunable artificial gauge fields”, *Nature Phys.* **9**, 738 (2013). Cited on page 2.
- [41] G. Jotzu, M. Messer, R. Desbuquois, M. Lebrat, T. Uehlinger, D. Greif, and T. Esslinger, “Experimental realization of the topological Haldane model with ultracold fermions”, *Nature* **515**, 237 (2014). Cited on page 2.

- [42] A. Eckardt, P. Hauke, P. Soltan-Panahi, C. Becker, K. Sengstock, and M. Lewenstein, “Frustrated quantum antiferromagnetism with ultracold bosons in a triangular lattice”, *EPL (Europhysics Letters)* **89**, 10010 (2010). Cited on page 2.
- [43] J. Struck, C. Ölschläger, R. Le Targat, P. Soltan-Panahi, A. Eckardt, M. Lewenstein, P. Windpassinger, and K. Sengstock, “Quantum simulation of frustrated classical magnetism in triangular optical lattices”, *Science* **333**, 996 (2011). Cited on page 2.
- [44] A. Eckardt, C. Weiss, and M. Holthaus, “Superfluid-insulator transition in a periodically driven optical lattice”, *Phys. Rev. Lett.* **95**, 260404 (2005). Cited on pages 2, 5, and 14.
- [45] A. Zenesini, H. Lignier, D. Ciampini, O. Morsch, and E. Arimondo, “Coherent control of dressed matter waves”, *Phys. Rev. Lett.* **102**, 100403 (2009). Cited on pages 2 and 14.
- [46] M. Grifoni and P. Hänggi, “Driven quantum tunneling”, *Phys. Rep.* **304**, 229 (1998). Cited on page 2.
- [47] W. Kohn, “Periodic thermodynamics”, *J. Stat. Phys.* **103**, 417 (2001). Cited on pages 3 and 15.
- [48] H. P. Breuer and F. Petruccione, *The theory of open quantum systems*, Oxford University Press (2002). Cited on pages 3 and 15.
- [49] R. Blümel, A. Buchleitner, R. Graham, L. Sirko, U. Smilansky, and H. Walther, “Dynamical localization in the microwave interaction of Rydberg atoms: The influence of noise”, *Phys. Rev. A* **44**, 4521 (1991). Cited on pages 3 and 15.
- [50] S. Kohler, T. Dittrich, and P. Hänggi, “Floquet-Markovian description of the parametrically driven, dissipative harmonic quantum oscillator”, *Phys. Rev. E* **55**, 300 (1997). Cited on pages 3 and 15.
- [51] H.-P. Breuer, W. Huber, and F. Petruccione, “Quasistationary distributions of dissipative nonlinear quantum oscillators in strong periodic driving fields”, *Phys. Rev. E* **61**, 4883 (2000). Cited on pages 3, 15, 22, and 32.
- [52] R. Ketzmerick and W. Wustmann, “Statistical mechanics of Floquet systems with regular and chaotic states”, *Phys. Rev. E* **82**, 021114 (2010). Cited on pages 3, 14, 22, and 32.
- [53] M. Langemeyer and M. Holthaus, “Energy flow in periodic thermodynamics”, *Phys. Rev. E* **89**, 012101 (2014). Cited on pages 3, 13, and 59.
- [54] D. W. Hone, R. Ketzmerick, and W. Kohn, “Time-dependent Floquet theory and absence of an adiabatic limit”, *Phys. Rev. A* **56**, 4045 (1997). Cited on page 4.
- [55] D. W. Hone, R. Ketzmerick, and W. Kohn, “Statistical mechanics of Floquet systems: The pervasive problem of near degeneracies”, *Phys. Rev. E* **79**, 051129 (2009). Cited on pages 4, 15, and 19.
- [56] R. Ketzmerick and W. Wustmann, “Switching mechanism in periodically driven quantum systems with dissipation”, *Phys. Rev. E* **80**, 021117 (2009). Cited on pages 4 and 30.

- [57] D. Vorberg, W. Wustmann, R. Ketzmerick, and A. Eckardt, “Generalized Bose-Einstein condensation into multiple states in driven-dissipative systems”, *Phys. Rev. Lett.* **111**, 240405 (2013). Cited on pages 4, 9, 22, 23, 27, 32, 35, 39, 41, 59, and 106.
- [58] D. Vorberg, W. Wustmann, H. Schomerus, R. Ketzmerick, and A. Eckardt, “Nonequilibrium steady states of ideal bosonic and fermionic quantum gases”, *Phys. Rev. E* **92**, 062119 (2015). Cited on pages 4, 9, 22, 23, 27, 35, 37, 39, 40, 41, 45, 49, 53, 55, 56, 59, 71, and 72.
- [59] E. Wertz, L. Ferrier, D. Solnyshkov, R. Johne, D. Sanvitto, A. Lemaître, I. Sagnes, R. Grousseau, A. V. Kavokin, P. Senellart, G. Malpuech, and J. Bloch, “Spontaneous formation and optical manipulation of extended polariton condensates”, *Nat. Phys.* **6**, 860 (2010). Cited on page 4.
- [60] H. Deng, H. Haug, and Y. Yamamoto, “Exciton-polariton Bose-Einstein condensation”, *Rev. Mod. Phys.* **82**, 1489 (2010). Cited on pages 4 and 79.
- [61] I. Carusotto and C. Ciuti, “Quantum fluids of light”, *Rev. Mod. Phys.* **85**, 299 (2013). Cited on pages 4, 75, and 79.
- [62] A. E. Siegman, “Lasers”, University Science Books, Sausalito **37**, 462 (1986). Cited on pages 4, 87, 89, and 98.
- [63] P. Kirton and J. Keeling, “Thermalization and breakdown of thermalization in photon condensates”, *Phys. Rev. A* **91**, 033826 (2015). Cited on page 4.
- [64] P. Kirton and J. Keeling, “Nonequilibrium model of photon condensation”, *Phys. Rev. Lett.* **111**, 100404 (2013). Cited on page 4.
- [65] H. Haken, “Laser theory”, in “Light and Matter”, 1, Springer (1970). Cited on page 4.
- [66] V. DeGiorgio and M. O. Scully, “Analogy between the laser threshold region and a second-order phase transition”, *Phys. Rev. A* **2**, 1170 (1970). Cited on page 4.
- [67] L. Mandel and E. Wolf, *Optical coherence and quantum optics*, Cambridge University Press (1995). Cited on page 4.
- [68] L. V. Butov, “Solid-state physics: A polariton laser”, *Nature* **447**, 540 (2007). Cited on page 5.
- [69] J. Kasprzak, D. D. Solnyshkov, R. André, L. S. Dang, and G. Malpuech, “Formation of an exciton polariton condensate: Thermodynamic versus kinetic regimes”, *Phys. Rev. Lett.* **101**, 146404 (2008). Cited on page 5.
- [70] B. Deveaud-Plédran, “The behaviour of exciton-polaritons”, *Nat. Photon.* **6**, 205 (2012). Cited on page 5.
- [71] L. V. Butov and A. V. Kavokin, “The behaviour of exciton-polaritons”, *Nat. Photon.* **6**, 2 (2012). Cited on page 5.
- [72] A. Chiocchetta, A. Gambassi, and I. Carusotto, “Laser operation and Bose-Einstein condensation: analogies and differences”, in “Universal Themes of Bose-Einstein Condensation”, Cambridge University Press (2017). Cited on page 5.

- [73] Y. Sun, P. Wen, Y. Yoon, G. Liu, M. Steger, L. N. Pfeiffer, K. West, D. W. Snoke, and K. A. Nelson, “Bose-Einstein condensation of long-lifetime polaritons in thermal equilibrium”, *Phys. Rev. Lett.* **118**, 016602 (2017). Cited on pages 5, 75, and 80.
- [74] M. Wouters, I. Carusotto, and C. Ciuti, “Spatial and spectral shape of inhomogeneous nonequilibrium exciton-polariton condensates”, *Phys. Rev. B* **77**, 115340 (2008). Cited on page 5.
- [75] A. Imamoglu, R. J. Ram, S. Pau, and Y. Yamamoto, “Nonequilibrium condensates and lasers without inversion: Exciton-polariton lasers”, *Phys. Rev. A* **53**, 4250 (1996). Cited on pages 5 and 79.
- [76] T. Byrnes, N. Y. Kim, and Y. Yamamoto, “Exciton-polariton condensates”, *Nature Phys.* **10**, 803 (2014). Cited on pages 5, 75, and 79.
- [77] J. M. Deutsch, “Quantum statistical mechanics in a closed system”, *Phys. Rev. A* **43**, 2046 (1991). Cited on page 5.
- [78] M. Srednicki, “Chaos and quantum thermalization”, *Phys. Rev. E* **50**, 888–901 (1994). Cited on page 5.
- [79] M. Rigol, V. Dunjko, and M. Olshanii, “Thermalization and its mechanism for generic isolated quantum systems”, *Nature* **452**, 854 (2008). Cited on page 5.
- [80] B. L. Altshuler, Y. Gefen, A. Kamenev, and L. S. Levitov, “Quasiparticle lifetime in a finite system: A nonperturbative approach”, *Phys. Rev. Lett.* **78**, 2803 (1997). Cited on page 5.
- [81] D. M. Basko, I. L. Aleiner, and B. L. Altshuler, “Metal-insulator transition in a weakly interacting many-electron system with localized single-particle states”, *Ann. Phys.* **321**, 1126 (2006). Cited on page 5.
- [82] M. Schreiber, S. S. Hodgman, P. Bordia, H. P. Lüschen, M. H. Fischer, R. Vosk, E. Altman, U. Schneider, and I. Bloch, “Observation of many-body localization of interacting fermions in a quasirandom optical lattice”, *Science* **349**, 842 (2015). Cited on page 5.
- [83] M. Rigol, V. Dunjko, V. Yurovsky, and M. Olshanii, “Relaxation in a completely integrable many-body quantum system: An *Ab Initio* study of the dynamics of the highly excited states of 1d lattice hard-core bosons”, *Phys. Rev. Lett.* **98**, 050405 (2007). Cited on page 5.
- [84] T. Langen, S. Erne, R. Geiger, B. Rauer, T. Schweigler, M. Kuhnert, W. Rohringer, I. E. Mazets, T. Gasenzer, and J. Schmiedmayer, “Experimental observation of a generalized Gibbs ensemble”, *Science* **348**, 207 (2015). Cited on page 5.
- [85] J. Z. Imbrie, “Diagonalization and many-body localization for a disordered quantum spin chain”, *Phys. Rev. Lett.* **117**, 027201 (2016). Cited on page 5.
- [86] A. Lazarides, A. Das, and R. Moessner, “Equilibrium states of generic quantum systems subject to periodic driving”, *Phys. Rev. E* **90**, 012110 (2014). Cited on page 5.

- [87] L. D'Alessio and M. Rigol, "Long-time behavior of isolated periodically driven interacting lattice systems", *Phys. Rev. X* **4**, 041048 (2014). Cited on page 5.
- [88] B. Gertjerenken and M. Holthaus, "Fluctuations of the order parameter of a mesoscopic Floquet condensate", *Phys. Rev. A* **90**, 053614 (2014). Cited on page 5.
- [89] C. Heinisch and M. Holthaus, "Entropy production within a pulsed Bose–Einstein condensate", *Z. Naturforsch. A* **71**, 875 (2016). Cited on page 5.
- [90] S. Choudhury and E. J. Mueller, "Stability of a Floquet Bose-Einstein condensate in a one-dimensional optical lattice", *Phys. Rev. A* **90**, 013621 (2014). Cited on page 5.
- [91] S. Choudhury and E. J. Mueller, "Transverse collisional instabilities of a Bose-Einstein condensate in a driven one-dimensional lattice", *Phys. Rev. A* **91**, 023624 (2015). Cited on page 5.
- [92] M. Weinberg, C. Ölschläger, C. Sträter, S. Prella, A. Eckardt, K. Sengstock, and J. Simonet, "Multiphoton interband excitations of quantum gases in driven optical lattices", *Phys. Rev. A* **92**, 043621 (2015). Cited on page 5.
- [93] T. Bilitewski and N. R. Cooper, "Scattering theory for Floquet-Bloch states", *Phys. Rev. A* **91**, 033601 (2015). Cited on page 5.
- [94] C. Sträter and A. Eckardt, "Interband heating processes in a periodically driven optical lattice", *Z. Naturforsch. A* **71**, 909 (2016). Cited on page 5.
- [95] A. Lazarides, A. Das, and R. Moessner, "Periodic thermodynamics of isolated quantum systems", *Phys. Rev. Lett.* **112**, 150401 (2014). Cited on pages 5 and 103.
- [96] A. Lazarides, A. Das, and R. Moessner, "Fate of many-body localization under periodic driving", *Phys. Rev. Lett.* **115**, 030402 (2015). Cited on pages 5 and 103.
- [97] J. Zhang, P. W. Hess, A. Kyprianidis, P. Becker, A. Lee, J. Smith, G. Pagano, I. D. Potirniche, A. C. Potter, A. Vishwanath, N. Y. Yao, and C. Monroe, "Observation of a discrete time crystal", *Nature* **543**, 217 (2017). Cited on page 5.
- [98] R. Moessner and S. L. Sondhi, "Equilibration and order in quantum Floquet matter", *Nature Phys.* **13**, 424 (2017). Cited on page 5.
- [99] I. Bloch, "Ultracold quantum gases in optical lattices", *Nature Phys.* **1**, 23 (2005). Cited on pages 6 and 27.
- [100] J. Hofbauer and K. Sigmund, *Evolutionary games and population dynamics*, Cambridge University Press (1998). Cited on pages 7 and 71.
- [101] M. Galbiati, L. Ferrier, D. D. Solnyshkov, D. Tanese, E. Wertz, A. Amo, M. Abbarchi, P. Senellart, I. Sagnes, A. Lemaître, E. Galopin, G. Malpuech, and J. Bloch, "Polariton condensation in photonic molecules", *Phys. Rev. Lett.* **108**, 126403 (2012). Cited on pages 8, 76, 79, 80, 81, 82, and 108.

- [102] H. A. M. Leymann, D. Vorberg, T. Lettau, C. Hopfmann, C. Schneider, M. Kamp, S. Höfling, R. Ketzmerick, J. Wiersig, S. Reitzenstein, and A. Eckardt, “Pump-power-driven mode switching in a microcavity device and its relation to Bose-Einstein condensation”, *Phys. Rev. X* **7**, 021045 (2017). Cited on pages 8, 9, 75, 76, 95, and 111.
- [103] A. Schnell, D. Vorberg, R. Ketzmerick, and A. Eckardt, “High-temperature nonequilibrium bose condensation induced by a hot needle”, *Phys. Rev. Lett.* **119**, 140602 (2017). Cited on pages 9 and 45.
- [104] S. Braun, J. P. Ronzheimer, M. Schreiber, S. S. Hodgman, T. Rom, I. Bloch, and U. Schneider, “Negative absolute temperature for motional degrees of freedom”, *Science* **339**, 52 (2013). Cited on pages 14 and 29.
- [105] K. Blum, *Density matrix theory and applications*, Plenum Press, New York (1996). Cited on page 15.
- [106] M. Nakatani and T. Ogawa, “Quantum master equations for composite systems: Is Born–Markov approximation really valid?”, *J. Phys. Soc.* **79** (2010). Cited on page 15.
- [107] M. Stollsteimer, *Thermodynamische Eigenschaften periodisch kontrollierter Quantensysteme*, Ph.D. thesis, Universitätsbibliothek der Universität Stuttgart (2006). Cited on page 15.
- [108] T. Mori and S. Miyashita, “Dynamics of the density matrix in contact with a thermal bath and the quantum master equation”, *J. Phys. Soc.* **77**, 124005 (2008). Cited on page 17.
- [109] W. Wustmann, *Statistical mechanics of time-periodic quantum systems*, Ph.D. thesis, Technische Universität Dresden (2010). Cited on pages 17, 30, and 32.
- [110] C. Fleming, N. I. Cummings, C. Anastopoulos, and B. L. Hu, “The rotating-wave approximation: consistency and applicability from an open quantum system analysis”, *J. Phys. A* **43**, 405304 (2010). Cited on page 18.
- [111] G. Lindblad, “On the generators of quantum dynamical semigroups”, *Commun. Math. Phys.* **48**, 119 (1976). Cited on page 18.
- [112] T. Dittrich, B. Oelschlägel, and P. Hänggi, “Driven tunnelling with dissipation”, *EPL* **22**, 5 (1993). Cited on pages 19 and 30.
- [113] S. Kohler, R. Utermann, P. Hänggi, and T. Dittrich, “Coherent and incoherent chaotic tunneling near singlet-doublet crossings”, *Phys. Rev. E* **58**, 7219 (1998). Cited on page 19.
- [114] T. Shirai, T. Mori, and S. Miyashita, “Condition for emergence of the Floquet-Gibbs state in periodically driven open systems”, *Phys. Rev. E* **91**, 030101 (2015). Cited on page 22.
- [115] M. B. Plenio and P. L. Knight, “The quantum-jump approach to dissipative dynamics in quantum optics”, *Rev. Mod. Phys.* **70**, 101 (1998). Cited on page 23.
- [116] K. Mølmer and Y. Castin, “Monte carlo wavefunctions in quantum optics”, *J. Opt. B* **8**, 49 (1999). Cited on page 23.

- [117] D. T. Gillespie, “A general method for numerically simulating the stochastic time evolution of coupled chemical reactions”, *J. Comput. Phys.* **22**, 403 (1976). Cited on page 23.
- [118] A. Gelman and D. B. Rubin, “Inference from iterative simulation using multiple sequences”, *Stat. Sci.* **7**, 457 (1992). Cited on page 25.
- [119] A. Griessner, A. J. Daley, S. R. Clark, D. Jaksch, and P. Zoller, “Dissipative dynamics of atomic hubbard models coupled to a phonon bath: dark state cooling of atoms within a bloch band of an optical lattice”, *New J. Phys.* **9**, 44 (2007). Cited on page 27.
- [120] A. Rapp, S. Mandt, and A. Rosch, “Equilibration rates and negative absolute temperatures for ultracold atoms in optical lattices”, *Phys. Rev. Lett.* **105**, 220405 (2010). Cited on page 29.
- [121] J. Dunkel and S. Hilbert, “Consistent thermostats forbids negative absolute temperatures”, *Nature Phys.* **10**, 67 (2014). Cited on page 29.
- [122] S. Hilbert, P. Hänggi, and J. Dunkel, “Thermodynamic laws in isolated systems”, *Phys. Rev. E* **90**, 062116 (2014). Cited on page 29.
- [123] D. Frenkel and P. B. Warren, “Gibbs, Boltzmann, and negative temperatures”, *Am. J. Phys.* **83**, 163–170 (2015). Cited on page 29.
- [124] C. E. Reid, “Energy eigenvalues and matrix elements for the quartic oscillator”, *J. Mol. Spectrosc.* **36**, 183 (1970). Cited on page 29.
- [125] T. Dittrich, P. Hänggi, G. Schon, and B. J. Kramer, *Quantum transport and dissipation*, volume 3, Wiley-vch Weinheim (1998). Cited on page 30.
- [126] P. Pfeifer and R. Levine, “A stationary formulation of time-dependent problems in quantum mechanics”, *J. Chem. Phys.* **79**, 5512 (1983). Cited on page 31.
- [127] U. Peskin and N. Moiseyev, “The solution of the time-dependent Schrödinger equation by the (t, t') method: Theory, computational algorithm and applications”, *The Journal of chemical physics* **99**, 4590 (1993). Cited on page 31.
- [128] I. C. Percival, “Regular and irregular spectra”, *J. Phys. B* **6**, L229 (1973). Cited on page 31.
- [129] M. V. Berry and M. Tabor, “Level clustering in the regular spectrum”, *Proc. R. Soc. A* **356**, 375 (1977). Cited on page 31.
- [130] A. Voros, “Semi-classical ergodicity of quantum eigenstates in the wigner representation”, *Stochastic behavior in classical and quantum Hamiltonian systems* 326 (1979). Cited on page 31.
- [131] K. Husimi, “Some formal properties of the density matrix”, *J. Phys. Soc.* **22**, 264 (1940). Cited on page 31.
- [132] O. Penrose and L. Onsager, “Bose-Einstein condensation and liquid helium”, *Phys. Rev.* **104**, 576 (1956). Cited on pages 34 and 37.

- [133] E. J. Mueller, T.-L. Ho, M. Ueda, and G. Baym, “Fragmentation of Bose-Einstein condensates”, *Phys. Rev. A* **74**, 033612 (2006). Cited on pages 34 and 103.
- [134] W. J. Mullin and A. R. Sakhel, “Generalized Bose–Einstein condensation”, *J. Low Temp. Phys.* **166**, 125 (2012). Cited on page 34.
- [135] R. Kubo, “Generalized cumulant expansion method”, *J. Phys. Soc.* **17**, 1100 (1962). Cited on page 39.
- [136] T. Köhler and K. Burnett, “Microscopic quantum dynamics approach to the dilute condensed Bose gas”, *Phys. Rev. A* **65**, 033601 (2002). Cited on page 39.
- [137] N. N. Bogoliubov, “On the theory of superfluidity”, *J. Phys. (USSR)* **11**, 23 (1947), reprinted in: D. Pines, *The Many-Body Problem* (W.A. Benjamin, New York, 1961), p. 292. Cited on page 42.
- [138] B. Sinervo and C. M. Lively, “The rock-paper-scissors game and the evolution of alternative male strategies”, *Nature* **380**, 240 (1996). Cited on pages 44 and 71.
- [139] M. Holthaus, E. Kalinowski, and K. Kirsten, “Condensate fluctuations in trapped Bose gases: Canonical vs. microcanonical ensemble”, *Ann. Phys.* **270**, 198 (1998). Cited on page 55.
- [140] V. V. Kocharovskiy, V. V. Kocharovskiy, M. Holthaus, C. R. Ooi, A. Svidzinsky, W. Ketterle, and M. O. Scully, “Fluctuations in ideal and interacting Bose–Einstein condensates: From the laser phase transition analogy to squeezed states and Bogoliubov quasiparticles”, *Advances In Atomic, Molecular, and Optical Physics* **53**, 291 (2006). Cited on page 55.
- [141] J. Schmitt, T. Damm, D. Dung, F. Vewinger, J. Klaers, and M. Weitz, “Observation of grand-canonical number statistics in a photon Bose-Einstein condensate”, *Phys. Rev. Lett.* **112**, 030401 (2014). Cited on page 56.
- [142] J. Schnakenberg, “Network theory of microscopic and macroscopic behavior of master equation systems”, *Rev. Mod. Phys.* **48**, 571 (1976). Cited on page 65.
- [143] J. Knebel, M. F. Weber, T. Krueger, and E. Frey, “Evolutionary games of condensates in coupled birth-death processes”, *Nat. Commun.* **6** (2015). Cited on pages 70, 71, 72, and 104.
- [144] J.-P. Brantut, C. Grenier, J. Meineke, D. Stadler, S. Krinner, C. Kollath, T. Esslinger, and A. Georges, “A thermoelectric heat engine with ultracold atoms”, *Science* **342**, 713 (2013). Cited on page 75.
- [145] S. Krinner, D. Stadler, D. Husmann, J.-P. Brantut, and T. Esslinger, “Observation of quantized conductance in neutral matter”, *Nature* **517**, 64 (2015). Cited on page 75.
- [146] T. Iadecola and C. Chamon, “Floquet systems coupled to particle reservoirs”, *Phys. Rev. B* **91**, 184301 (2015). Cited on page 77.
- [147] J. D. Plumhof, T. Stöferle, L. Mai, U. Scherf, and R. F. Mahrt, “Room-temperature Bose-Einstein condensation of cavity exciton-polaritons in a polymer.”, *Nat. Mater.* **13** (2014). Cited on page 79.

- [148] S. Pau, G. Björk, J. Jacobson, H. Cao, and Y. Yamamoto, “Microcavity exciton-polariton splitting in the linear regime”, *Phys. Rev. B* **51**, 14437 (1995). Cited on page 80.
- [149] G. Björk, A. Karlsson, and Y. Yamamoto, “Definition of a laser threshold”, *Phys. Rev. A* **50**, 1675 (1994). Cited on page 86.
- [150] K. D. Choquette, D. A. Richie, and R. E. Leibenguth, “Temperature dependence of gain-guided vertical-cavity surface emitting laser polarization”, *Appl. Phys. Lett.* **64**, 2062 (1994). Cited on page 95.
- [151] M. Sondermann, M. Weinkath, T. Ackemann, J. Mulet, and S. Balle, “Two-frequency emission and polarization dynamics at lasing threshold in vertical-cavity surface-emitting lasers”, *Phys. Rev. A* **68**, 033822 (2003). Cited on page 95.
- [152] D. Sun, E. Towe, P. H. Ostdiek, J. W. Grantham, and G. J. Vansuch, “Polarization control of vertical-cavity surface-emitting lasers through use of an anisotropic gain distribution in [110]-oriented strained quantum-well structures”, *IEEE J. Sel. Top. Quantum Electron.* **1**, 674 (1995). Cited on page 95.
- [153] J. Martin-Regalado, J. L. A. Chilla, J. J. Rocca, and P. Brusenbach, “Polarization switching in vertical-cavity surface emitting lasers observed at constant active region temperature”, *Appl. Phys. Lett.* **70**, 3350 (1997). Cited on page 95.
- [154] T. Ackemann and M. Sondermann, “Characteristics of polarization switching from the low to the high frequency mode in vertical-cavity surface-emitting lasers”, *Appl. Phys. Lett.* **78**, 3574 (2001). Cited on page 95.
- [155] L. Ge, D. Liu, A. Cerjan, S. Rotter, H. Cao, S. G. Johnson, H. E. Türeci, and A. D. Stone, “Interaction-induced mode switching in steady-state microlasers”, *Opt. Express* **24**, 41 (2016). Cited on page 95.
- [156] S. S. Alharthi, A. Hurtado, V. M. Korpijarvi, M. Guina, I. D. Henning, and M. J. Adams, “Circular polarization switching and bistability in an optically injected 1300 nm spin-vertical cavity surface emitting laser”, *Appl. Phys. Lett.* **106**, 021117 (2015). Cited on page 95.
- [157] G. S. Agarwal and S. Dattagupta, “Higher-order phase transitions in systems far from equilibrium: Multicritical points in two-mode lasers”, *Phys. Rev. A* **26**, 880 (1982). Cited on page 95.
- [158] P. Gartner and C. M. Halati, “Laser transition in the thermodynamic limit for identical emitters in a cavity”, *Phys. Rev. A* **93**, 013817 (2016). Cited on page 95.
- [159] S. Reitzenstein, “Semiconductor quantum dot–microcavities for quantum optics in solid state”, *IEEE J. Sel. Top. Quantum Electron.* **18**, 1733 (2012). Cited on page 95.
- [160] L. He, S. K. Özdemir, and L. Yang, “Whispering gallery microcavity lasers”, *Laser Photon. Rev.* **7**, 60 (2013). Cited on page 95.

-
- [161] K. J. Vahala, “Optical microcavities”, *Nature* **424**, 839 (2003). Cited on page 95.
- [162] K. Panajotov, B. Nagler, G. Verschaffelt, A. Georgievski, H. Thienpont, J. Danckaert, and I. Veretennicoff, “Impact of in-plane anisotropic strain on the polarization behavior of vertical-cavity surface-emitting lasers”, *Appl. Phys. Lett.* **77**, 1590 (2000). Cited on pages 95 and 99.
- [163] S. M. Ulrich, C. Gies, S. Ates, J. Wiersig, S. Reitzenstein, C. Hofmann, A. Löffler, A. Forchel, F. Jahnke, and P. Michler, “Photon statistics of semiconductor microcavity lasers”, *Phys. Rev. Lett.* **98**, 043906 (2007). Cited on page 96.
- [164] P. R. Rice and H. J. Carmichael, “Photon statistics of a cavity-qed laser: A comment on the laser–phase-transition analogy”, *Phys. Rev. A* **50**, 4318 (1994). Cited on page 97.
- [165] C. J. Pethick and H. Smith, *Bose-Einstein condensation in dilute gases*, Cambridge university press (2002). Cited on page 103.
- [166] V. Bagnato and D. Kleppner, “Bose-Einstein condensation in low-dimensional traps”, *Phys. Rev. A* **44**, 7439 (1991). Cited on page 103.
- [167] B. Fischer and R. Weill, “When does single-mode lasing become a condensation phenomenon?”, *Opt. Express* **20**, 26704 (2012). Cited on page 104.
- [168] G. Bianconi and A.-L. Barabási, “Bose-Einstein condensation in complex networks”, *Phys. Rev. Lett.* **86**, 5632 (2001). Cited on page 104.
- [169] Z. Burda, D. Johnston, J. Jurkiewicz, M. Kaminski, M. A. Nowak, G. Papp, and I. Zahed, “Wealth condensation in Pareto macroeconomies”, *Phys. Rev. E* **65**, 026102 (2002). Cited on page 104.
- [170] M. R. Evans and T. Hanney, “Nonequilibrium statistical mechanics of the zero-range process and related models”, *J. Phys. A* **38**, R195 (2005). Cited on page 104.
- [171] M. R. Evans, T. Hanney, and S. N. Majumdar, “Interaction-driven real-space condensation”, *Phys. Rev. Lett.* **97**, 010602 (2006). Cited on page 104.

List of publications

- **D. Vorberg**, W. Wustmann, R. Ketzmerick, and A. Eckardt, *Generalized Bose-Einstein condensation into multiple states in driven-dissipative systems*. Phys. Rev. Lett. **111**, 240405 (2013)
- **D. Vorberg**, W. Wustmann, H. Schomerus, R. Ketzmerick, and A. Eckardt, *Nonequilibrium steady states of ideal bosonic and fermionic quantum gases*. Phys. Rev. E **92**, 062219 (2015)
- H. A. M. Leymann^{*}, **D. Vorberg**^{*}, T. Lettau^{*}, C. Hopfmann, C. Schneider, M. Kamp, S. Höfling, R. Ketzmerick, J. Wiersig, S. Reitzenstein, A. Eckardt, *Pump-power-driven mode switching in a microcavity device and its relation to Bose-Einstein condensation*. Phys. Rev. X **7**, 021045 (2017).
- A. Schnell, **D. Vorberg**, R. Ketzmerick, A. Eckardt, *High-temperature nonequilibrium Bose condensation induced by a hot needle*. Phys. Rev. Lett. **119**, 140602 (2017).

^{*}These authors contributed equally to this work

Danksagungen

Besonders herzlich danke ich meinem Betreuer Prof. Roland Ketzmerick für sein entgegengebrachtes Vertrauen und die hervorragende Betreuung und Unterstützung auf meinem Weg zur Promotion.

Dr. André Eckardt danke ich von Herzen für die wissenschaftliche Betreuung und die bereichernde Zusammenarbeit. Nicht nur habe ich viel von seinen Ideen und Ratschlägen gelernt, sondern sein Enthusiasmus für die Forschung ist für mich zum Vorbild geworden.

Ich bedanke mich für die gute Zusammenarbeit im Rahmen unterschiedlicher Projekte bei Thomas Lettau, Dr. Alexander Leymann, Alexander Schnell, Prof. Hennig Schomerus, Prof. Jan Wiersig, Dr. Waltraut Wustmann und allen anderen Koautoren. Das gemeinsame Forschen hat mir viel Freude bereitet und zahlreiche Ideen entstanden durch den wissenschaftlichen Austausch miteinander.

Für die freundschaftliche Arbeitsatmosphäre danke ich der gesamten Arbeitsgruppe und den Kollegen am Max-Planck-Institut für Physik komplexer Systeme und am Institut für Theoretische Physik. Insbesondere erwähnen möchte ich Dr. Thomas Bilitewski, Dr. Martin Körber, Dr. Steffen Lange, Dr. Alexander Leymann, Dr. Clemens Löbner, Franziska Onken, Dr. Martin Richter, Dr. Arko Roy, Dr. Krishanu Roychowdhury, Dr. Shashi Srivastava, Maximilian Schulz, Alexander Schnell, Christoph Sträter, Dr. Nur Ünal und Botao Wang. Meinem Kollegen, Freund und Trauzeugen Dr. Wladimir Tschischik spreche ich ganz besonderen Dank aus für die vielen Diskussionen über die Physik und das Leben.

Der Studienstiftung des deutschen Volkes gilt mein Dank für die finanzielle und ideelle Förderung im Rahmen des Promotionsstipendiums.

Der *Machine Learning Reading Group*, die jede Woche ein Highlight war, danke ich für die spannenden Diskussionen über die unterschiedlichsten Facetten künstlicher Intelligenz.

Für die vielen hilfreichen Hinweise beim Korrekturlesen schulde ich Dr. André Eckardt, Dr. Alexander Leymann, Dr. Arko Roy, Alexander Schnell, Christoph Sträter, Dr. Nur Ünal und Dr. Wladimir Tschischik meinen Dank.

Ich danke den Entwicklern der Software, die erst diese Forschung und dessen Präsentation ermöglicht haben. Hierzu zählen Python, SciPy, PyX, PyXGraph (vielen Dank an Prof. Arnd Bäcker für die tolle Bibliothek zum Erstellen von Graphiken) und Latex.

Meinen Eltern Annegret und Holger Vorberg danke ich für ihre liebevolle Unterstützung.

Ich danke meiner Frau Kerstin, die mir während der Promotion mit unserem Sohn Jakob das größte Geschenk machte.

Versicherung

Die Arbeit zu dem Thema

*Generalized Bose-Einstein Condensation
in Driven-dissipative Quantum Gases*

wurde am Max-Planck-Institut für Physik komplexer Systeme in Dresden und am Institut für Theoretische Physik der Technischen Universität Dresden unter der wissenschaftlichen Betreuung von Prof. Roland Ketzmerick durchgeführt.

Hiermit versichere ich, dass ich die vorliegende Arbeit ohne unzulässige Hilfe Dritter und ohne Benutzung anderer als der angegebenen Hilfsmittel angefertigt habe; die aus fremden Quellen direkt oder indirekt übernommenen Gedanken sind als solche kenntlich gemacht. Die Arbeit wurde bisher weder im Inland noch im Ausland in gleicher oder ähnlicher Form einer anderen Prüfungsbehörde vorgelegt.

Ich erkenne die Promotionsordnung der Fakultät Physik der Technischen Universität Dresden vom 23. Februar 2011 an.

Daniel Vorberg

Ort, Datum